

**ANALYSIS OF ORDINARY BRIDGES CROSSING FAULT-  
RUPTURE ZONES**

**by**

**Rakesh K. Goel  
California Polytechnic State University, San Luis Obispo**

**and**

**Anil K. Chopra  
University of California, Berkeley**

**Research Conducted for the  
California Department of Transportation  
Contract No. 59A0435**

**Earthquake Engineering Research Center  
University of California at Berkeley  
February 2008**

**Report No. UCB/EERC-2008/01**

## ABSTRACT

Recent earthquakes have demonstrated the vulnerability of bridges that cross fault-rupture zones. While avoiding building bridges across faults may be the best practice, it may not always be possible to do so, especially in regions of high seismicity, such as California. While site-specific seismological studies to define spatially-varying ground motions and rigorous nonlinear response history analysis (RHA) are necessary for important bridges on “lifeline” routes, such investigations may be too onerous for “ordinary” bridges whose design is governed by the California Department of Transportation (CALTRANS) Seismic Design Criteria (SDC). The overall objective of this research investigation is to develop rational, simplified methods – simpler than nonlinear response history analysis (RHA) – rooted in structural dynamics theory, for estimating seismic demand for “ordinary” bridges crossing fault-rupture zones.

Shear keys at abutment of bridges are designed to provide transverse restraint to the superstructure during service load and moderate earthquakes. During the maximum design earthquake, the shear keys are designed as sacrificial elements to protect the abutment stem-wall, wing-walls, and piles from damage, implying that the shear keys will break off before damage occurs in piles or abutment walls. However, recent experiments conducted on the seismic performance of shear keys designed according to current CALTRANS design criteria indicate that “actual” break-off strength of shear keys may be significantly higher than the design value. Therefore, the first phase of this investigation focused on developing an improved understanding of the role that shear keys play in affecting the seismic response of “ordinary” bridges crossing fault-rupture zones.

For this purpose, seismic responses of bridges subjected to spatially-uniform and spatially-varying ground motions for three shear-key conditions – nonlinear shear keys that break-off and cease to provide transverse restraint if deformed beyond certain limit; elastic shear keys that do not break-off and continue to provide transverse restraint throughout the ground shaking; and no shear keys – are examined. It is shown that seismic demands for a bridge with nonlinear shear keys can generally be bounded by the demands for a bridge with elastic shear keys and bridge with no shear keys for both types of ground motions. While ignoring shear keys provides conservative estimates of seismic demands for bridges subjected to spatially-uniform ground motion, such a practice may lead to underestimation of some seismic demands in bridges in

fault-rupture zones that are subjected to spatially-varying ground motion. Therefore, estimating the upper bounds of seismic demands in bridges crossing fault-rupture zones requires analysis for two shear-key conditions: no shear keys and elastic shear keys. It is also demonstrated that seismic response of bridges crossing fault-rupture zones may be very sensitive to the strength of shear keys indicating that computation of this response, even with nonlinear RHA, may be unreliable in the absence of realistic and accurate force-deformation models for shear keys.

The second phase of this investigation focused on developing two approximate procedures for estimating peak responses of linearly-elastic “ordinary” bridges crossing fault-rupture zones: response spectrum analysis (RSA) procedure and a linear static analysis procedure. These procedures estimate the peak response by superposing peak values of quasi-static and dynamic responses. The peak quasi-static response in both procedures is computed by static analysis of the bridge with peak values of all support displacements applied simultaneously. In RSA, the peak dynamic response is estimated by dynamic analysis including all significant modes, which is simplified in the latter procedure to static analysis of the bridge for appropriately selected forces; usually only one mode – the most dominant mode – is sufficient in the RSA procedure. Appearing in these procedures is the “effective” influence vector that differs from the influence vector for spatially-uniform excitation, and the response spectrum used in the RSA procedure differs from the standard CALTRANS SDC spectrum. Both of these simplified procedures have been shown to provide estimates of peak response that are close enough to results of the “exact” response history analysis to be useful for practical application. They are suitable for analysis of bridges with elastic shear keys or with no shear keys, the two shear-key cases that must be considered according to findings in the first phase of this investigation.

The third and final phase of this investigation extended the approximate procedures developed in the second phase to estimate seismic demands for “ordinary” bridges deforming into their inelastic range. This phase of investigation led to development of three approximate procedures for estimating seismic demands for bridges crossing fault-rupture zones and deforming into their inelastic range: modal pushover analysis (MPA), linear dynamic analysis, and linear static analysis. These procedures estimate the total seismic demand by superposing peak values of quasi-static and dynamic parts, as in the case of linearly-elastic bridges. The peak quasi-static demand in all three procedures is computed by *nonlinear static analysis* of the bridge subjected to peak values of all support displacements applied simultaneously. In the MPA and

the linear dynamic analysis procedures, the peak dynamic demand is estimated by *nonlinear static (or pushover) analysis* and *linear static analysis*, respectively, for forces corresponding to the most-dominant mode. In the linear static analysis procedure, the peak dynamic demand is estimated by *linear static analysis* of the bridge due to lateral forces appropriate for bridges crossing fault-rupture zones. The three approximate procedures are shown to provide estimates of seismic demands that are accurate enough to be useful for practical applications. The linear static analysis procedure, which is much simpler than the other two approximate procedures, is recommended for practical analysis of “ordinary” bridges because it eliminates the need for mode shapes and vibration periods of the bridge. In light of the procedures developed in this investigation, deficiencies in the current procedures being used by bridge engineers for analysis of bridges in fault-rupture zones are identified.

## **ACKNOWLEDGMENTS**

This research investigation is supported by the California Department of Transportation (CALTRANS) under Contract No. 59A0435 with Dr. Mahmoud Khojasteh as the project manager. This support is gratefully acknowledged. Also acknowledged is the collaboration of Professor Douglas Dreger and Gabriel Hurtado of University of California at Berkeley, who simulated the ground motions used in this investigation. We also appreciate the advice of: Sami Megally of PBS&J Inc. and Azadeh Bozorgzadeh at the University of California, San Diego on modeling of shear keys; Prof. Ansgar Neuenhofer of Cal Poly, San Luis Obispo on response combination rules; and we thank Foued Zayati of CALTRANS on current procedures for analysis of bridges crossing fault-rupture zones. Finally, we acknowledge the editorial expertise provided by Claire Johnson of University of California, Berkeley.

# CONTENTS

ABSTRACT.....	I
ACKNOWLEDGMENTS .....	IV
CONTENTS.....	V
1. INTRODUCTION .....	1
2. STRUCTURAL SYSTEMS AND RESPONSE QUANTITIES.....	3
2.1 Structural Systems and Modeling.....	3
2.2 Response Quantities .....	6
3. GROUND MOTIONS .....	7
3.1 Spatially-Uniform Ground Motion.....	7
3.2 Spatially-Varying Ground Motion Across Fault-Rupture Zones .....	8
3.2.1 Vertical Strike-Slip Faults.....	9
3.2.2 Other Types of Faults.....	11
3.2.3 Response Spectrum.....	12
4. ROLE OF SHEAR KEYS IN SEISMIC BEHAVIOR.....	15
4.1 Introduction .....	15
4.2 Shear-Key Modeling .....	16
4.3 Seismic Response of Bridges with Shear Keys.....	18
4.3.1 Spatially-Uniform Ground Motion .....	18
4.3.2 Spatially-Varying Ground Motion Across Fault-Rupture Zones.....	20
4.4 Upper Bounds of Seismic Demands.....	22
5. LINEAR ANALYSIS .....	26
5.1 Introduction .....	26
5.2 Response History Analysis.....	26
5.2.1 Multiple-Support Excitation .....	26
5.2.2 Proportional Multiple-Support Excitation .....	27
5.2.3 Evaluation of Proportional Multiple-Support Excitation Approximation .....	29
5.3 Estimation of Peak Response .....	31
5.3.1 Response Spectrum Analysis (RSA) Procedure .....	33
5.3.2 Linear Static Analysis Procedure.....	34
5.4 Significant Vibration Modes .....	35
5.4.1 Vibration Periods and Modes.....	35
5.4.2 Modal Contribution Factors and Significant Modes.....	37
5.5 Accuracy of Proposed Procedures.....	41
6. NONLINEAR ANALYSIS .....	44
6.1 Introduction .....	44
6.2 Superposing Quasi-static and Dynamic Parts of Response.....	44
6.2.1 Is Quasi-Static Solution Adequate? .....	46

6.3 Estimation of Peak Response.....	47
6.3.1 Modal Pushover Analysis (MPA ).....	47
496.3.2 ..... Linear Dynamic Analysis	51
6.3.3 Linear Static Analysis.....	51
6.4 Accuracy of Approximate Procedures .....	52
6.5 Application to Bridges with Nonlinear Shear Keys .....	54
7. COMMENTS ON CURRENT PROCEDURES .....	58
7.1 Procedures based on Fault Rupture Load Cases .....	58
7.2 A Simplistic Procedure.....	59
8. CONCLUSIONS.....	61
8.1 Role of Shear Keys.....	61
8.2 Linear Analysis.....	62
8.3 Nonlinear Analysis .....	63
8.4 Current Procedures.....	64
REFERENCES .....	66
APPENDIX A. GROUND MOTIONS FOR OTHER EARTHQUAKE MAGNITUDES.....	68
APPENDIX B. SHEAR-KEY MODELING .....	72
B.1 STRENGTH OF SHEAR KEYS .....	72
B.2 FORCE-DEFORMATION RELATIONSHIP OF SHEAR KEY .....	74
APPENDIX C. PROPERTIES OF INELASTIC SDF SYSTEM.....	76
APPENDIX D. EXAMPLE ANALYSIS .....	79
D.1 STATEMENT OF THE PROBLEM .....	79
D.2 VIBRATION PERIODS AND MODES .....	81
D.3 MODAL CONTRIBUTION FACTORS .....	81
D.4 QUASI-STATIC RESPONSE .....	84
D.5 PEAK DYNAMIC RESPONSES.....	85
D.5.1 MPA Procedure.....	85
D.5.2 Linear Dynamic Analysis .....	88
D.5.3 Linear Static Analysis.....	89

## 1. INTRODUCTION

Recent earthquakes have demonstrated the vulnerability of bridges that cross fault-rupture zones. Several bridges were seriously damaged as a result of rupture of causative faults in the 1999 Chi-Chi earthquake (EERI, 2001; Yen, 2002), 1999 Kocaeli earthquake (EERI, 2000), and 1999 Duzce earthquake (Ghasemi et al., 2000). While avoiding building bridges across faults may be the best practice, it may not always be possible to do so, especially in regions of high seismicity, such as California. It is estimated that that more than 5% of all bridges in California may either cross faults or lie in very close proximity to fault-rupture zones.

Bridges crossing fault-rupture zones will experience ground offset across the fault and hence spatially-varying ground motion. While site-specific seismological studies to define spatially-varying ground motions and rigorous nonlinear response history analysis (RHA) are necessary for important bridges on “lifeline” routes, such investigations may be too onerous for “ordinary” bridges whose design is governed by the CALTRANS Seismic Design Criteria (SDC) (CALTRANS, 2006). “Ordinary” bridges are defined as normal weight concrete bridges with span lengths less than 90 m supported on the substructure by pin/rigid connections or conventional bearings. The bent caps of “ordinary” bridges terminate inside of the exterior girders, and their foundations consist of spread footings, piles, or pile shafts with underlying soil that is not susceptible to liquefaction, lateral spreading, or scour. A large fraction of bridge inventory in California falls in the category of “ordinary” bridges. For such structures, simplified procedures for estimating seismic demands are needed to facilitate their seismic evaluation and design. Therefore, overall objective of this research investigation is to develop rational, simplified methods – simpler than nonlinear response history analysis (RHA) – rooted in structural dynamics theory, for estimating seismic demand of bridges crossing fault-rupture zones.

This investigation has been implemented in three phases: (1) understanding the role of shear keys in seismic behavior, (2) development of linear analysis procedures, and (3) development of nonlinear analysis procedures. Comments on the procedures currently being used by bridge engineers for analysis of “ordinary” bridges crossing fault-rupture zones are included.

This report has been organized as follows. Chapter 2 presents the structural systems, modeling approach, and the response quantities considered. Chapter 3 describes the ground

motions considered in this investigation. Chapter 4 examines the role of shear keys in seismic behavior of bridges in fault-rupture zones. Chapter 5 develops procedures for linear analysis of bridges crossing fault-rupture zones, which are extended in Chapter 6 to nonlinear analysis of bridges. Chapter 7 comments on analysis procedures currently being used by bridge engineers in light of the procedures developed in Chapters 5 and 6. Finally, Chapter 8 presents conclusions and recommendations of this investigation.

## 2. STRUCTURAL SYSTEMS AND RESPONSE QUANTITIES

### 2.1 Structural Systems and Modeling

The structural systems considered in this investigation are as follows: (1) a three-span symmetric bridge (Figure 2.1a); (2) a three-span unsymmetric bridge (Figure 2.1b); (3) a four-span symmetric bridge (Figure 2.1c); and (4) a four-span unsymmetric bridge (Figure 2.1d). These bridges, with no skew, are supported on abutments at the two ends and intermediate single-column bents. The span lengths and bent heights are shown in Figure 2.1. The bases of columns in the bents are fixed (restrained in all six degrees-of-freedom). The deck, a multi-cell box girder, is expected to accommodate two traffic lanes (Figure 2.2). The columns selected are 1.5 m diameter circular sections, with helical transverse (or hoop) steel and longitudinal steel arranged at its periphery (Figure 2.3). The area of longitudinal steel is selected between 2% and 3% of the gross columns area, and hoop steel selected is 1% of the column volume to represent well confined columns; such heavy reinforcement is appropriate for columns in bridges crossing fault-rupture zones. Although not reported here for reason of brevity, a parametric analysis for different ratio of longitudinal and hoop steel indicated that the observations and conclusions presented in this report are relatively insensitive to these parameters.

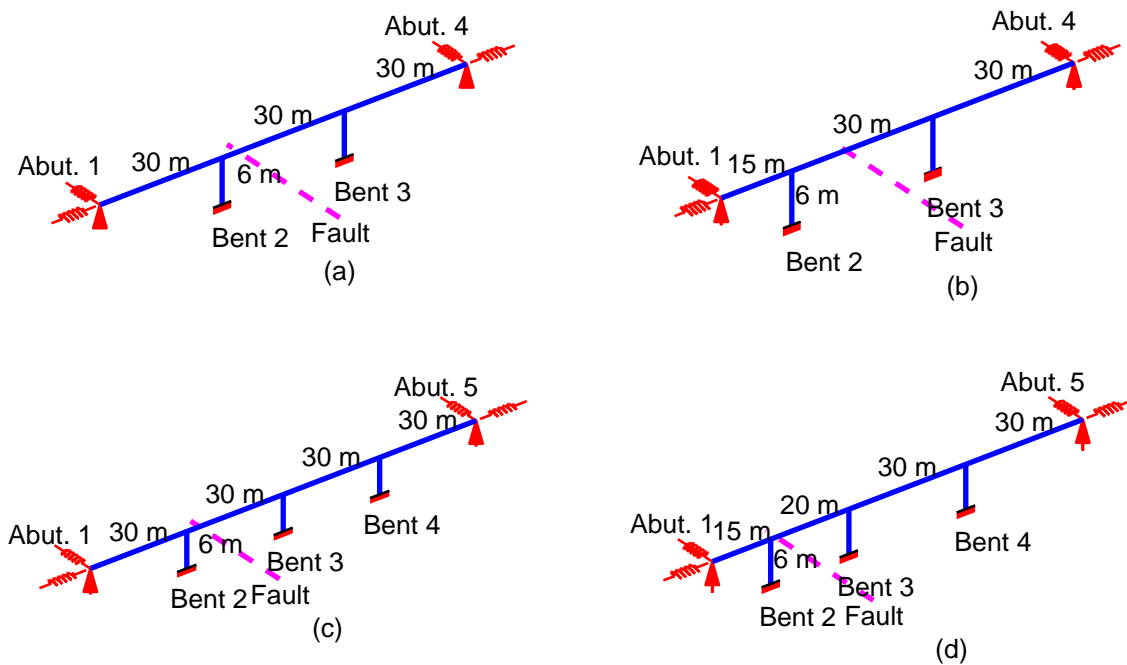


**Figure 2.1. Bridges considered: (a) three-span symmetric bridge, (b) three-span unsymmetric bridge; (c) four-span symmetric bridge; (4) four-span unsymmetric bridge.**

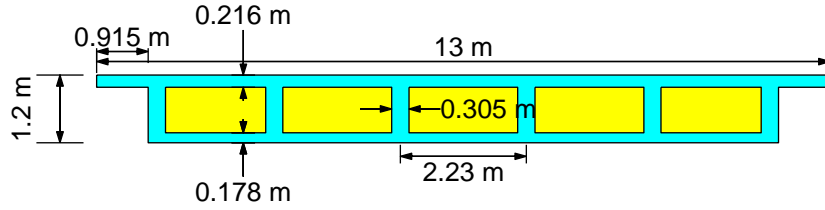


**Figure 2.2. Cross section of the bridge deck.**

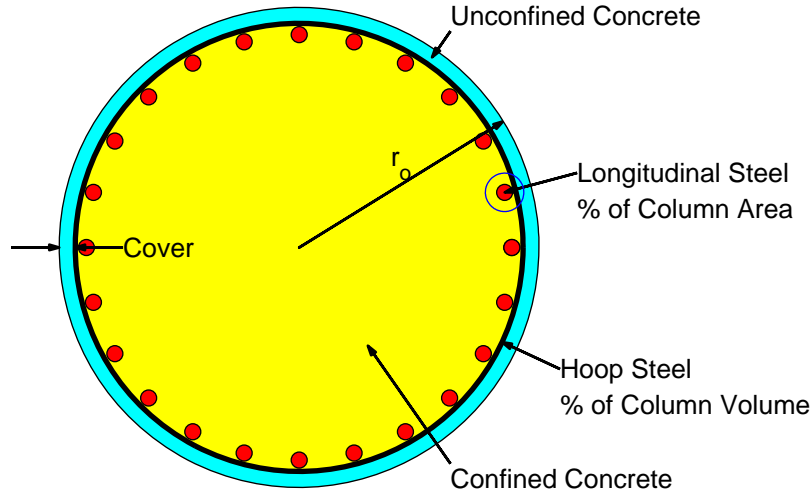


**Figure 2.3. Column cross-section.**

The structural systems considered in this investigation do not necessarily represent “actual” bridges. They were selected in consultation with CALTRANS engineers to investigate the bridge behavior for varying parametric conditions: the number of spans (three-span versus four-span bridges) and asymmetry in bridge geometry (symmetric-bridges versus asymmetric bridges). It is assumed that the conclusions gleaned from analyzing the seismic behavior of these structural systems bridges will be generally applicable for most “actual” bridges.

The selected bridge systems were analyzed using the structural analysis software Open System for Earthquakes Engineering Simulation (*OpenSees*) (McKenna and Fenves, 2001), whereby the girder was modeled as linearly-elastic beam column elements. In order to capture the distribution of mass along the length of the deck, five elements per span was used. Consistent with CALTRANS’ recommendations, the gross values for moment of inertia and polar moment of inertia were used for a pre-stressed multi-cell box deck girder. The columns were modeled as linear beam-column element for linear analysis and nonlinear beam-column elements with fiber

section for nonlinear analysis. Details on the modeling are available in McKenna and Fenves (2001).

The inherent damping for all selected bridges was modeled with Rayleigh's damping (Chopra, 2007):  $\mathbf{c} = a_0\mathbf{m} + a_1\mathbf{k}$ , where  $\mathbf{m}$  is the mass matrix of the system,  $\mathbf{k}$  is the initial elastic stiffness matrix of the system, and  $a_0$  and  $a_1$  are the mass- and stiffness-proportionality coefficients. In order to keep damping ratio to be about 5% in most significant modes of the selected systems, values of  $a_0$  and  $a_1$  were selected to be 0.4134 and 0.004837, respectively.

The abutments were modeled as springs in the longitudinal and transverse directions. The longitudinal springs were elastic-perfectly-plastic springs with a gap to account for the gap between end of the deck and the abutment back-wall, which is provided to accommodate thermal movement. The stiffness,  $K_L$ , and strength,  $F_{yL}$ , of the longitudinal springs were computed according to CALTRANS recommendations (CALTRANS, 2006: Section 7.8.1):

$$K_L = 11500W \frac{H}{1.7} \text{ kN/m} \quad (2.1a)$$

$$F_{yL} = 239A \frac{H}{1.7} \text{ kN} \quad (2.1b)$$

where  $W$  and  $H$  are the width and height of the back-wall in meters, and  $A$  is the area of back-wall in  $\text{m}^2$  for a seat-type abutment.

The transverse springs model the contributions of the foundation system as well as the shear keys. While CALTRANS provided recommendations on the stiffness of transverse springs that model pile-supported foundation, no clear guidelines were given to model shear keys that exhibit highly nonlinear behavior with brittle failure. The modeling procedure used in this investigation for the transverse springs represents the shear-key-pile-foundation system is presented in Chapter 4.

It is useful to emphasize that nonlinearity in the structural systems was restricted to the columns and the shear keys (where appropriate). The girder was assumed to remain linear elastic. These assumptions were based on consultations with CALTRANS engineers, who indicated nonlinearity (or hinging) in the girder to be unacceptable. Furthermore, soil-structure interaction

at the two abutments was not explicitly considered because the scope of this investigation is limited to “ordinary” bridges, and such detailed analysis may not be necessary.

## **2.2 Response Quantities**

The response quantities considered in this investigation are the column drift and deck displacement at the abutment. The column drift, which indicates deformation demand in the column, is defined as the displacement at top of the column relative to its base displacement. The deck displacement at the abutment, which is used to estimate the relative displacement of the deck from the abutment, is defined as the displacement of the deck at the abutment relative to the displacement at the top of the abutment.

### 3. GROUND MOTIONS

This investigation examined the seismic demands for selected structural systems subjected to two types of ground motions: (1) spatially-uniform ground motion resulting from near-field or far-field earthquakes; and (2) spatially-varying ground motion resulting from rupture of a fault. Following is a description of these ground motions.

#### 3.1 Spatially-Uniform Ground Motion

For this study, the ground motion recorded during the 1994 Northridge earthquake at the Sylmar County Hospital Parking Lot in the north-south direction (Figure 3.1) was selected as the spatially-uniform ground motion, with a peak ground acceleration, velocity, and displacement of 0.844g, 1.29 m/s, and 0.325 m, respectively. This motion represents strong shaking that may occur in regions where fault rupture does not extend all the way to the ground surface. This motion is applied as uniform excitation to all supports of the selected bridge in the transverse direction.

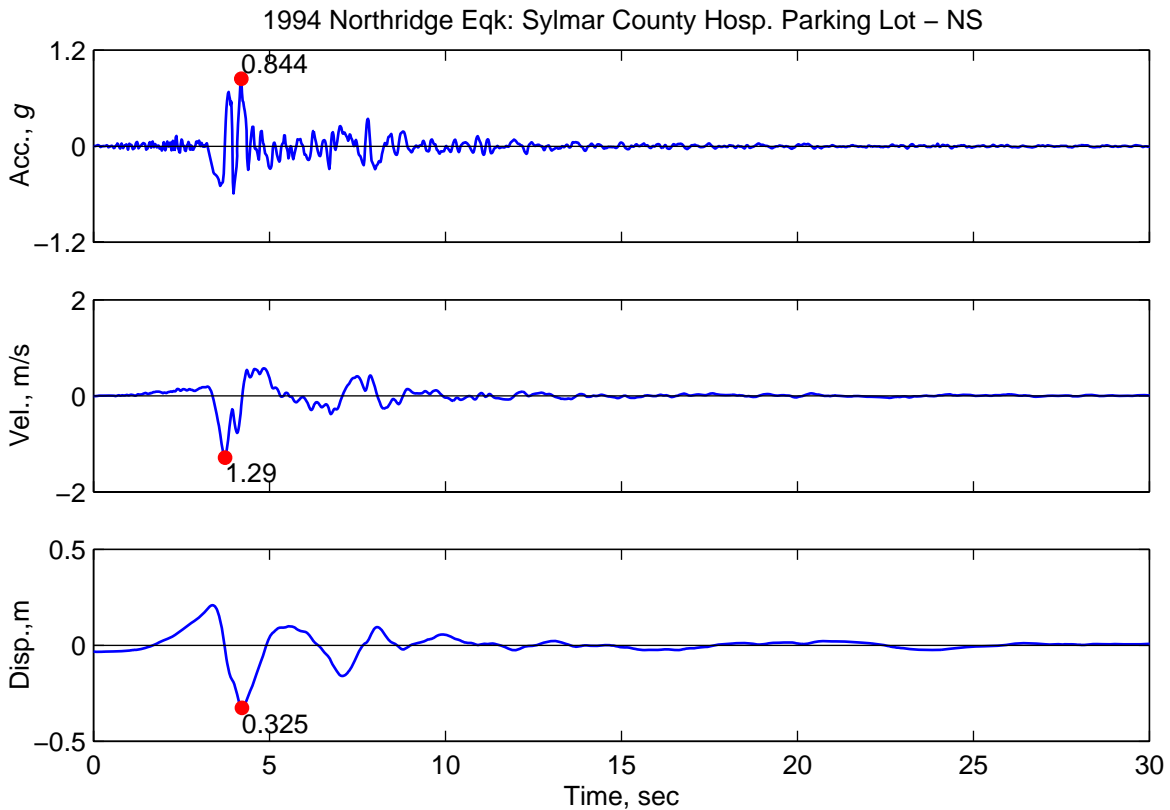
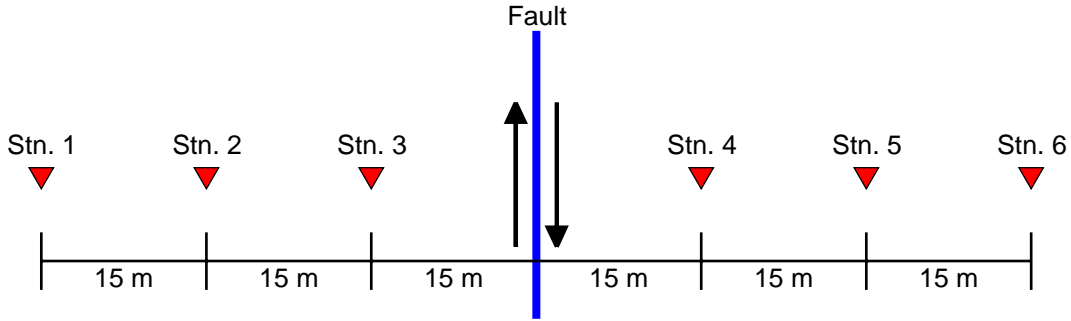


Figure 3.1. Spatially-uniform ground motion considered.

### 3.2 Spatially-Varying Ground Motion Across Fault-Rupture Zones

Ground motions in fault-rupture zones are to be defined at bridge supports in very close proximity to the fault (Figure 2.1). Unfortunately, to date, ground motions have never been recorded at such fine spacing in close proximity to the causative fault. For this investigation, motions were simulated at stations spaced 15 m apart (Figure 3.2) due to a magnitude 6.5 earthquake in the fault-normal, fault-parallel, and vertical directions across a fault rupture zone. The simulation method utilized a fourth order accurate staggered-grid elastic finite-difference code, ELAS3D, developed at Lawrence Livermore National Laboratory (Larsen and Schultz, 1995). Stress-free boundary conditions were used to model the free-surface, and absorbing boundary conditions (Clayton and Engquist, 1977) were used to damp artificial reflections from the grid boundary. Further details of the procedure to generate ground motions are available elsewhere (Dreger et al. 2007). Resulting from this simulation, the fault-parallel and fault-normal components of ground acceleration, velocity, and displacement at stations 1-6 are discussed next. The vertical motions are not considered in this investigation because they do not lead to column drift or deck displacement at abutment, the two response quantities of interest.

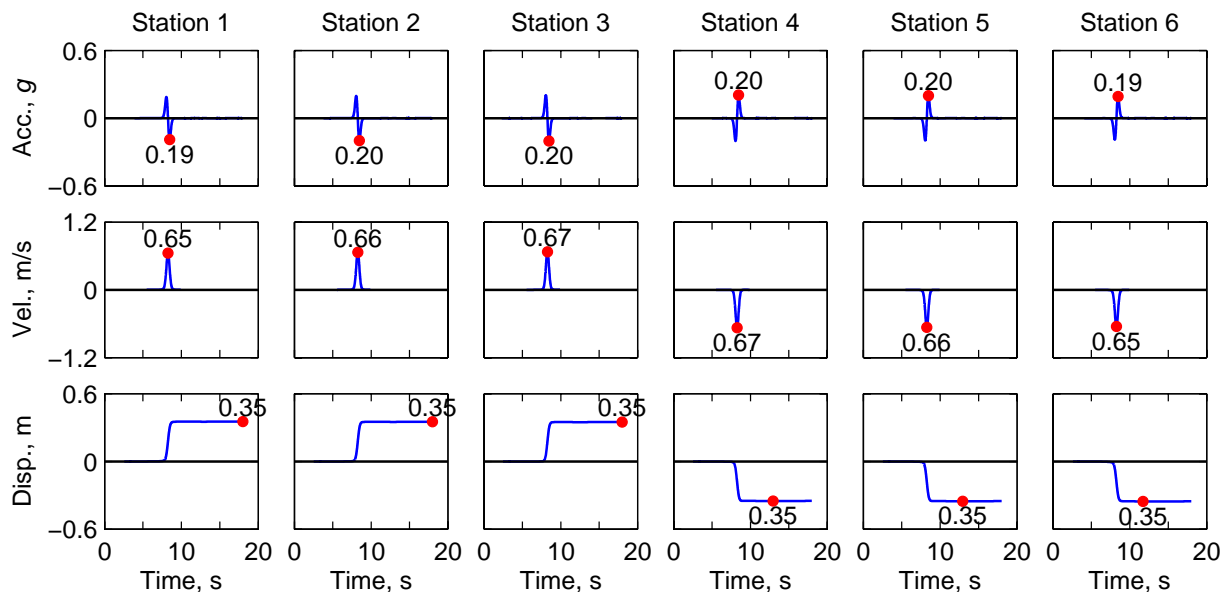
For the selected location of the fault with respect to various bents of the selected structural systems (see Figure 2.1), the simulated motions were applied at various supports of the three-span bridges as follows: motions at stations 1, 3, 4, and 6 were applied to abutment 1, bent 2, bent 3, and abutment 4, respectively, of the three-span symmetric bridge (Figure 2.1a); and motions at stations 2, 3, 4, and 6 were applied to abutment 1, bent 2, bent 3, and abutment 4, respectively, of the three-span unsymmetric bridge (Figure 2.1b). The motions were available only at abutment 1, bent 2, bent 3, and bent 4 (stations 1, 3, 4, and 6) of the four-span symmetric bridge, and at bent 3 and bent 4 (stations 4 and 6) of the four-span unsymmetric bridge. Because spatial variation among motions on the same side of the fault is minimal (as demonstrated later), motions at abutment 5 of the four-span symmetric bridge were assumed to be identical to those at station 6 (Figure 2.1c); and motions at abutment 1, bent 2, and abutment 5 of the four-span unsymmetric bridge were assumed to be those at stations 2, 3, and 6, respectively (Figure 2.1d).



**Figure 3.2. Location of stations across the fault where spatially-varying ground motions were simulated.**

### 3.2.1 Vertical Strike-Slip Faults

The fault-parallel motions across a strike-slip fault exhibit time variation of ground displacement that is a gradual step function, ground velocity that is a single-sided pulse, and ground acceleration that is a double-sided pulse (Figure 3.3). As expected, the ground in fault-rupture zones exhibits a permanent displacement (or static offset) that occurs over rise-time  $T_r$ . At distance close to the fault, the static displacement is one-half of the average slip of the fault. Both the static-offset (or average slip) and rise-time are related to the earthquake magnitude [Somerville et al. (1999); also see Appendix A].



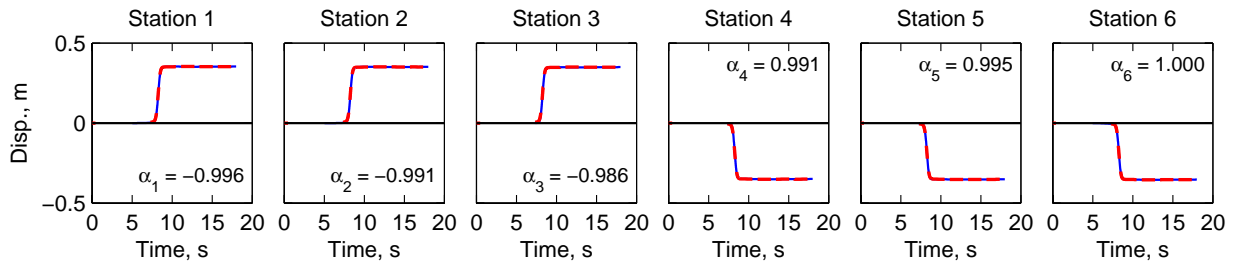
**Figure 3.3. Displacement, velocity, and acceleration in fault-parallel direction at six stations across a strike-slip fault during magnitude 6.5 earthquake.**

Figure 3.3 also shows that the simulated fault-parallel motions are anti-symmetric about the fault plane, i.e., fault-parallel motions at stations located equidistant from the fault but on opposite sides are essentially the same time functions, but are opposite in algebraic signs. Furthermore, the motions at stations 1, 2, and 3 on one side of the fault are essentially identical, and motions at stations 4, 5, and 6 on the other side of the fault are also almost identical. This indicates that motions at various stations (or locations) across the fault are essentially proportional to each other. Thus the displacement at support  $l$ ,

$$u_{gl}(t) = \alpha_l u_g(t) \quad (3.1)$$

in which  $u_g(t)$  is the displacement history of motion at a reference location, and  $\alpha_l$  is the proportionality constant for the  $l$ th support. The support motion defined by Equation (3.1) is referred to as proportional multiple-support excitation in rest of this report. The validity of this hypothesis is demonstrated in Figure 3.4, where motions obtained from Equation (3.1), with station 6 selected as the reference location, are compared with the simulated motions. The numerical values of  $\alpha_l$ , computed as the ratio of the peak displacements at the  $l$ th station and at the reference location (station 6) noted in Figure 4 are close to +1 or -1.

The fault-normal displacements across a strike-slip fault are essentially identical across the fault (Figure 3.5). Therefore, such motions may be treated as spatially-uniform excitation. The fault-normal displacements across a vertical strike-slip fault generally do not exhibit static-offset, except at locations close to start and end of the fault rupture; such motions are not included here for brevity but are available in another report (Dreger et al., 2007).



**Figure 3.4. Comparison of Equation (3.1) (dashed line) with simulated displacements (solid line) in the fault parallel direction as a result of rupture on a strike-slip fault;  $\alpha_l$  are as noted.**

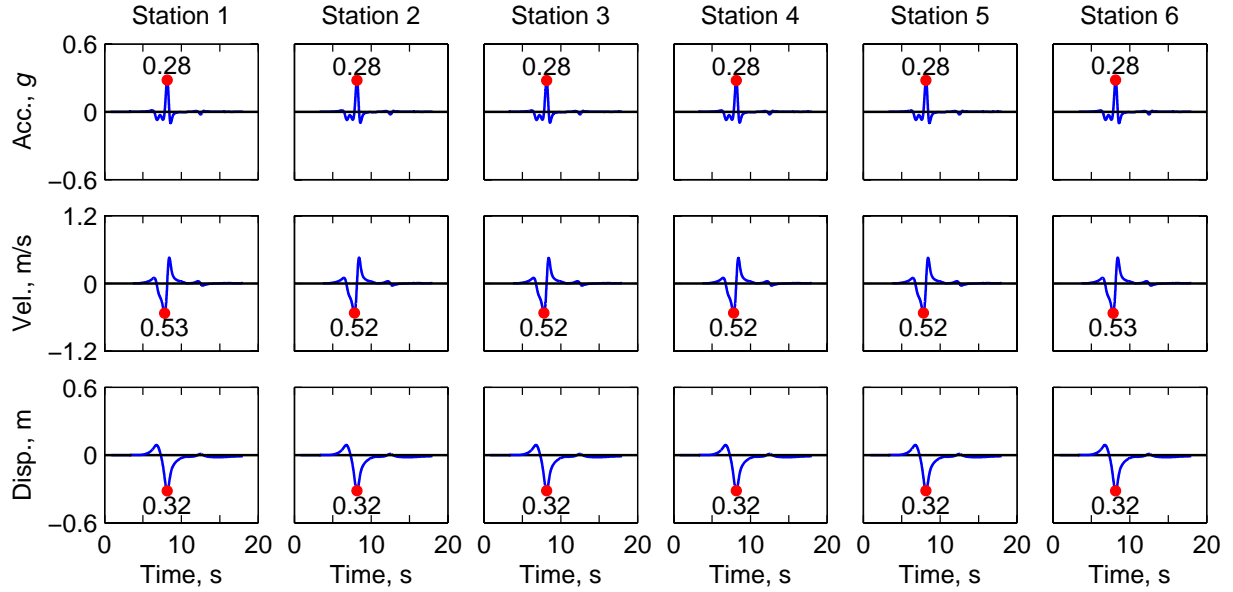


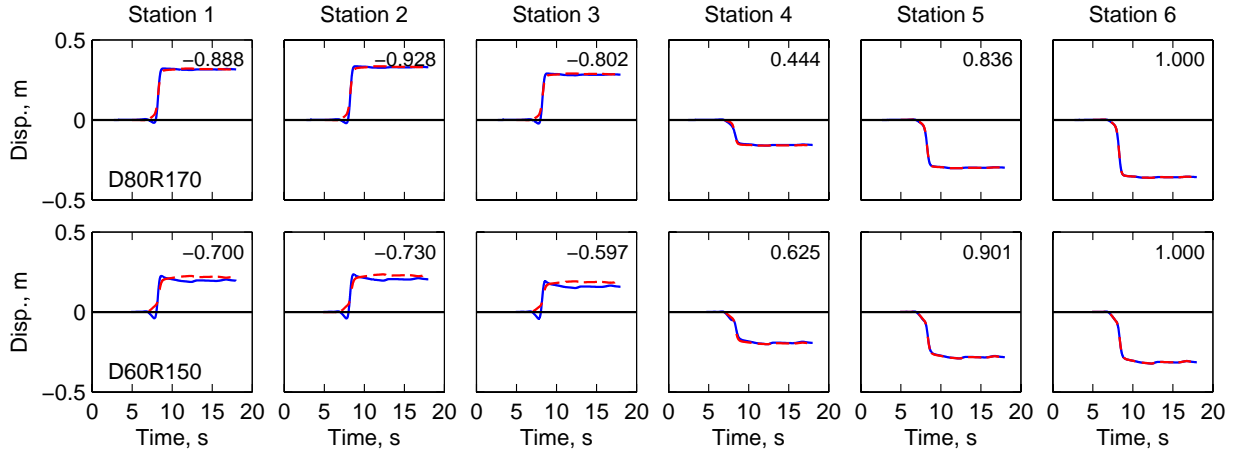
**Figure 3.5. Displacement, velocity, and acceleration in fault-normal direction at six stations across a strike-slip fault during magnitude 6.5 earthquake.**

### 3.2.2 Other Types of Faults

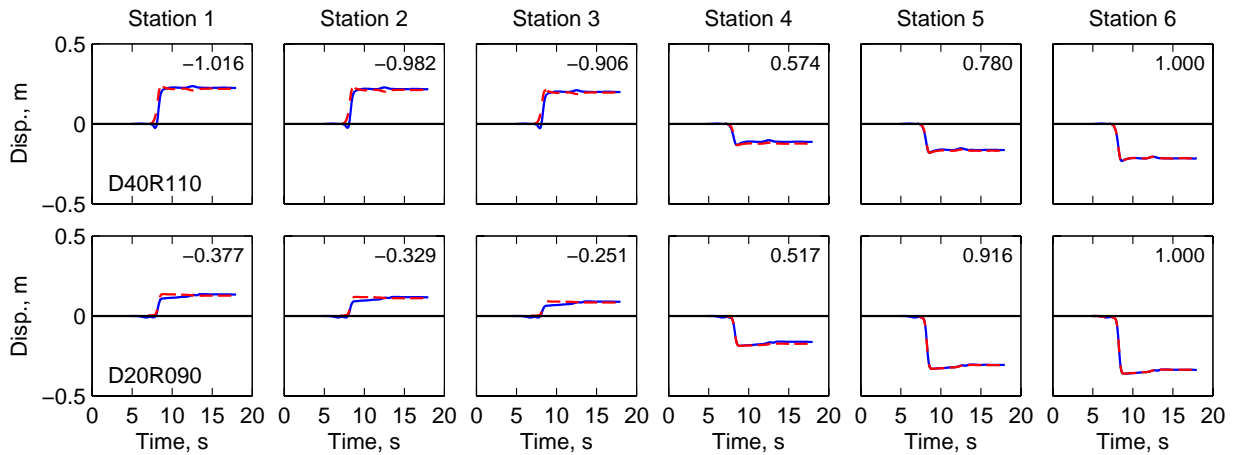
The validity of Equation (3.1), demonstrated in the preceding section for a strike-slip fault<sup>+</sup>, is found to be approximately valid for fault-parallel component of ground displacements across other types of faults (Figure 3.6): a fault with dip of 80° and rake of 170° (D90R170) and a fault with dip of 60° and rake of 150° (D60R150). For faults other than strike-slip, however,  $\alpha_l$  differ significantly from  $\pm 1$ . Note that the dip angle is the angle of the fault plane with respect to a horizontal plane on the surface of the earth; and the rake angle is the angle of slip direction on the fault with respect to a horizontal line on the fault surface.

The fault-normal component of ground displacements across dipping faults exhibit similar trends (Figure 3.7): (1) displacements exhibit static-offset and vary across the fault; and (2) the spatially-varying excitation can be modeled approximately as proportional multiple-support excitation with  $\alpha_l$  differing from  $\pm 1$ .

<sup>+</sup> Dip = 90° and rake of 180°. Dip is the angle the fault plane makes with a horizontal plane; rake is the slip direction in degrees relative to the strike of the fault.



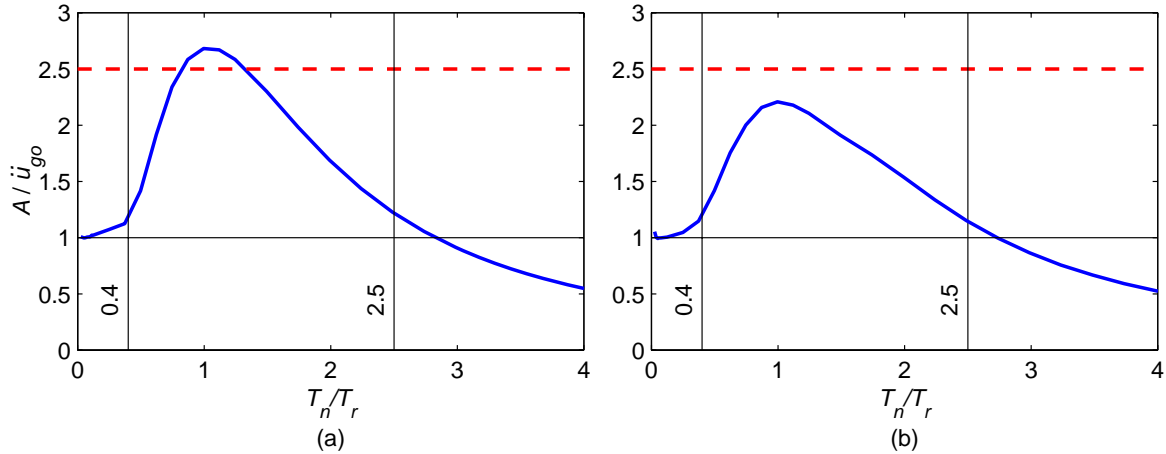
**Figure 3.6. Comparison of Equation (3.1) (dashed line) with simulated displacements (solid line) in the fault-parallel direction as a result of rupture on a fault with two different dip-rake angle combinations;  $\alpha_l$  are as noted.**



**Figure 3.7. Comparison of Equation (3.1) (dashed line) with simulated displacements (solid line) in the fault-normal direction as a result of rupture on a fault with two different dip-rake angle combinations;  $\alpha_l$  are as noted.**

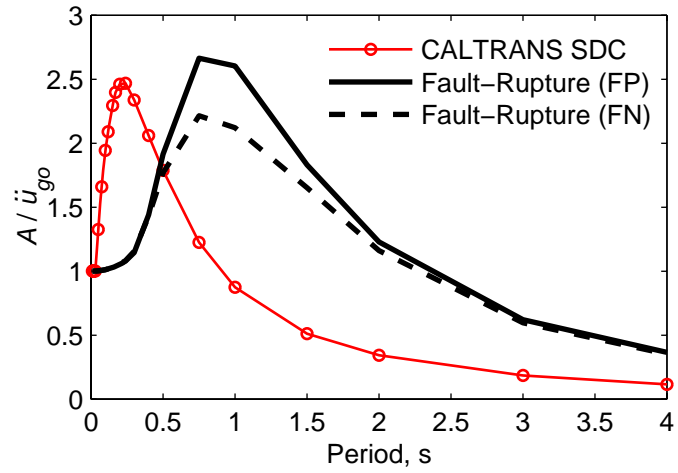
### 3.2.3 Response Spectrum

Figure 3.8 shows the pseudo-acceleration response spectrum for the fault-parallel and fault-normal components of ground motion, with permanent offset, in very close proximity (say, roughly, 15 meters) to the causative fault. The pseudo-acceleration scale has been normalized by the peak ground acceleration ( $A/\ddot{u}_{go}$ ), and the period scale by the rise-time ( $T_n/T_r$ ). When presented in such normalized form, the spectrum is valid for earthquakes over a wide range of magnitudes (Appendix A).



**Figure 3.8. Normalized 5%-damped elastic response spectrum for ground motions in fault-rupture zones: (a) fault-parallel component on a vertical strike-slip fault with dip of  $90^\circ$  and rake of  $180^\circ$ ; (b) fault-normal component on a fault with dip of  $40^\circ$  and rake of  $110^\circ$ .**

The CALTRANS SDC spectrum is inappropriate for analysis of bridges crossing fault-rupture zones because it differs considerably from the response spectrum for expected ground motions. This becomes apparent by comparing the normalized response spectrum for ground motions in fault-rupture zones with the CALTRANS SDC spectrum (Figure 3.9). Note that the various spectra in Figure 3.9 are normalized by dividing the spectral acceleration,  $A$ , with the peak ground acceleration,  $\ddot{u}_{g0}$ . Furthermore, the CALTRANS SDC spectrum included in Figure 3.9 is for peak ground acceleration (PGA) of 0.4g, soil type B, and earthquake magnitude  $6.5 \pm 0.25$ . Although CALTRANS SDC provides spectrum for PGA values in the range of 0.1g to 0.6g for each earthquake magnitude and soil type, only one spectrum for 0.4g PGA is included here for clarity.



**Figure 3.9. Comparison of normalized 5%-damped elastic response spectrum for ground motions in fault-rupture zone with the CALTRANS SDC spectrum.**

## 4. ROLE OF SHEAR KEYS IN SEISMIC BEHAVIOR

### 4.1 Introduction

Reinforced-concrete bridges in California typically consist of a multi-cell box girder deck supported on abutments at two ends and single or multiple intermediate bents. The abutment consists of two wing-walls, a back-wall, shear keys (exterior), a seat, footing, and piles if needed (Figure 4.1). The shear keys at abutment of bridges are designed to provide transverse restraint to the superstructure during service load and moderate earthquakes. During the maximum design earthquake, however, the shear keys are designed as sacrificial elements to protect the abutment stem-wall, wing-walls, and piles from damage, implying that the shear keys will break off before damage occurs in piles or abutment walls. The current CALTRANS SDC for shear keys in “ordinary” bridges limit the capacity of shear keys to be smaller of 30% of the dead load vertical reaction at the abutment and 75% of the total lateral pile capacity (CALTRANS, 2006).

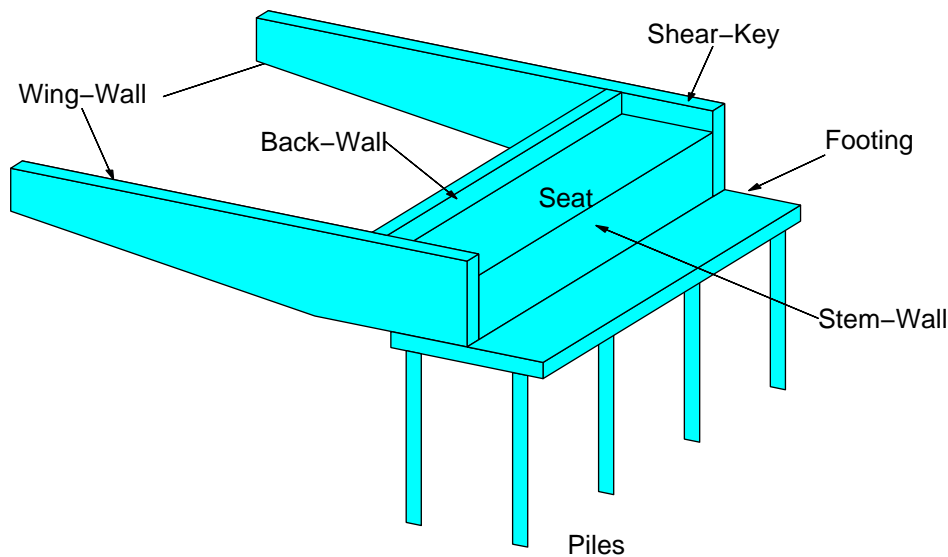


**Figure 4.1. Typical abutment details.**

Recent experiments conducted on the seismic performance of shear keys designed according to current CALTRANS design criteria indicate that “actual” break-off strength of shear keys may be significantly higher than the design value (Bozorgzadeh et al., 2003, 2006; Megally et al., 2001). While shear keys with such higher break-off strengths may lead to damage in abutment walls and piles, for bridges subjected to spatially-uniform ground motion they tend to limit the deformation demands in other critical locations, such as column drifts and displacement of the

deck at the abutments. Therefore, shear keys are generally ignored when idealizing a bridge because it is assumed that it provides upper bound estimates of the seismic displacement demands. Given that, it is not clear if ignoring shear keys will always provide upper bound estimates of these demands for bridges that cross fault-rupture zones and hence be subjected to spatially-varying ground motion.

The objective of this phase of the investigation is to develop an improved understanding of the role that shear keys play in affecting the seismic response of “ordinary” bridges crossing fault-rupture zones. In particular, the seismic response of bridges subjected to spatially-uniform ground motion as well as bridges subjected to spatially-varying ground motion expected in fault-rupture zones is examined with different shear-key conditions.

## **4.2 Shear-Key Modeling**

As mentioned in Chapter 2, the structural models include transverse springs to model the contributions of the foundation system as well as the shear keys. While procedures to model the contribution of the pile-foundation system are available (CALTRANS, 2006), no clear guidelines are available to model shear keys. Experiments conducted at University of California at San Diego (UCSD) (Bozorgzadeh et al., 2003, 2006; Megally et al., 2001) on shear keys with different detailing have shown that shear keys exhibit highly nonlinear behavior with brittle failure. Based on these experiments, details to improve the shear key behavior have been proposed, including various mechanisms to establish failure load of shear keys. However, force-deformation (or hysteretic) behavior of shear keys to be used in seismic analysis of bridges has not yet been finalized.

This investigation utilized a simple tri-linear force-deformation model (Figure 4.2) based on the experiment results obtained from the UCSD research on shear keys (Megally et al., 2001). The reference (or starting) strength of the shear key at each abutment was assumed to be equal to 30% of the dead load vertical reaction at that abutment. Details of the development of the force-deformation behavior of the shear key are presented in Appendix B.

The tests conducted at UCSD did not include the flexible piles that support the abutment. Pile flexibility is included in obtaining the abutment force-deformation behavior by assuming that the shear key and the piles act as springs in series. The modified force-deformation relationship of the abutment with shear-key-pile system is shown in Figure 4.2; a stiffness of

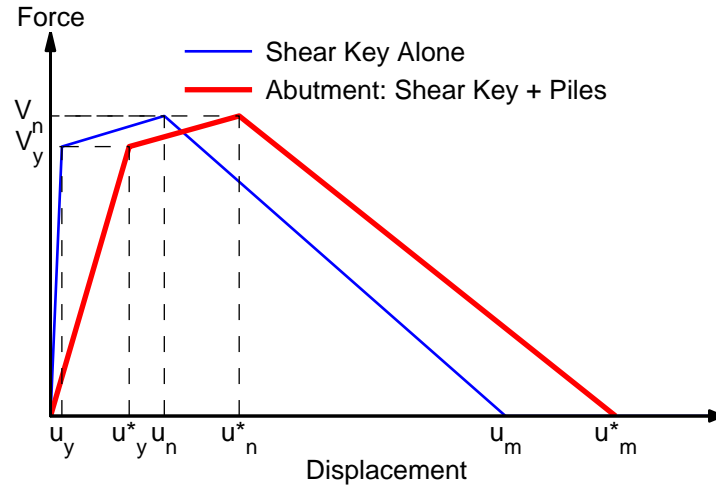


**Figure 4.2. Force-deformation behavior of shear keys and abutment.**

7000 kN/m per pile was selected per CALTRANS recommendations (CALTRANS, 2006), assuming a total of 12 piles per abutment. Note that including pile flexibility makes displacements  $u_y^*$ ,  $u_n^*$ , and  $u_m^*$  larger than  $u_y$ ,  $u_n$ , and  $u_m$ , but it does not affect the forces  $V_y$  and  $V_n$ .

For shear-keys at the abutment, three cases were considered. In the first case, shear keys do not engage during the design ground shaking, which is an appropriate model if shear keys are designed and constructed to break-off soon after onset of the design ground shaking. For this case, denoted as the bridge without shear keys, no springs were specified in the transverse direction at the abutment. In the second case, shear keys remain elastic and do not break-off during the ground shaking, which is an appropriate model if shear keys are much stronger than the design break-off strength. For this case, denoted as the bridge with elastic shear keys, elastic springs with stiffness equal to the initial abutment stiffness (see Figure 4.2) were specified in the transverse direction. The third case considered nonlinear behavior of shear keys. For this case, denoted as the bridge with nonlinear shear keys, shear keys were modeled as nonlinear springs in the transverse direction with force-deformation behavior specified by the tri-linear relationship presented in Figure 4.2. In the second and third cases, shear keys were assumed to provide transverse restraint in both positive and negative direction of the deck displacement, with

identical force-deformation behavior in the two directions. Note that bridge columns were permitted to respond beyond the linear elastic range for all shear-key conditions.

In addition to the three shear-key cases defined above, also investigated was how seismic demands for the bridge vary depending on the strength of the shear keys. For this purpose, the normalized shear key strength was varied between zero and 4, where the value one denotes a shear key with the strength equal to 30% of the dead load reaction at the abutment. As the normalized shear key strength approaches zero, the bridge behavior approaches that of a bridge without shear keys. For values of normalized shear key strength much larger than 1, the bridge behavior approaches that of a bridge with elastic shear keys.

### **4.3 Seismic Response of Bridges with Shear Keys**

This section investigates the influence of shear keys on the seismic response of the three-span symmetric bridge subjected to two types of excitations: (1) spatially-uniform ground motion (Figure 3.1), and (2) spatially-varying ground motion characteristic of fault-rupture zones (Figure 3.3). For each type of ground motion, examined first are the response histories of the bridge with three shear-key conditions – without shear keys, nonlinear shear keys, and elastic shear keys – followed by the variation of peak values of seismic demands with shear key strength.

#### **4.3.1 Spatially-Uniform Ground Motion**

Figure 4.3 shows the time-variation of column drift and deck displacement at the abutment of the three-span symmetric bridge for the three shear-key cases subjected to spatially-uniform ground motion. These results show that smallest of both responses occur for the bridge with elastic shear keys; the shear keys continue to provide transverse restraint throughout the ground shaking, leading to a stiffer structural system. In contrast, the largest of both responses occur for the bridge without shear keys, where there isn't any transverse restraint. The responses in the bridge with nonlinear shear keys, whereby shear keys initially provide transverse restraint but break-off if deformed beyond a certain limit, are initially identical to that of the bridge with elastic shear keys. After shear keys break-off on both sides of the deck, a bridge with nonlinear shear keys oscillates in a manner essentially similar to the bridge without shear keys, but about a different permanent drift.

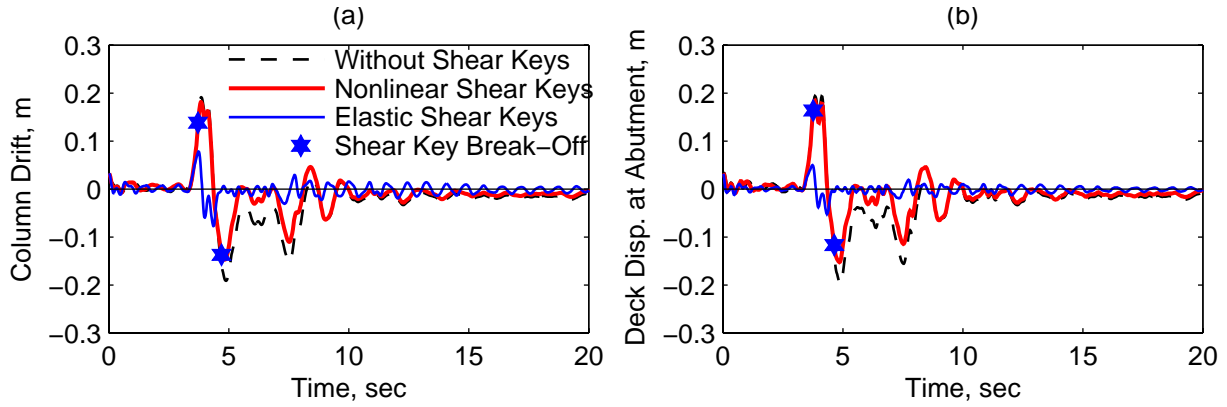


**Figure 4.3. Response history for a three-span symmetric bridge subjected to spatially-uniform ground motion: (a) column drift in bent 2, and (b) deck displacement at abutment 1.**

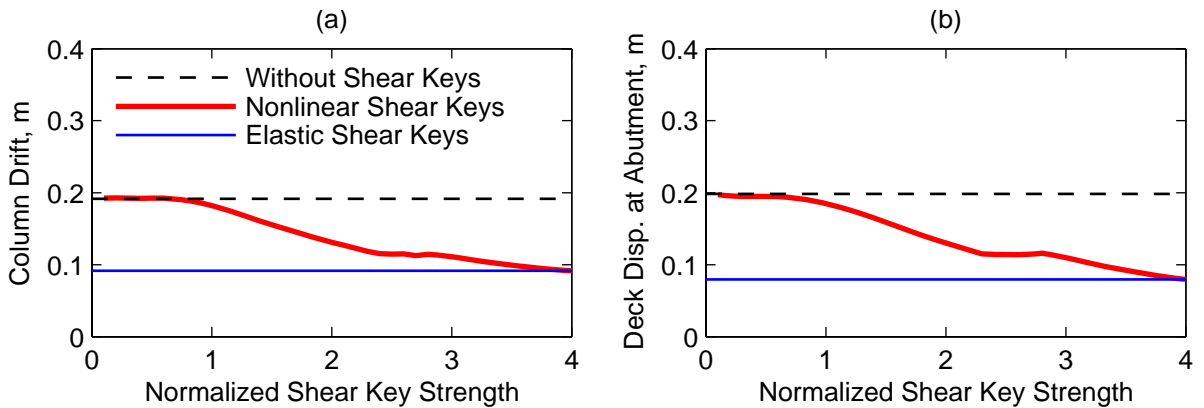


**Figure 4.4. Variation of peak responses with normalized shear key strength for a three-span symmetric bridge subjected to spatially-uniform ground motion: (a) column drift in bent 2, and (b) deck displacement at abutment 1.**

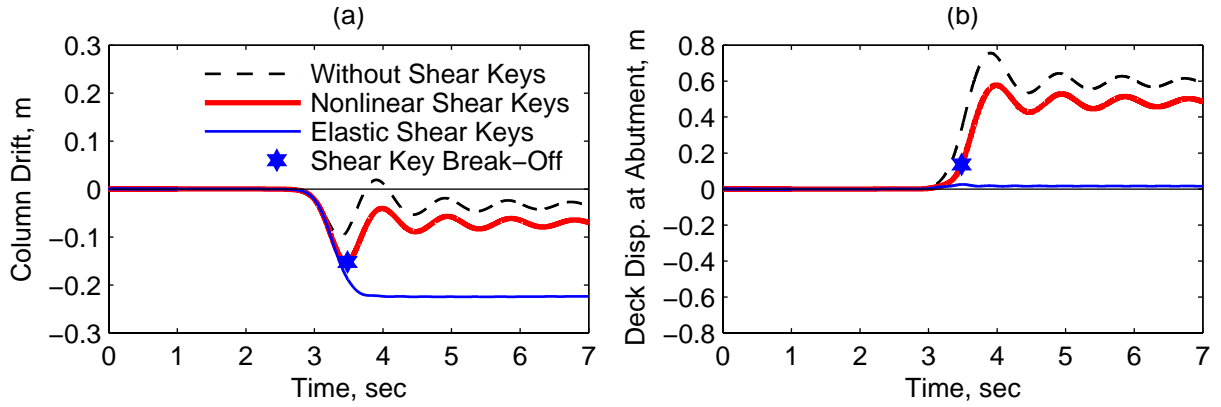
Figure 4.4 shows how the peak column drift and peak deck displacement at an abutment vary with normalized strength of the nonlinear shear key in a bridge with nonlinear shear keys. Also included for reference are the peak demands for the bridge with elastic shear keys and the bridge without shear keys; for obvious reasons, these demands are independent of the normalized shear key strength. As expected, the results presented show that the seismic demands for a bridge with nonlinear shear keys of very low strength approach those of the bridge without shear keys and the seismic demands for a bridge with very strong shear keys approach those of the bridge with elastic shear keys. For intermediate values of normalized shear key strength, seismic demands for the bridge with nonlinear shear keys fall between or are bounded by the demand values for the bridge without shear keys and bridge with elastic shear keys.

### 4.3.2 *Spatially-Varying Ground Motion Across Fault-Rupture Zones*

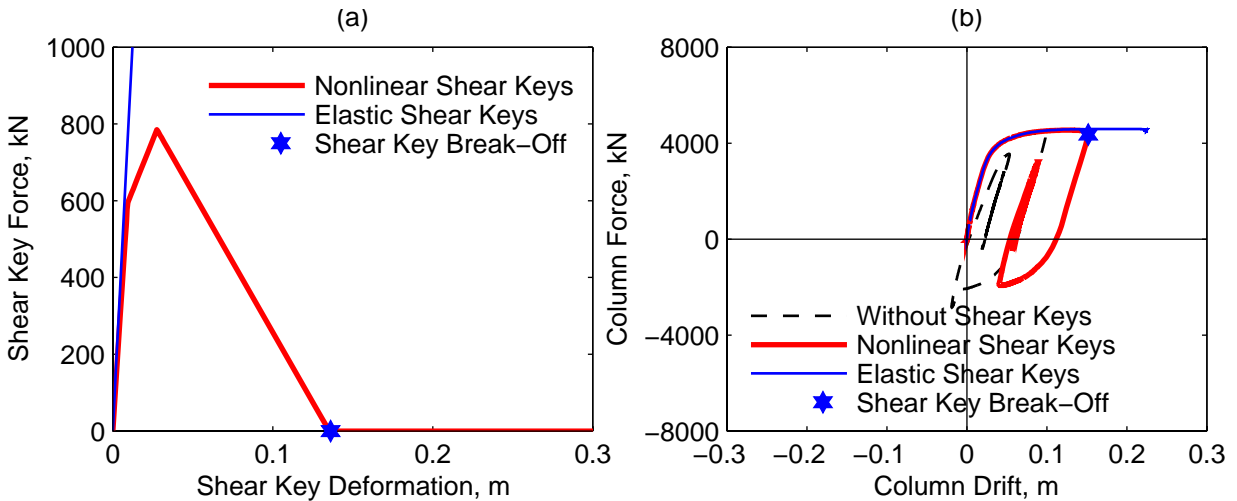
Figure 4.5 shows the time-variation of column drift and deck displacement at an abutment of the three-span symmetric bridge for the three shear-key cases subjected to spatially-varying ground motion expected in a fault-rupture zone (Figure 3.3). Comparing the results for the three cases, the smallest column drift occurred for the bridge without shear keys, whereas the smallest deck displacement occurred for the bridge with elastic shear keys. In contrast, among the three cases, the largest column drift occurred for the bridge with elastic shear keys and the largest deck displacement occurred for the bridge without shear keys. Thus seismic response trends for a bridge crossing a fault-rupture zone differ from that of this bridge subjected to spatially-uniform ground motion. In the first case, among the three shear key cases, the largest response may occur either in the bridge without shear keys (e.g., deck displacement at the abutment) or in the bridge with elastic shear keys (e.g., column drift) (see Figure 4.5), whereas in the second case, the seismic demand is largest for the bridge without shear keys (see Figure 4.3).

Figure 4.5 demonstrates that, as observed previously for spatially-uniform ground motion, the response of the bridge (with nonlinear shear keys) crossing a fault rupture-zone is initially identical to that of the bridge with elastic shear keys. After break-off of shear keys, the bridge oscillated in a manner similar to the bridge without shear keys, but about a different permanent displacement. The different permanent displacement, both column drift and deck displacement at the abutment (Figure 4.5), in the bridge with nonlinear shear keys after break-off of shear keys occurred due to different permanent offset that occurs in the bridge columns (as will be demonstrated next). Note that the strength and stiffness of the bridge after shear-key break-off is entirely due to the bridge columns.

Figure 4.6 shows the force-deformation relations for a shear key and a column in a bridge crossing a fault-rupture zone. As expected, the shear keys exhibited linearly-elastic force-deformation relationship for the bridge with elastic shear keys, and selected tri-linear force-deformation relationship for the bridge with nonlinear shear keys (Figure 4.6a). In the latter case, the shear key ceased to provide any resistance at a deformation of about 0.13 m, denoted as the shear key break-off point (Figure 4.6a). The shear key is loaded only in one direction (without any unloading or reloading) because the ground displacement, which resembles a step function with finite rise time (Figure 3.3), deformed the shear key only in one direction. The column



**Figure 4.5. Response histories for a three-span bridge subjected to spatially-varying ground motion: (a) column drift in bent 2, and (b) deck displacement at abutment 1.**



**Figure 4.6. Force-deformation relations for a three-span symmetric bridge subjected to spatially-varying ground motion: (a) shear-key at abutment 1, and (b) column in bent 2.**

experienced significant inelastic action for all three shear-key conditions (Figure 4.6b), with the extent of inelastic action depending on the condition of the shear-keys. The column deformed farthest into the inelastic range in the bridge with elastic shear keys and the least in the bridge without shear keys. The column experienced permanent drift for all three shear-key conditions, which was largest in the bridge with elastic shear keys and smallest in the bridge without shear keys.

Figure 4.7 shows how peak column drift and peak deck displacement at the abutment varied with normalized strength of nonlinear shear keys, along with the peak demands for the bridge with elastic shear keys and for the bridge without shear keys. As in the case of spatially-uniform

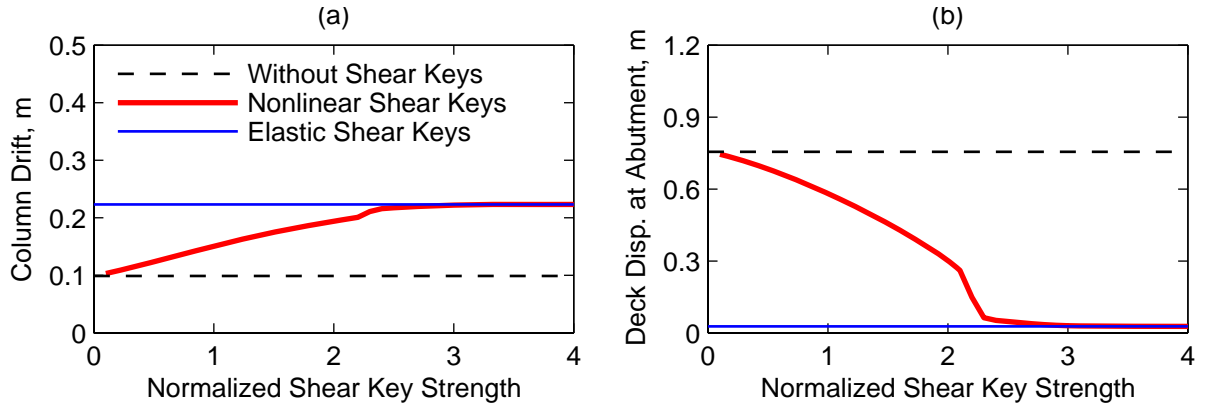


**Figure 4.7. Variation of peak responses with normalized shear key strength for a three-span symmetric bridge subjected to spatially-varying ground motion: (a) column drift in bent 2, and (b) deck displacement at abutment 1.**

ground motion (Figure 4.4), even for a bridge crossing a fault-rupture zone, the seismic demands in the bridge with elastic shear keys and without shear keys provided upper and lower bounds for seismic demands on a bridge with nonlinear shear keys (Figure 4.7). The bridge without shear keys provides an upper bound for deck displacement at the abutment and the bridge with elastic shear keys provided a lower bound (Figure 4.7b). This trend reversed, however, for column drift for which the bridge with elastic shear keys provided an upper bound and the bridge without shear keys led to a lower bound (Figure 4.7a).

Figure 4.7 also shows that seismic response of bridges crossing fault-rupture zones may be very sensitive to the strength of shear keys. For example, column drift in a bridge with very strong shear keys (normalized shear key strength greater than two) is more than twice that in a bridge with very weak shear keys (normalized shear key strength approaching zero) (Figure 4.7a). The deck displacement at abutment in a bridge with very strong shear keys is almost negligible but becomes very large in a bridge with very weak shear keys (Figure 4.7b).

#### 4.4 Upper Bounds of Seismic Demands

Design practice generally requires an upper bound of seismic demand for various parametric conditions. Therefore, it is useful to re-examine the results of Figures 4.4 and 4.7 to establish which of the three shear-key conditions provides an upper bound of seismic demand.

The results of Figure 4.4 for a three-span symmetric bridge subjected to spatially-uniform ground motions show that the seismic demands in the bridge without shear keys provide an upper bound of both seismic demands (column drift and deck displacement at the abutment) on

the bridge with nonlinear shear keys. This implies that the current practice of ignoring transverse restraint provided by shear keys in estimating seismic displacement demands of bridges is valid for spatially-uniform ground motion.

The results of Figure 4.7 for a three-span symmetric bridge subjected to spatially-varying ground motion in a fault-rupture zone demonstrate that ignoring transverse restraint provided by shear keys, i.e., by analyzing a bridge without shear keys, may not always provide an upper bound value for all seismic demand quantities. For the selected bridge, while ignoring shear keys provides an upper bound for deck displacement at the abutment (Figure 4.7b), the column drift is underestimated (Figure 4.7a), however, including elastic shear keys provides an upper bound for column drift. Therefore, a bridge should be analyzed for both shear-key cases (without shear keys and with elastic shear keys) to establish upper bounds for all seismic demands in the bridge. For the bridge subjected to spatially-varying ground motion expected in a fault-rupture zone, the traditional practice of ignoring transverse restraint provided by shear keys may lead to underestimation of some seismic demands.

The generality of the preceding conclusion is further supported by an examination of the peak seismic demands in three other bridges: a three-span unsymmetric bridge, a four-span symmetric bridge, and a four-span unsymmetric bridge. The results of Figures 4.8 to 4.10 permit the following observations: (1) Each of the two responses (the peak deck displacement at an abutment and peak column drift) of the three other bridges are generally bounded by the seismic demand estimates for two shear key cases: without shear keys and with elastic shear keys; (2) The bridge without shear keys provides an upper bound for deck displacement at an abutment; and (3) The bridge with elastic shear keys generally provides an upper bound for column drift. The first and second observations are generally valid, but exceptions at a few values of shear-key strength are noted in Figures 4.8a and 4.9a. Note, these deviations are minor, therefore, a design value for the column drift in a bridge with nonlinear shear keys can be estimated to a useful degree of accuracy by analyzing a bridge with elastic shear keys.

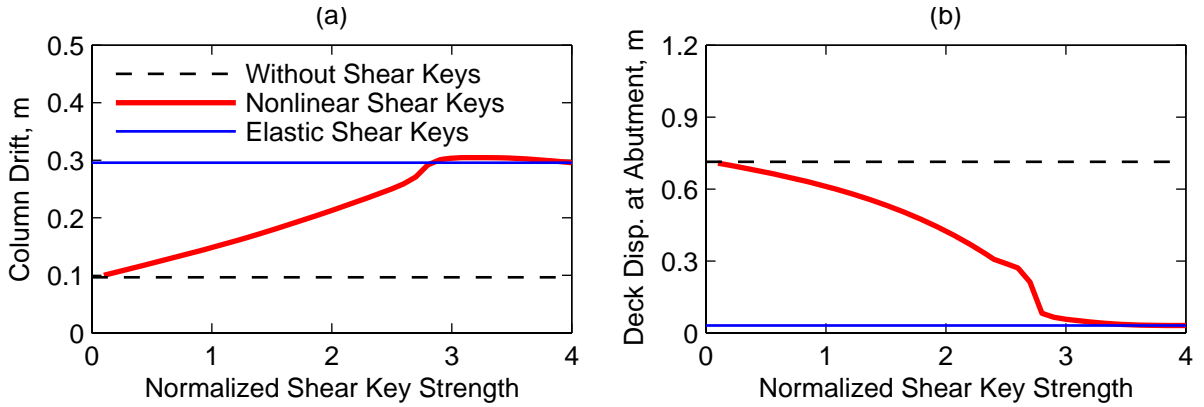


**Figure 4.8. Variation of peak responses with normalized shear key strength for a three-span unsymmetric bridge subjected to spatially-varying ground motion: (a) column drift in bent 3, and (b) deck displacement at abutment 4.**

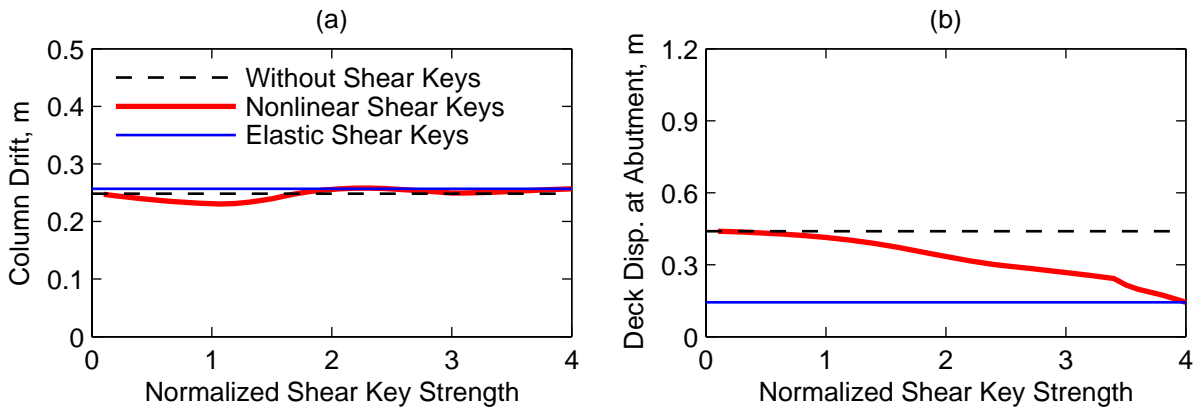


**Figure 4.9. Variation of peak responses with normalized shear key strength for a four-span symmetric bridge subjected to spatially-varying ground motion: (a) column drift in bent 3, and (b) deck displacement at abutment 1.**

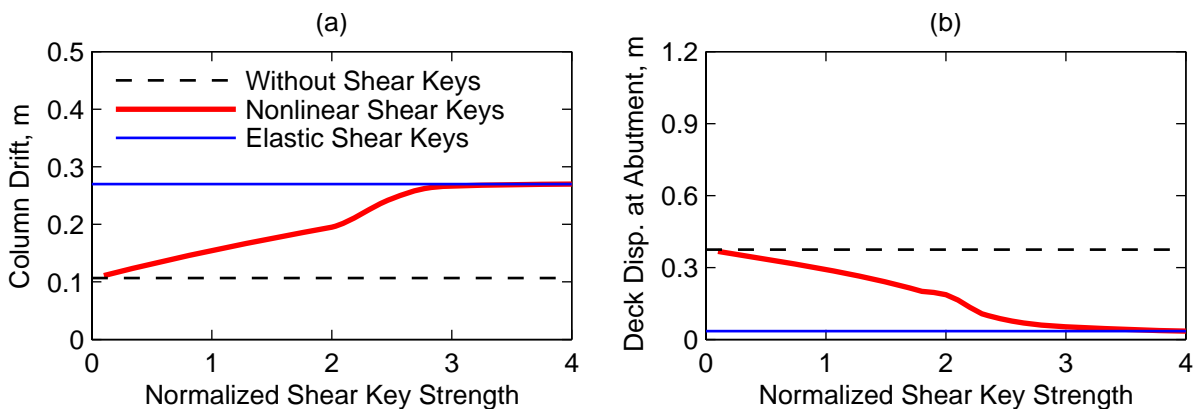


**Figure 4.10. Variation of peak responses with normalized shear key strength for a four-span unsymmetric bridge subjected to spatially-varying ground motion: (a) column drift in bent 4, and (b) deck displacement at abutment 5.**

The occurrence of larger deck displacement at an abutment for a bridge without shear keys and larger column drift in a bridge with elastic shear keys can be explained based on observations on the deflected shape of a bridge to static application of support displacements that are expected during fault-rupture. For this purpose, consider the deflected shape of the three-span symmetric bridge subjected to equal but opposite motions on two sides of the fault that ruptures between bent 2 and bent 3 (Figure 4.11). The bridge without shear keys rotates essentially as a rigid body about a vertical axis (Figure 4.11a). For such a deflected shape, the displacement of the girder at its two edges, i.e., at the two abutments, are the largest; however, drift in the columns, i.e., displacement of a column at the top relative to its bottom, is essentially zero. Although, the bridge with elastic shear keys exhibits rotational displacements about the vertical axis, it no longer rotates as a rigid body about the vertical axis but involves deformation of the girder (Figure 4.11b). Because of stiffness of the shear keys, the displacement at the two edges of the girder and hence deck displacements at the two abutments are smaller compared to the bridge without shear keys. The column drifts, however, are larger in the bridge with elastic shear keys. This occurs because the column bottom moves with the ground but the top is restricted from moving due to restraint provided by the girder that is not completely free to rotate as a rigid body about the vertical axis due to restraint imposed by the shear keys at its two ends. Although results are not presented here for reasons of brevity, similar reasons led to larger deck displacement at abutments in bridges without shear keys and larger column drift in bridges with elastic shear keys for other systems considered in this investigation.

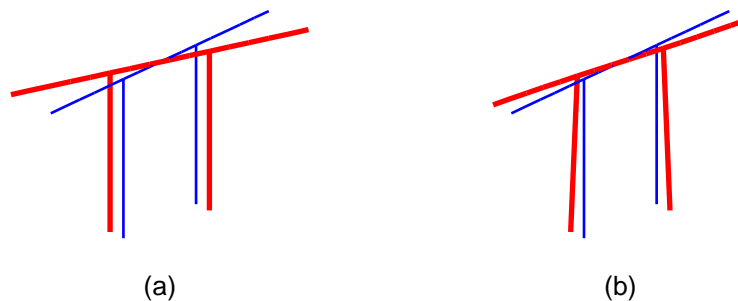


**Figure 4.11. Deflected shape of a three-span symmetric bridge: (a) bridge without shear keys; and (b) bridge with elastic shear keys.**

## 5. LINEAR ANALYSIS

### 5.1 Introduction

The objective this phase of investigation is to develop rational, simplified methods – simpler than response history analysis (RSA) – rooted in structural dynamics theory, for estimating seismic demand of bridges crossing fault-rupture zones. This Chapter presents such simplified analysis procedures for bridges, assuming they remain linearly elastic, which are extended in Chapter 6 to estimate seismic demands for bridges responding in their inelastic range. The development of the simplified procedures utilizes special features of the spatially-varying ground motions in fault-rupture zones identified in Chapter 3 (see Equation 3.1).

### 5.2 Response History Analysis

#### 5.2.1 Multiple-Support Excitation

Equations governing the motions of a linearly elastic structure subjected to multiple-support excitation are formulated by separating the displacements at the  $N$  DOFs of the super-structure in two parts (Chopra, 2007: Sec 9.7): (1)  $\mathbf{u}^s$  the quasi-static displacements due to static application of the displacements  $\mathbf{u}_g$  imposed at the supports, and (2)  $\mathbf{u}$  the dynamic displacements, governed by

$$\mathbf{m}\ddot{\mathbf{u}} + \mathbf{c}\dot{\mathbf{u}} + \mathbf{k}\mathbf{u} = -\mathbf{m} \sum_{l=1}^{N_g} \boldsymbol{\iota}_l \ddot{u}_{gl}(t) \quad (5.1)$$

where  $\mathbf{m}$ ,  $\mathbf{c}$ , and  $\mathbf{k}$  are the mass, damping, and stiffness matrices corresponding to structural DOF;  $\ddot{u}_{gl}(t)$  is the acceleration at support  $l$ ;  $\boldsymbol{\iota}_l$  is the influence vector defined as the displacements in the superstructure DOF due to unit displacement at the  $l$ th support DOF; and  $N_g$  is the number of components of support displacements. The total response is then given by

$$\mathbf{u}^t(t) = \mathbf{u}^s(t) + \mathbf{u}(t) = \sum_{l=1}^{N_g} \boldsymbol{\iota}_l u_{gl}(t) + \sum_{l=1}^{N_g} \left[ \sum_{n=1}^N \Gamma_{nl} \boldsymbol{\phi}_n D_{nl}(t) \right] \quad (5.2)$$

in which  $D_{nl}(t)$  is the deformation response of the  $n$ th-mode SDF system subjected to ground motion  $\ddot{u}_{gl}(t)$ ,  $\boldsymbol{\phi}_n$  is the  $n$ th natural mode of vibration, and  $\Gamma_{nl} = \boldsymbol{\phi}_n^T \mathbf{m} \boldsymbol{\iota}_l / \boldsymbol{\phi}_n^T \mathbf{m} \boldsymbol{\phi}_n$ .

### 5.2.2 Proportional Multiple-Support Excitation

For such excitation defined by Equation (3.1), Equation (5.1) simplifies to

$$\mathbf{m}\ddot{\mathbf{u}} + \mathbf{c}\dot{\mathbf{u}} + \mathbf{k}\mathbf{u} = -\mathbf{m}\mathbf{t}_{\text{eff}}\ddot{u}_g(t) \quad (5.3)$$

where the “effective” influence vector

$$\mathbf{t}_{\text{eff}} = \sum_{l=1}^{N_g} \alpha_l \mathbf{t}_l \quad (5.4)$$

is the vector of displacements at all structural degrees of freedom due to simultaneous static application of all support displacements with value equal to  $\alpha_l$  at the  $l$ th support, and  $\ddot{u}_g(t)$  is the acceleration at the reference support.

The right side of Equation (5.3) can be interpreted as effective earthquake forces:

$$\mathbf{p}_{\text{eff}}(t) = -\mathbf{m}\mathbf{t}_{\text{eff}}\ddot{u}_g(t) \quad (5.5)$$

The spatial distribution of these effective forces is defined by the vector  $\mathbf{s} = \mathbf{m}\mathbf{t}_{\text{eff}}$  and their time variation by  $\ddot{u}_g(t)$ . The force distribution  $\mathbf{s}$  can be expanded as a summation of modal inertia force distribution  $s_n$  (Chopra, 2007: Section 13.2):

$$\mathbf{m}\mathbf{t}_{\text{eff}} = \sum_{n=1}^N \mathbf{s}_n = \sum_{n=1}^N \Gamma_n \mathbf{m}\boldsymbol{\phi}_n \quad (5.6)$$

where  $\Gamma_n = \boldsymbol{\phi}_n^T \mathbf{m}\mathbf{t}_{\text{eff}} / \boldsymbol{\phi}_n^T \mathbf{m}\boldsymbol{\phi}_n$ . The effective earthquake forces can then be expressed as

$$\mathbf{p}_{\text{eff}}(t) = \sum_{n=1}^N \mathbf{p}_{\text{eff},n}(t) = \sum_{n=1}^N -\mathbf{s}_n \ddot{u}_g(t) \quad (5.7)$$

The contributions of the  $n$ th mode to  $\mathbf{s}$  and to  $\mathbf{p}_{\text{eff}}$  are:

$$\mathbf{s}_n = \Gamma_n \mathbf{m}\boldsymbol{\phi}_n \quad \mathbf{p}_{\text{eff},n}(t) = -\mathbf{s}_n \ddot{u}_g(t) \quad (5.8)$$

The response of a linearly-elastic multi-degree-of-freedom (MDF) system to  $\mathbf{p}_{\text{eff},n}(t)$  is entirely in the  $n$ th mode, with no contributions from other modes. Thus

$$\mathbf{u}_n(t) = \Gamma_n \boldsymbol{\phi}_n D_n(t) \quad (5.9)$$

where  $D_n(t)$  is the deformation response of the  $n$ th-mode SDF system subjected to the reference ground motion  $\ddot{u}_g(t)$ . It is governed by

$$\ddot{D}_n + 2\zeta_n \omega_n \dot{D}_n + \omega_n^2 D_n = -\ddot{u}_g(t) \quad (5.10)$$

Any response quantity  $r(t)$  – deformations, internal element forces, etc. – can be expressed as

$$r_n(t) = r_n^{\text{st}} A_n(t) \quad (5.11)$$

where  $r_n^{\text{st}}$  denotes the modal static response, the static value of  $r$  due to external forces  $\mathbf{s}_n$ , and

$$A_n(t) = \omega_n^2 D_n(t) \quad (5.12)$$

is the pseudo-acceleration response of the  $n$ th-mode SDF system (Chopra, 2007; Section 13.1). The response of the system to the total excitation  $\mathbf{p}_{\text{eff}}(t)$  is obtained by superimposing the modal responses given by Equations (5.9) and (5.11):

$$\mathbf{u}(t) = \sum_{n=1}^N \mathbf{u}_n(t) = \sum_{n=1}^N \Gamma_n \boldsymbol{\phi}_n D_n(t) \quad (5.13a)$$

$$r(t) = \sum_{n=1}^N r_n(t) = \sum_{n=1}^N r_n^{\text{st}} A_n(t) \quad (5.13b)$$

The total displacements of the structure are then given by

$$\mathbf{u}^t(t) = \mathbf{u}^s(t) + \mathbf{u}(t) = \mathbf{l}_{\text{eff}} u_g(t) + \sum_{n=1}^N \Gamma_n \boldsymbol{\phi}_n D_n(t) \quad (5.14)$$

Note that the responses to individual support motions appear in the summation over  $N_g$  in Equation (5.2) but they are represented indirectly in the effective influence vector that affects  $\Gamma_n$  and  $D_n(t)$  in Equation (5.14).

Equation (5.14) for total response of a bridge crossing fault-rupture zone to proportional multiple-support excitation resembles Equation (5.15) for a bridge located on one side of the fault subjected to spatially-uniform excitation (Chopra, 2007: Sec. 9.4):

$$\mathbf{u}^t(t) = \mathbf{u}^s(t) + \mathbf{u}(t) = \boldsymbol{\iota} u_g(t) + \sum_{n=1}^N \Gamma_n \boldsymbol{\phi}_n D_n(t) \quad (5.15)$$

where  $\boldsymbol{\iota}$  is the influence vector of displacements resulting from static application of a unit ground displacement simultaneously at all supports, and  $\Gamma_n = \boldsymbol{\phi}_n^T \mathbf{m} \boldsymbol{\iota} / \boldsymbol{\phi}_n^T \mathbf{m} \boldsymbol{\phi}_n$ . However, the influence vectors that appear explicitly in Equations (5.14) and (5.15) and implicitly in  $\Gamma_n$  and  $D_n(t)$ , are very different. In Equation (5.14),  $\boldsymbol{\iota}_{\text{eff}}$  represents the structural displacements due to static application of all support displacement with value equal to  $\alpha_l$  at the  $l$ th support, which is anti-symmetric about a strike-slip fault. In Equation (5.15),  $\boldsymbol{\iota}$  represents the structural displacements due to rigid body displacement of the base (or all support displacements) equal to 1, which is symmetric about the fault.

### 5.2.3 Evaluation of Proportional Multiple-Support Excitation Approximation

The accuracy of this approximation is evaluated by comparing bridge response computed by two methods of response history analysis: the “exact” Equation (5.2) for multiple-support excitation and Equation (5.14), which is based on approximating the excitation by Equation (3.1). Digressing briefly, RHA was not implemented by the modal approach of Equations (5.2) and (5.14), but for expedience by directly applying ground displacements to various supports in the *OpenSees* computer program.

The results presented in Figures 5.1 and 5.2 show that the proportional multiple-support excitation provides accurate results. The percentage errors in column drifts may appear large for some cases shown in Figure 5.2, but they do not seem consequential because column drifts for these cases are generally very small. The results of Figures 5.1 to 5.2 also permit another important observation: among the three faults considered, the strike-slip fault (dip angle = 90° and rake angle = 180°) causes the largest seismic demands in the transverse direction of the bridge. This indicates that a conservative estimate of the seismic demands due to the fault-parallel component of the motions in a fault-rupture zones may be obtained by assuming strike-slip orientation for the fault if dip and rake angles of the fault are not available.

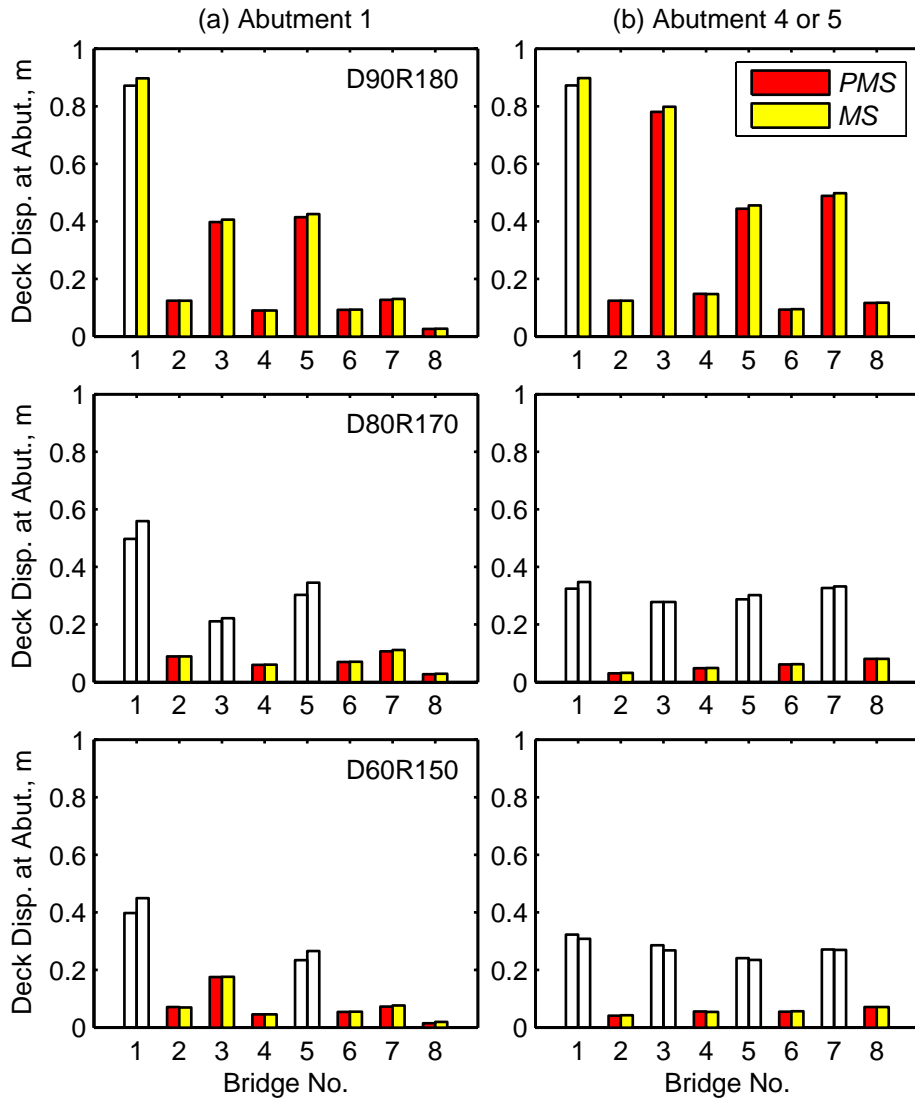


**Figure 5.1. Comparison of deck displacement at abutments from analyses using multiple-support (MS) excitation and proportional multiple-support (PMS) excitation approximation for three combination of dip angles – 90°, 70°, and 60° – and rake angles – 180°, 170°, and 150°.**

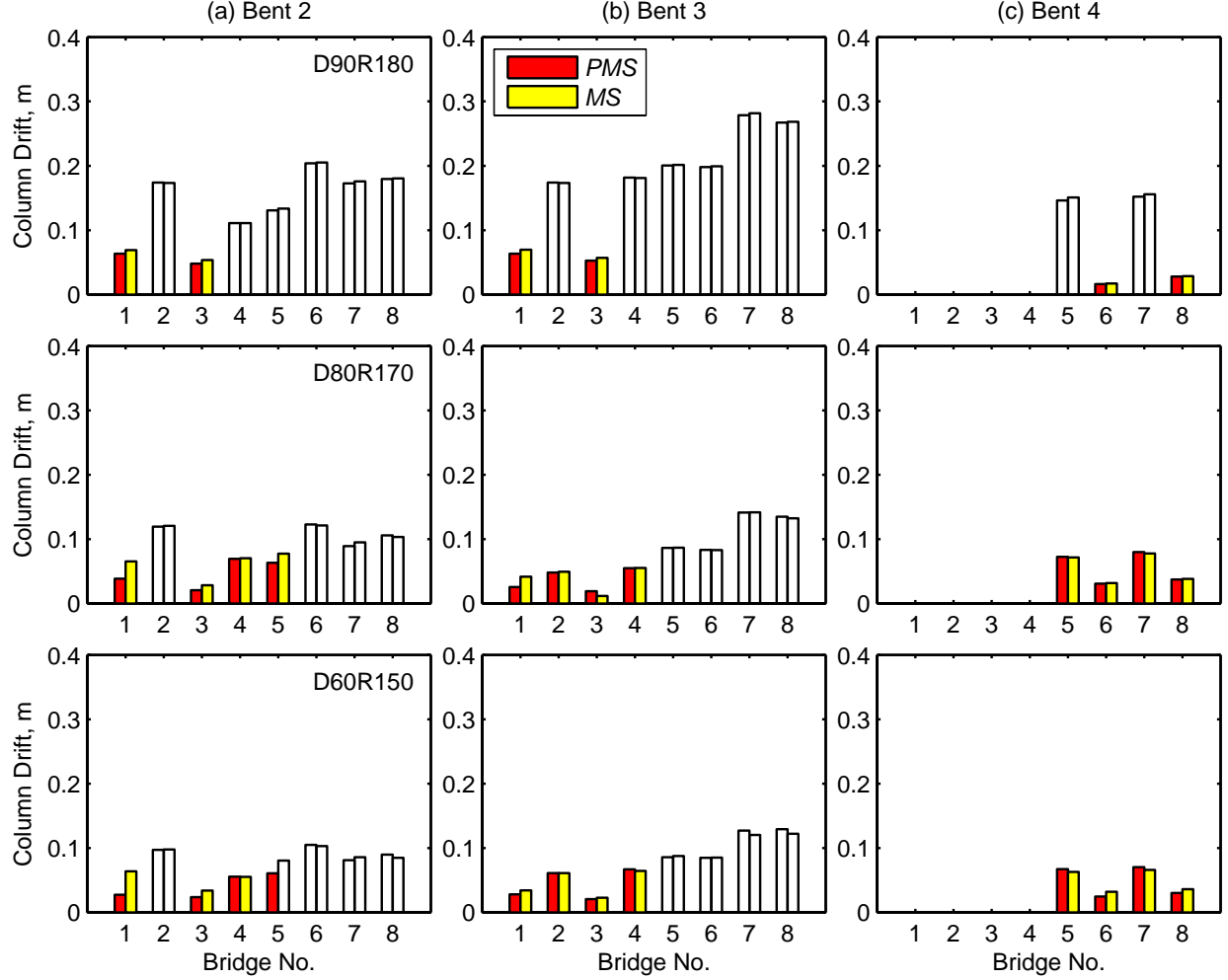


**Figure 5.2. Comparison of column drifts from analyses using multiple-support (MS) excitation and proportional multiple-support (PMS) excitation approximation for three combinations of dip angles –  $90^\circ$ ,  $70^\circ$ , and  $60^\circ$  – and rake angles –  $180^\circ$ ,  $170^\circ$ , and  $150^\circ$ .**

### 5.3 Estimation of Peak Response

Of primary interest in practical design of new bridges or evaluation of existing bridges crossing fault-rupture zones is their peak response to earthquake excitation. Procedures specially designed for bridges crossing fault-rupture zones are proposed where the peak value of the total response,  $\mathbf{u}_o^t$  and  $r_o^t$ , is estimated by adding peak values of the quasi-static response,  $\mathbf{u}_o^s$  and  $r_o^s$ , and dynamic response,  $\mathbf{u}_o$  and  $r_o$  :

$$\mathbf{u}_o^t \approx \mathbf{u}_o^s + \mathbf{u}_o \quad r_o^t \approx r_o^s + r_o \quad (5.16)$$

Such superposition of peak quasi-static and dynamic responses is reasonable because for motions

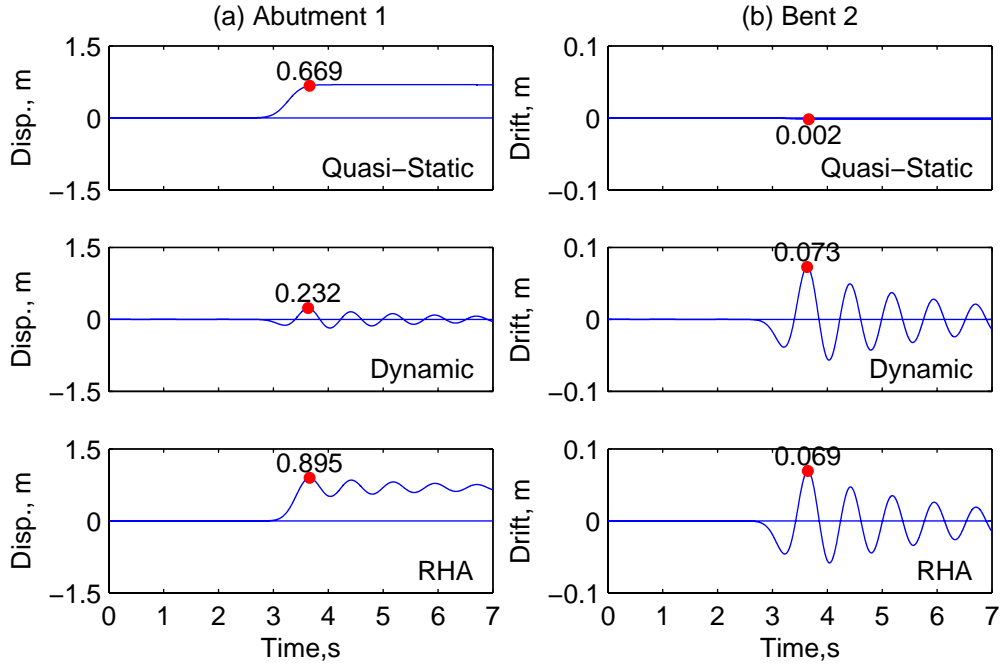


**Figure 5.3. History of quasi-static and dynamic responses along with the total response from response history analysis (RHA) of a three-span symmetric bridge: (1) Deck displacement at abutment 1, and (b) Column drift at bent 2. Results are for response in the transverse direction due to fault-parallel motions on a strike-slip fault.**

in fault-rupture zones, the peak value of the dynamic part of the response generally occurs during time phase after the quasi-static part of the response reaches, and maintains, its peak value. This is demonstrated in Figure 5.3 for a three-span symmetric bridge. Equation (5.16) may be interpreted as a special case of the multi-support response spectrum analysis procedure (Der Kiureghian and Neuenhofer, 1992) for ground motions in fault-rupture zones because the support motions and peak values of quasi-static and dynamic responses are correlated (Neuenhofer, 2007).

The peak value of the quasi-static response,  $r_o^s$ , is due to static application of the peak values of ground displacements,  $\alpha_l u_{go}$ , simultaneously at all supports where  $u_{go}$  is the peak value of the ground displacement at the reference support. Presented next are two procedures to determine the peak value of dynamic response: response spectrum analysis and static analysis.

### 5.3.1 Response Spectrum Analysis (RSA) Procedure

The peak dynamic response is estimated by using SRSS or CQC rule, as appropriate, to combine the peak modal responses. Although not rigorously valid for ground motions in close proximity to the causative fault, these modal combinations will be used and their accuracy evaluated. The peak value of the dynamic response,  $r_o$ , is computed by implementing the following steps:

1. Compute the vibration periods,  $T_n$ , and mode shapes,  $\phi_n$ , of the bridge.
2. Identify the significant modes that need to be considered in the dynamic analysis based on the modal contribution factors as follows:
  - 2.1 Compute the “effective” influence vector,  $\mathbf{t}_{\text{eff}}$ , the vector of displacements in the structural DOF obtained by static analysis of the bridge due to support displacements  $\alpha_l$ , applied simultaneously in the appropriate direction: fault parallel or fault normal.
  - 2.2 Compute the static response,  $r^{\text{st}}$ , by static analysis of the bridge due to forces  $\mathbf{m}\mathbf{t}_{\text{eff}}$  applied at the structural DOF.
  - 2.3 Compute the modal static response,  $r_n^{\text{st}}$ , from static analysis of the bridge due to forces  $\mathbf{s}_n = \Gamma_n \mathbf{m}\phi_n$  applied at the structural DOF, where  $\Gamma_n = \phi_n^T \mathbf{m}\mathbf{t}_{\text{eff}} / \phi_n^T \mathbf{m}\phi_n$ .
  - 2.4 Compute the modal contribution factor for the  $n$ th mode,  $\bar{r}_n = r_n^{\text{st}} / r^{\text{st}}$  (Chopra 2007: Section 12:10).
  - 2.5 Repeat Steps 2.3 and 2.4 for all modes.
  - 2.6 Select the number of significant modes,  $J$ , such that the error in the static value response quantity  $r$ ,  $e_J = 1 - \sum_{n=1}^J \bar{r}_n$ , is less than acceptable value, e.g., 0.05.
3. Compute the peak value of the  $n$ th mode dynamic response,  $r_{no} = r_n^{\text{st}} A_n$  in which  $r_n^{\text{st}}$  is the modal static response (Step 2.3) and  $A_n$  is the ordinate of the pseudo-acceleration spectrum for the reference support acceleration  $\ddot{u}_g(t)$  corresponding to the  $n$ th-mode SDF system.
4. Repeat Step 3 for all significant modes identified in Step 2.
5. Combine the peak modal response by SRSS or CQC modal combination rule, as appropriate, to obtain the peak dynamic response,  $r_o$ .

### 5.3.2 Linear Static Analysis Procedure

To develop a procedure that is especially convenient for practical application, the RSA procedure is simplified to recognize the particular characteristics of ground motions in close proximity to the causative fault, based on two observations:

1. In many cases, the individual modal responses tend to attain their peak values at essentially the same time. This is demonstrated in Figure 5.4, where the individual terms in the modal summation of Equation (5.14) are presented for the first three participating modes together with the total response. Thus, the algebraic sum of the peak responses (instead of CQC or SRSS combinations) should provide a reasonable estimate of the peak value of the combined response.
2. For bridges with period of the most dominant mode,  $T_r/T_n > 2.5$ ,  $A/\ddot{u}_{go} \approx 1$  (Figure 3.8) and the excitation will affect the structure like the effective force  $\mathbf{p}_{\text{eff}}(t)$  applied statically.

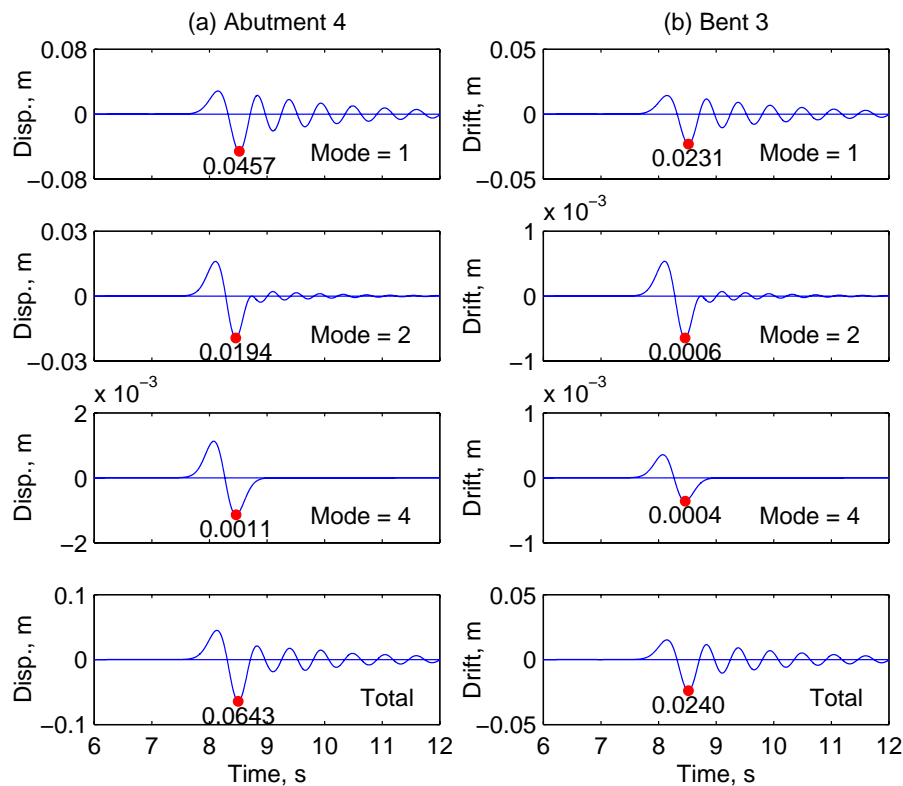


**Figure 5.4. History of modal responses for first three significant modes and total response of a three-span asymmetric bridge: (1) Deck displacement at abutment 4, and (b) Column drift at bent 3. Results are for response in the transverse direction due to fault-parallel motions on a strike-slip fault.**

Thus, the peak dynamic response can simply be computed by static analysis of the structure due to lateral forces  $(\mathbf{p}_{\text{eff}})_o = \mathbf{m}\mathbf{l}_{\text{eff}}\ddot{u}_{go}$ . For a bridge with period of the most-dominant mode in the range  $0.4 < T_n/T_r \leq 2.5$ , the value of  $A$  may be conservatively approximated to be about 2.5 times  $\ddot{u}_{go}$ , i.e.,  $A \approx 2.5\ddot{u}_{go}$  (Figure 3.8), and the peak dynamic response may be computed by static analysis of the structure due to lateral forces  $= 2.5\mathbf{m}\mathbf{l}_{\text{eff}}\ddot{u}_{go}$ . If all vibration periods (or at least period of the most-dominant mode) fall in the range  $T_n/T_r > 2.5$ ,  $A$  is either close to  $\ddot{u}_{go}$  or less than  $\ddot{u}_{go}$  (Figure 3.8), and the peak dynamic response may be conservatively estimated by static analysis of the bridge due to lateral forces  $= \mathbf{m}\mathbf{l}_{\text{eff}}\ddot{u}_{go}$ .

An especially simple procedure, which avoids computing the vibration period of the bridge and estimating the rise-time of the fault-offset, is achieved at the expense of using a conservative value of the lateral forces  $= 2.5\mathbf{m}\mathbf{l}_{\text{eff}}\ddot{u}_{go}$ ; this is the basis for the static analysis procedure presented next. The peak value of the dynamic response,  $r_o$ , is computed by implementing the following steps:

1. Compute the effective influence vector,  $\mathbf{l}_{\text{eff}}$ , as the vector of displacements in the structural DOF obtained by static analysis of the bridge due to support displacements  $\alpha_l$ , applied simultaneously.
2. Estimate the dynamic response  $r_o$  by static analysis of the bridge due to lateral forces  $= 2.5\mathbf{m}\mathbf{l}_{\text{eff}}\ddot{u}_{go}$ .

## 5.4 Significant Vibration Modes

Presented in this section are vibration periods, mode shapes, and modal contribution factor values of the selected bridges required in RSA procedure.

### 5.4.1 *Vibration Periods and Modes*

The first six vibration periods and modes of the four selected bridges, each with two shear key conditions, are presented in Figures 5.5 to 5.8. The bridge modes may be categorized by their primary motion – transverse, longitudinal, torsional, or vertical – although some modes may exhibit coupling between two motions, e.g., longitudinal and vertical (Mode 3 in Figure 5.5a),

transverse and torsional (Mode 1 in Figure 5.6a). While the fundamental mode of symmetric bridges exhibits no coupling with torsional motion (Mode 1 in Figures 5.5 and 5.7), coupling occurs between transverse and torsional motions for unsymmetric bridges (Mode 1 in Figures 5.6 and 5.8). Furthermore, both symmetric and unsymmetric bridge exhibit a predominantly torsional mode with no or little coupling with transverse motion (Mode 2 in Figures 5.5a, 5.6a, 5.7a, 5.7b, 5.8a, and 5.8b and Mode 3 in Figures 5.5b and 5.6b). Some transverse modes exhibit flexural deformation of the deck (e.g., Mode 5 in Figure 5.5a), especially for bridges with elastic shear keys (Mode 1 in Figures 5.5b, 5.6b, 5.7b, and 5.8b).

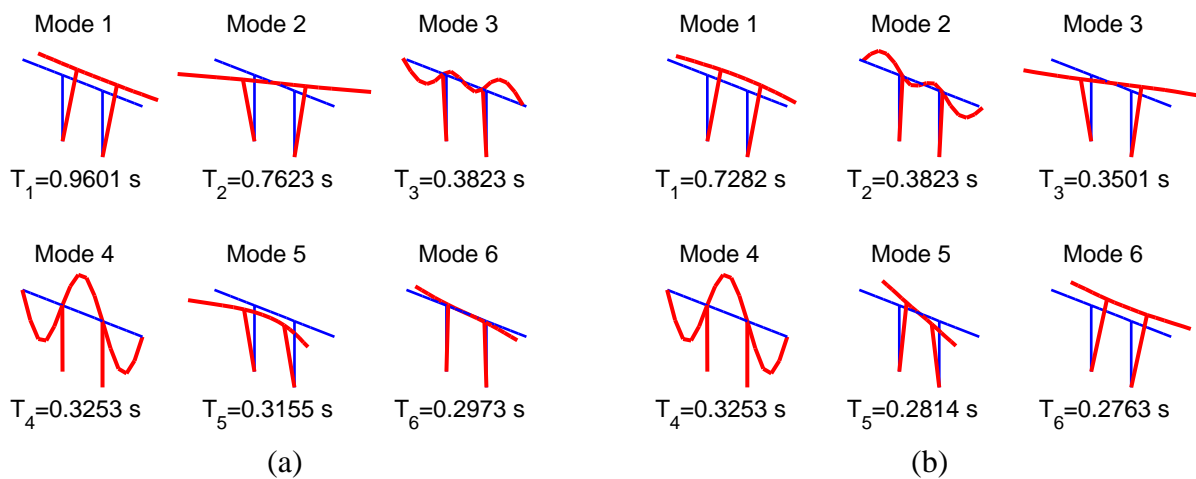


**Figure 5.5. Vibration periods and mode shapes of a three-span symmetric bridge: (a) without shear keys, and (b) with elastic shear keys.**

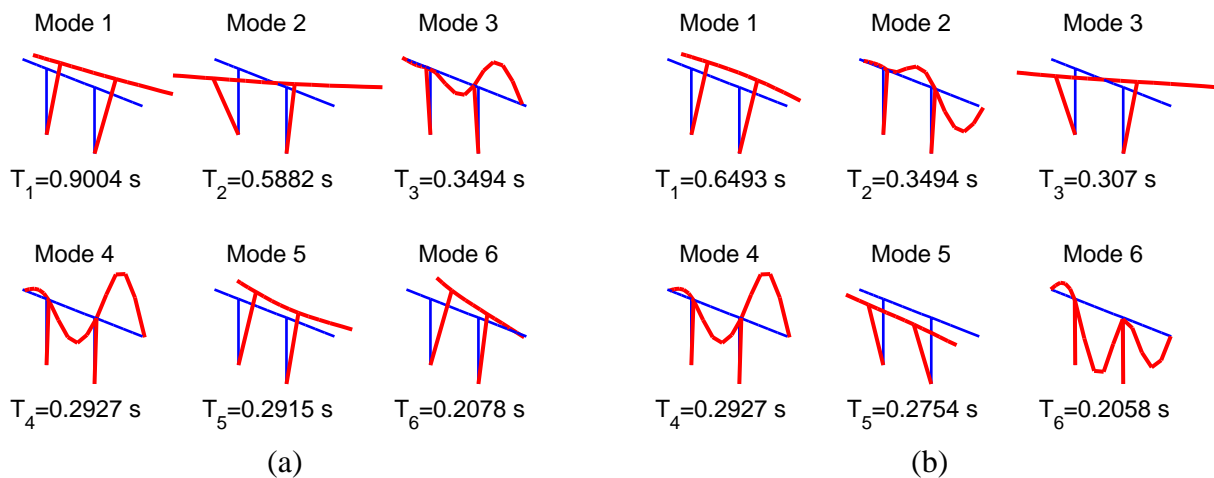


**Figure 5.6. Vibration periods and mode shapes of a three-span unsymmetric bridge: (a) without shear keys, and (b) with elastic shear keys.**

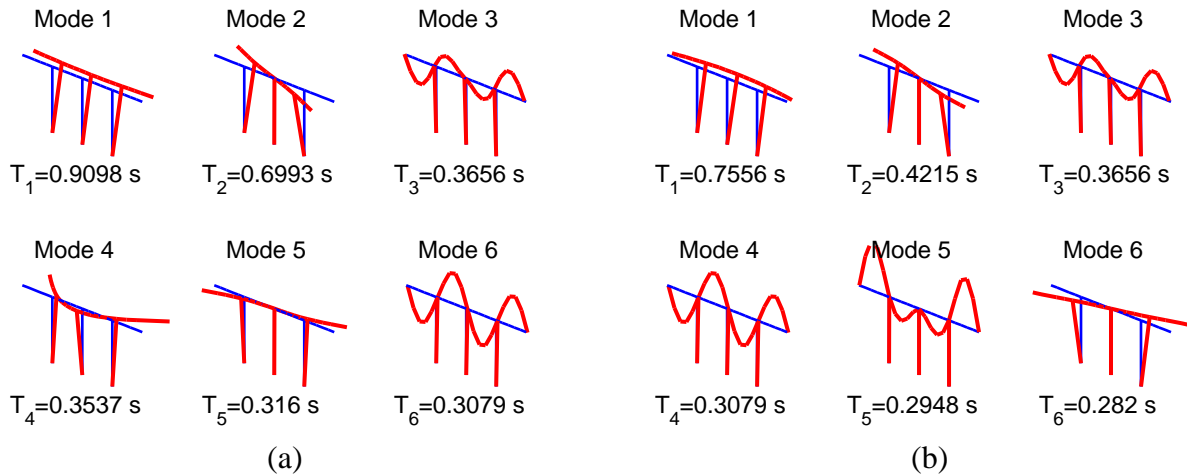


**Figure 5.7. Vibration periods and mode shapes of a four-span symmetric bridge: (a) without shear keys, and (b) with elastic shear keys.**

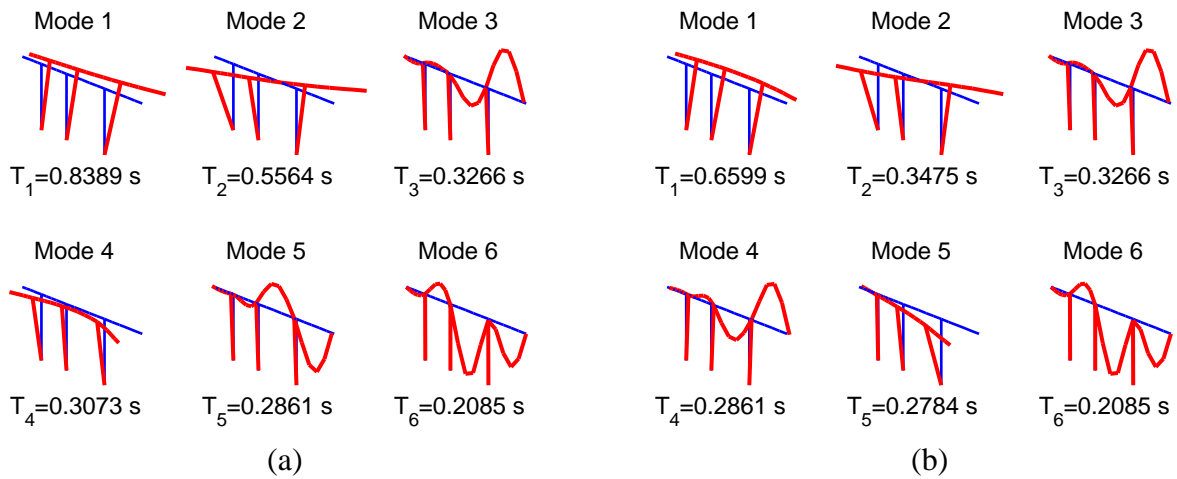


**Figure 5.8. Vibration periods and mode shapes of a four-span unsymmetric bridge: (a) without shear keys, and (b) with elastic shear keys.**

#### 5.4.2 Modal Contribution Factors and Significant Modes

Associated with the effective influence vector for fault-parallel motions, the deflected shapes of the four selected bridges, each with two shear key cases, are presented in Figures 5.9 and 5.10 for proportional multiple-support excitation for bridges crossing fault-rupture zones and spatially-uniform excitation for bridges on one side of the fault, respectively. The effective influence vectors exhibit significant torsional motion about the vertical axis for a bridge across a fault (Figure 5.9), in contrast to the translational motion of the bridge on one side of the fault (Figure 5.10).

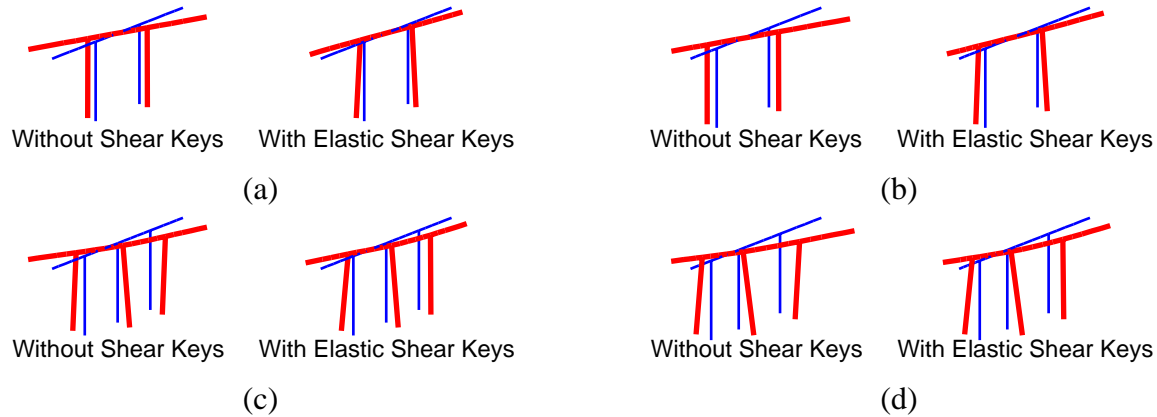


**Figure 5.9. Deflected shapes of bridges crossing fault-rupture zones associated with the “effective” influence vector for excitation in fault-parallel direction: (a) three-span symmetric; (b) three-span unsymmetric; (c) four-span symmetric; and (d) four-span unsymmetric.**

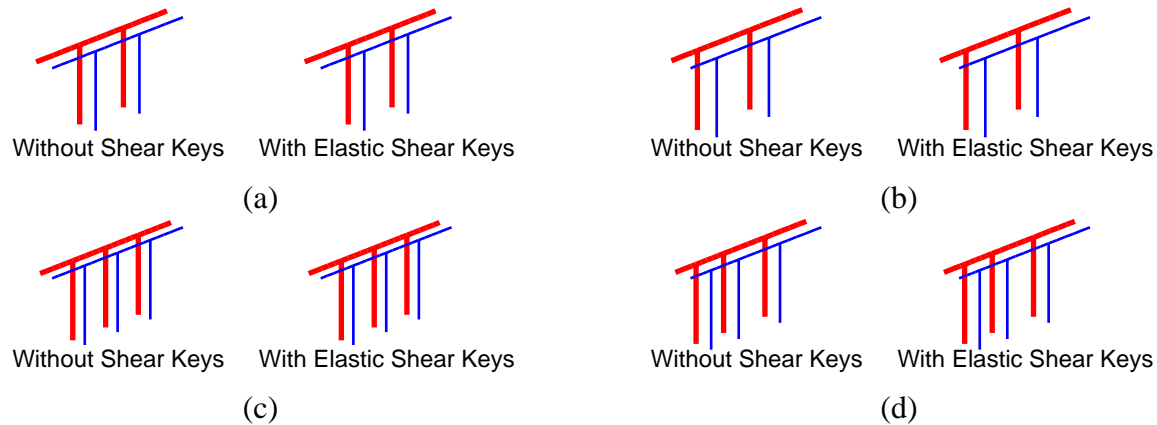


**Figure 5.10. Deflected shapes of bridges on one side of the fault associated with the “effective” influence vector for excitation in fault-parallel direction: (a) three-span symmetric; (b) three-span unsymmetric; (c) four-span symmetric; and (d) four-span unsymmetric.**

Tables 5.1 to 5.4 list the values of the modal contribution factors for two selected responses (drift in bent 2 and displacement at abutment 1) for bridges crossing fault-rupture zones as well as bridges on one side of the fault, and fault-parallel ground motion; modes with modal contribution factors  $> 0.05$  are also identified with darker shade. These results permit several important observations on the type and number of modes that need to be considered for the dynamic analysis.

First, the types of vibration modes excited in bridges crossing fault-rupture zones are entirely different from the modes excited in bridges on one side of the fault: for a three-span symmetric bridge, predominantly torsional modes are excited in the first cases, whereas only

transverse modes are excited in the second case. The modal contribution factors are non-zero only for the torsional modes of the bridge crossing a fault (second and sixth modes for the bridge without shear keys and third and fifth mode for the bridge with elastic shear keys (see Table 5.1 and Figure 5.5); and are non-zero only for transverse modes in the case of the bridge on one side of the fault (first and fifth modes for the bridge without shear keys and first and sixth modes for bridge with elastic shear keys (see Table 5.1 and Figure 5.5). For the other three bridges, the modal contribution is largest for predominantly torsional modes in the case of bridges crossing faults and for predominantly transverse modes in the case of bridges on one side of the fault (Tables 5.2 to 5.4), indicating that the contribution of such modes would be largest.

Second, many more modes may be required to accurately estimate the seismic demands in bridges with elastic shear keys compared to those without shear keys and in unsymmetric bridges compared to symmetric bridges. For example, the modal contribution factor for the three-span symmetric bridge crossing a fault is significant only for one mode in the case of a bridge without shear keys but for two modes for bridge with elastic shear keys (Table 5.1). For the three-span unsymmetric bridge crossing a fault, it is significant for three modes of the bridge without shear keys (Table 5.2) compared to only one mode if the bridge has no shear keys (Table 5.1). Similar trends are observed for the four-span bridges (Tables 5.3 and 5.4).

Third, the number and types of modes to be included in dynamic analysis may depend on the seismic demand being evaluated. For example, the first and second modes may be sufficient to estimate the deck displacement at abutment 1 of the three-span unsymmetric bridge without shear keys crossing a fault, whereas four modes – first, second, fifth, and sixth – may be necessary to estimate the drift in bent 2 (Table 5.2).

Finally, the modal contribution factors may be larger than 1.0 for some modes and negative for other modes (Table 5.2); opposing algebraic signs indicate cancellation of modal responses.

**Table 5.1. Modal combination factors for three-span symmetric bridge and a strike-slip fault. Results are presented for bridge with fault crossing between bent 2 and bent 3, and bridge on one side of fault.**

Mode	Bridge without Shear Keys					Bridge With Shear Keys				
	Period (sec)	Across Fault		One Side		Period (sec)	Across Fault		One Side	
		Bent 2 Drift	Abut 1 Disp.	Bent 2 Drift	Abut 1 Disp.		Bent 2 Drift	Abut 1 Disp.	Bent 2 Drift	Abut 1 Disp.
1	0.960	0	0		0.863	0.728	0	0		0.689
2	0.762		0.992	0	0	0.382	0	0	0	0
3	0.382	0	0	0	0	0.350		0.602	0	0
4	0.325	0	0	0	0	0.325	0	0	0	0
5	0.315	0	0		0.155	0.281		0.396	0	0
6	0.297	0.005	0.008	0	0	0.276	0	0		0.301
7	0.268	0	0	0	0	0.268	0	0	0	0
8	0.196	0	0	0	0	0.196	0	0	0	0
9	0.184	0	0	0.005	-0.010	0.170	0	0	-0.004	0.030
10	0.158	0	0	0.007	-0.008	0.152	0	0	0.007	-0.020

**Table 5.2. Modal combination factors for three-span unsymmetric bridge and a strike-slip fault. Results are presented for bridge with fault crossing between bent 2 and bent 3, and bridge on one side of fault.**

Mode	Bridge without Shear Keys					Bridge With Shear Keys				
	Period (sec)	Across Fault		One Side		Period (sec)	Across Fault		One Side	
		Bent 2 Drift	Abut 1 Disp.	Bent 2 Drift	Abut 1 Disp.		Bent 2 Drift	Abut 1 Disp.	Bent 2 Drift	Abut 1 Disp.
1	0.900				0.837	0.649	0.098	0.046		0.843
2	0.588		1.394	-0.027	-0.055	0.349	0	0	0	0
3	0.349	0	0	0	0	0.307				-0.160
4	0.293	0	0	0	0	0.293	0	0	0	0
5	0.291	-0.063	-0.026		0.146	0.275				0.149
6	0.208	0.053	0.024	0.046	0.081	0.206	0	0	0	0
7	0.206	0	0	0	0	0.199				0.159
8	0.142	0	-0.002	0	0.001	0.140	-0.002	-0.008	0	0.003
9	0.128	0.001	0.007	0	-0.009	0.119	0.006	0.028	0.001	0.007
10	0.096	0	0	0	0	0.096	0	0.002	0	-0.001

**Table 5.3. Modal combination factors for four-span symmetric bridge and a strike-slip fault. Results are presented for bridge with fault crossing between bent 2 and bent 3, and bridge on one side of fault.**

Mode	Bridge without Shear Keys					Bridge With Shear Keys				
	Period (sec)	Across Fault		SU		Period (sec)	Across Fault		One Side	
		Bent 2 Drift	Abut 1 Disp.	Bent 2 Drift	Abut 1 Disp.		Bent 2 Drift	Abut 1 Disp.	Bent 2 Drift	Abut 1 Disp.
1	0.910				0.841	0.756				0.655
2	0.699		1.102	0	0	0.422		0.796	0	0
3	0.366	0	0	0	0	0.366	0	0	0	0
4	0.354	0	0	0.038	0.202	0.308	0	0	0	0
5	0.316	0.042	0.056	0	0	0.295	0	0	0	0
6	0.308	0	0	0	0	0.282		0.661	0	0
7	0.295	0	0	0	0	0.274				0.294
8	0.259	0.018	-0.006	0.035	-0.033	0.236	0	-0.036	0.001	0.091
9	0.227	0	0	0	0	0.227	0	0	0	0
10	0.189	-0.011	-0.003	0.013	-0.01	0.187	1.497	-0.013	0.015	-0.041

**Table 5.4. Modal combination factors for four-span unsymmetric bridge and a strike-slip fault. Results are presented for bridge with fault crossing between bent 2 and bent 3, and bridge on one side of fault.**

Mode	Bridge without Shear Keys					Bridge With Shear Keys				
	Period (sec)	Across Fault		SU		Period (sec)	Across Fault		One Side	
		Bent 2 Drift	Abut 1 Disp.	Bent 2 Drift	Abut 1 Disp.		Bent 2 Drift	Abut 1 Disp.	Bent 2 Drift	Abut 1 Disp.
1	0.839				0.691	0.660				0.797
2	0.556				0.104	0.347		1.299	0.020	0.033
3	0.327	0	0	0	0	0.327	0	0	0	0
4	0.307				0.124	0.286	0	0	0	0
5	0.286	0	0	0	0	0.278		0.102	0.017	-0.036
6	0.209	0	0	0	0	0.209	0	0	0	0
7	0.204				0.118	0.191				0.138
8	0.194	0.019	0.005	0.019	-0.022	0.179	0.074	-0.024	0.022	0.069
9	0.161	0.031	0.034	-0.003	-0.015	0.155		0.229	0	-0.002
10	0.115	0	0	0	0	0.115	0.002	0.001	0	0

### 5.5 Accuracy of Proposed Procedures

The procedures presented to estimate the peak response are based on two approximations: (1) superposing the peak values of quasi-static and dynamic responses (Equation 5.16); and (2) estimating the peak dynamic response by the RSA or the linear static analysis procedure. In this section, the combined errors due to both approximations are investigated by comparing the peak values of the responses determined by approximate procedures and by RHA (Equation 5.14), the

“exact” procedure. For this purpose, presented are the transverse responses of bridges due to fault-parallel motions resulting from a rupture on a vertical strike-slip fault (Figures 5.11 and 5.12), and the longitudinal responses due to fault-normal motions resulting from a rupture on a fault with dip of  $40^\circ$  and rake of  $110^\circ$  (Figures 5.13 and 5.14). Note that for the selected bridges and orientation of the fault, fault-parallel ground motions cause response only in the transverse direction of the bridge and fault-normal motions lead to response only in the longitudinal direction of the bridge. Also included are results from the RSA procedure considering contribution of only the dominant mode, the mode with the largest modal contribution factor; these results are denoted as RSA:1-Mode.

The presented results show that both versions of RSA lead to estimates of seismic demands that are very close to those from the “exact” RHA procedure, indicating that the most-dominant mode contributes essentially all of the dynamic response of the selected systems.

The presented results also show that the linear static analysis procedure that avoids dynamic analysis also provides a reasonably good estimate of the seismic demand, which is slightly conservative in most cases. Such an overestimation is expected because the simplified procedure is based on an upper bound estimate of the pseudo-acceleration  $= 2.5\ddot{u}_{go}$ . However, it underestimates the seismic demand slightly in a few cases, e.g., bent 2 drift for bridges 3 and 7 (Figure 5.13a) because these bridges have two nearly most-dominant modes and contribution of these two modes to some seismic demands tend to cancel out.

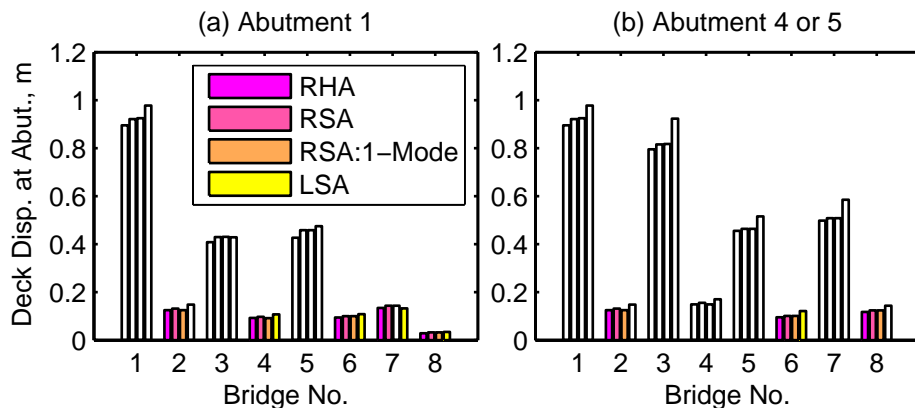


**Figure 5.11. Comparison of transverse deck displacement at abutments determined by three proposed procedures – RSA, RSA:1-Mode, and linear static analysis (LSA) – with those from the “exact” RHA procedure. Results are for fault-parallel ground motions associated with a vertical strike-slip fault.**

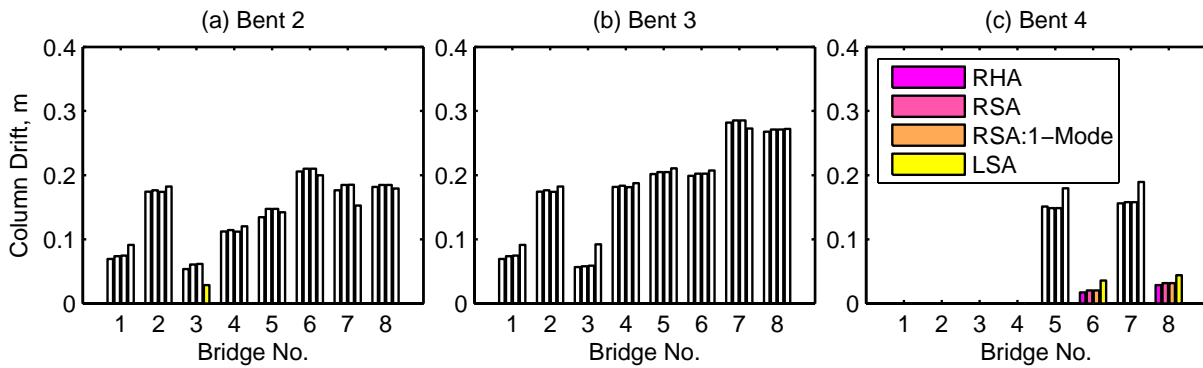


**Figure 5.12. Comparison of transverse column drifts determined by the three proposed procedures – RSA, RSA:1-Mode, and linear static analysis (LSA) – with those from the “exact” RHA procedure. Results are for fault-parallel ground motions associated with a vertical strike-slip fault.**

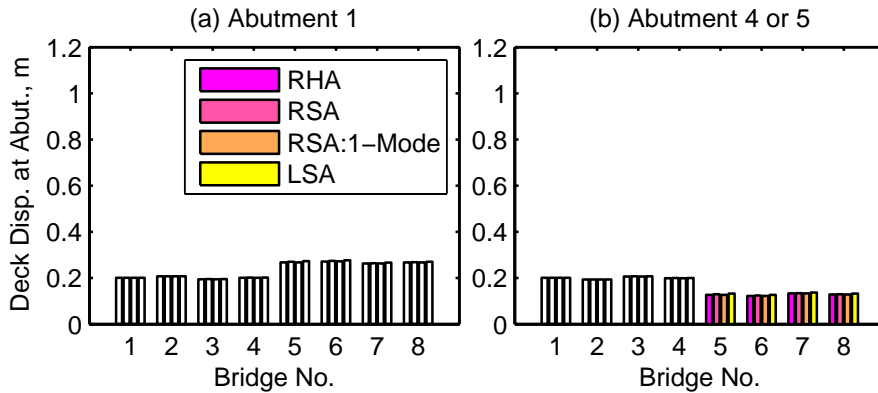


**Figure 5.13. Comparison of longitudinal deck displacement at abutments determined by the three proposed procedures – RSA, RSA:1-Mode, and linear static analysis (LSA) – with those from the “exact” RHA procedure. Results are for fault-normal ground motions associated with a fault with dip of 40° and rake of 110°.**

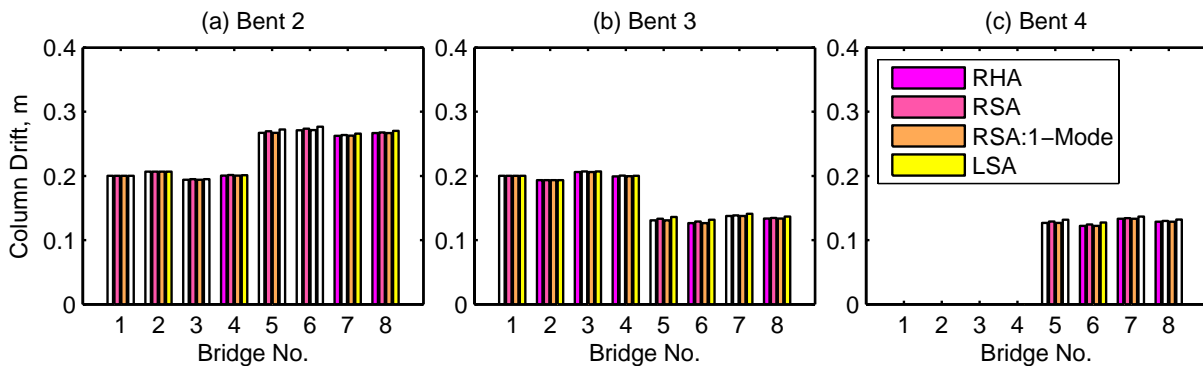


**Figure 5.14. Comparison of longitudinal column drifts determined by the three proposed procedures – RSA, RSA:1-Mode, and linear static analysis (LSA) – with those from the “exact” RHA procedure. Results are for fault-normal ground motions associated with a fault with dip of 40° and rake of 110°.**

## 6. NONLINEAR ANALYSIS

### 6.1 Introduction

Chapter 5 presented development of a response spectrum analysis (RSA) procedure and a linear static analysis procedure for estimating dynamic part of seismic demands in linearly-elastic bridges crossing fault-rupture zones and demonstrated that both these procedures, when combined with the quasi-static demands due to ground offset across the fault, provide estimates of peak responses that are close to the “exact” results from RHA. However, bridges crossing fault-rupture zones are expected to be deformed beyond their linear elastic range. Therefore, the objective of the investigation reported in this Chapter is to extend the aforementioned procedures to estimate seismic demands for “ordinary” bridges deforming into their inelastic range.

Presented first is the theoretical background followed by development of three approximate procedures for analysis of nonlinear bridges crossing fault-rupture zones. Subsequently, accuracy of these procedures is evaluated.

### 6.2 Superposing Quasi-static and Dynamic Parts of Response

Inelastic response analysis of bridges subjected to multiple-support excitation requires a step-by-step solution of equations governing the total displacements  $\mathbf{u}^t$  of the bridge for ground motions directly imposed on the support degrees of freedom of the system. This procedure, denoted as “exact” nonlinear RHA, is too onerous for estimating seismic demands for “ordinary” bridges. With the objective of developing practical procedures, we explore whether an approximate solution based on superposition of the peak values of the quasi-static and dynamic part of the response [Equation (5.16)] provides acceptable estimates for the inelastic seismic demands for bridges. The peak values of quasi-static and dynamic responses,  $\mathbf{u}_o^s$  and  $\mathbf{u}_o$ , are computed by two independent nonlinear analyses of the bridge: (1)  $\mathbf{u}_o^s$  is determined by nonlinear static analysis of the bridge subjected to peak values of ground displacements,  $\alpha_l u_{g_o}$ , simultaneously applied at all supports; and (2)  $\mathbf{u}_o$  is determined by nonlinear dynamic analysis, i.e., solving the equations of motion:

$$\mathbf{m}\ddot{\mathbf{u}} + \mathbf{c}\dot{\mathbf{u}} + \mathbf{f}_s(\mathbf{u}, \dot{\mathbf{u}}) = -\mathbf{m}\mathbf{l}_{\text{eff}}\ddot{u}_g(t) \quad (6.1)$$

The peak values of seismic demands obtained by this approximate superposition procedure are compared against those from “exact” nonlinear RHA in Figures 6.1 and 6.2 for eight selected bridges. The presented results indicate that this approximate procedure generally leads to a conservative – but not excessively conservative – estimate of deck displacements at abutments (Figure 6.1) and column drifts (Figure 6.2). Exceptions occur for column drift in bent 2 of bridges 5 and 7 where the superposition leads to slightly smaller estimate (Figure 6.2a).

The preceding results indicate that, although superposition of peak quasi-static and dynamic responses determined by two independent nonlinear analyses is not “strictly” valid, this approach provides estimates of seismic demands that are accurate to a useful degree. This is the approach adopted to develop a practical procedure for estimating inelastic seismic demands for bridges.

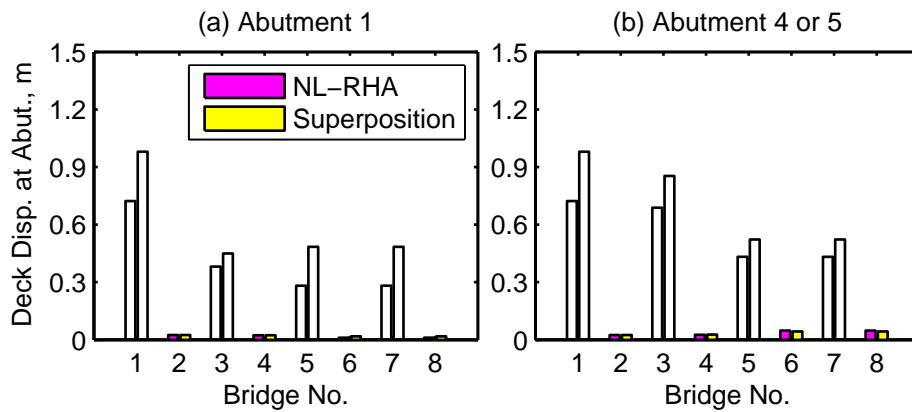


**Figure 6.1. Comparison of transverse deck displacements at abutments determined by two analyses: “exact” nonlinear RHA (NL-RHA) and superposition of peak values of nonlinear quasi-static and nonlinear dynamic response. Results are for fault-parallel ground motions associated with a strike-slip fault.**

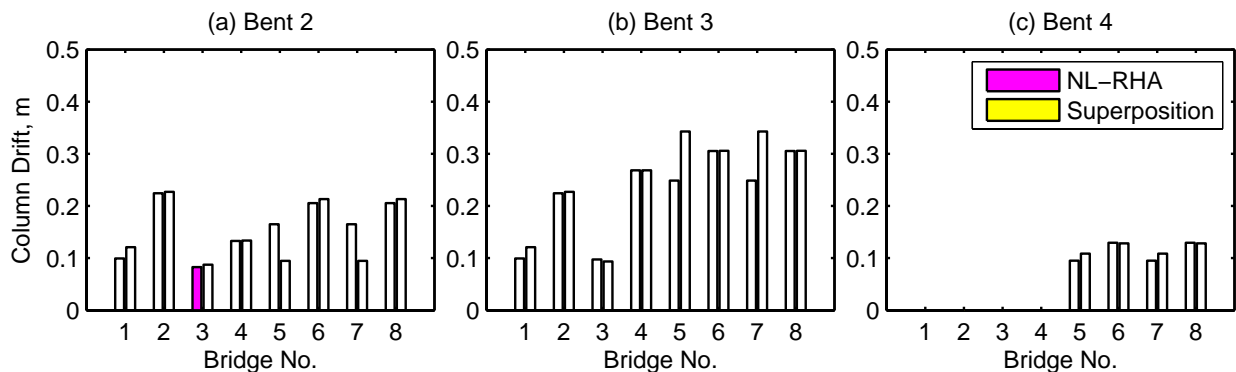


**Figure 6.2. Comparison of transverse column drifts determined by two analyses: “exact” nonlinear RHA (NL-RHA) and superposition of peak values of nonlinear quasi-static and nonlinear dynamic response. Results are for fault-parallel ground motions associated with a strike-slip fault.**

### 6.2.1 Is Quasi-Static Solution Adequate?

Because the displacement offset associated with fault rupture dominates the earthquake excitation, can the structural response be approximated by the quasi-static solution alone? To address this question, the peak values of the total response are presented in Figures 6.3 and 6.4, together with the peak values of the quasi-static and dynamic parts of the response. These results indicate that the peak values of the total deck displacement at bridge abutments may be estimated from nonlinear quasi-static analysis alone (Figure 6.3); however, the quasi-static response alone is inadequate in estimating column drifts in bridges without shear keys (see bridges 1, 3, 5, and 7 in Figure 6.4a; bridges 1 and 3 in Figure 6.4b; and bridges 5 and 7 in Figure 6.4c).

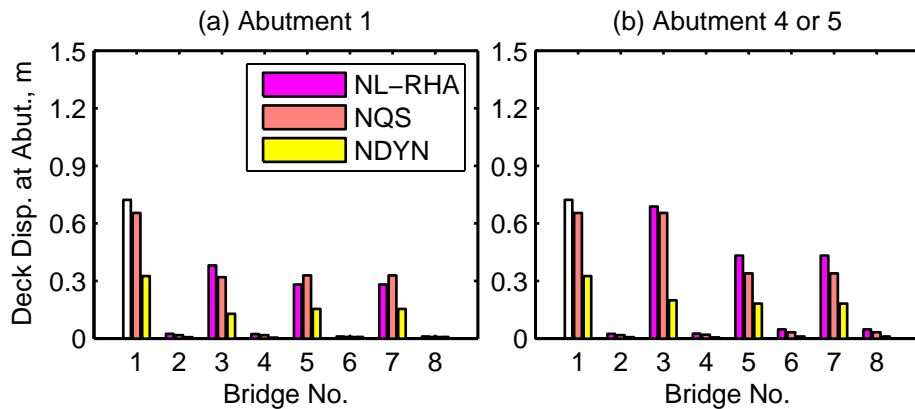


**Figure 6.3. Comparison of transverse deck displacements at abutments determined by three analyses: nonlinear RHA (NL-RHA), nonlinear quasi-static (NQS), and nonlinear dynamic (NDYN). Results are for fault-parallel ground motions associated with a strike-slip fault.**

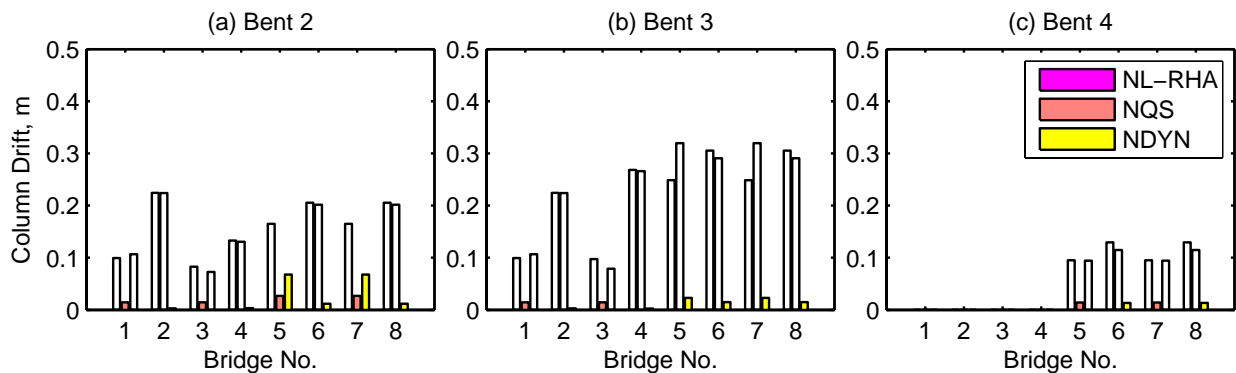


**Figure 6.4. Comparison of transverse column drifts determined by three analyses: nonlinear RHA (NL-RHA), nonlinear quasi-static (NQS), and nonlinear dynamic (NDYN). Results are for fault-parallel ground motions associated with a strike-slip fault.**

### 6.3 Estimation of Peak Response

Approximate procedures proposed herein are based on superposing quasi-static and the dynamic parts of the response, an approach demonstrated to be appropriate in a preceding section. Thus, the peak value of the total response is estimated by

$$r^t = r_{o+g}^s + r_o \quad (6.2)$$

where  $r_{o+g}^s$  is the peak value of the quasi-static part of the response (including the effects of gravity loads) and  $r_o$  is the peak value of the dynamic part of the response.

In all three approximate procedures, the peak value of the quasi-static part of the response including the effects of gravity loads,  $r_{o+g}^s$ , is computed by nonlinear static analysis of the bridge due to ground displacements,  $\alpha_l u_{go}$ , applied simultaneously at all supports, where  $u_{go}$  is the peak value of the ground displacement at the reference support. Gravity loads are applied prior to the static analysis and the part of the response,  $r_g$ , due to gravity loads is noted.

Presented next are three procedures to estimate the peak value of the dynamic part of the response: modal pushover analysis, linear dynamic analysis, and linear static analysis\.

#### 6.3.1 Modal Pushover Analysis (MPA )

The MPA procedure developed earlier for estimating seismic demands for buildings (e.g., Chopra, 2007: Section 19.7.3) is adapted for bridges crossing fault-rupture zones. The MPA procedure is specialized only for the most-dominant mode because, as demonstrated in Chapter 5, only this mode is generally sufficient to accurately estimate the response of many bridges. The procedure is summarized next in step-by-step form:

1. Compute the vibration periods,  $T_n$ , and mode shapes,  $\phi_n$ , of the bridge.
2. Identify the most-dominant mode that needs to be considered in the dynamic analysis based on the modal contribution factors of the *linearly-elastic bridge* as follows:
  - 2.1 Compute the “effective” influence vector,  $\iota_{\text{eff}}$ , as the vector of displacements in the structural DOF obtained by linear static analysis of the bridge due to support displacements  $\alpha_l$  applied simultaneously as demonstrated in Chapter 5; this

“effective” influence vector has no resemblance to the one for spatially-uniform excitation.

- 2.2 Compute the response,  $r^{\text{st}}$ , by static analysis of the bridge due to forces equal to  $\mathbf{m}\boldsymbol{\iota}_{\text{eff}}$  applied at the structural DOF.
  - 2.3 Compute the modal static response,  $r_n^{\text{st}}$ , by static analysis of the bridge due to forces  $\mathbf{s}_n = \Gamma_n \mathbf{m}\boldsymbol{\phi}_n$  applied at the structural DOF, where  $\Gamma_n = \boldsymbol{\phi}_n^{\text{T}} \mathbf{m}\boldsymbol{\iota}_{\text{eff}} / \boldsymbol{\phi}_n^{\text{T}} \mathbf{m}\boldsymbol{\phi}_n$ .
  - 2.4 Compute the modal contribution factor for the  $n$ th mode,  $\bar{r}_n = r_n^{\text{st}} / r^{\text{st}}$  (Chopra 2007: Section 12.10).
  - 2.5 Repeat steps 2.3 and 2.4 for all modes.
  - 2.6 Select the most-dominant mode as the mode with the largest modal contribution factor.
3. Compute the peak value of dynamic response,  $r_{no}$ , in the most-dominant mode of the bridge by nonlinear static (or pushover) analysis as follows:
    - 3.1 Develop the pushover curve,  $\beta_n - u_{rn}$ , for the modal force distribution,  $\mathbf{f}_n^* = \beta_n \mathbf{m}\boldsymbol{\phi}_n$ , in which  $\beta_n$  is the force-scale factor, and  $u_{rn}$  is the displacement of the bridge at a reference point. Gravity loads are applied before pushover analysis and P- $\Delta$  effects are included. Note the value of the reference point displacement due to gravity loads,  $u_{rg}$ .
    - 3.2 Convert the  $\beta_n - u_{rn}$  pushover curve to the force-displacement,  $F_{sn}/L_n - D_n$ , relation for the inelastic SDF system by utilizing  $F_{sn}/L_n = \beta_n/\Gamma_n$  and  $D_n = u_{rn}/\Gamma_n \phi_{rn}$  in which  $\phi_{rn}$  is the value of  $\boldsymbol{\phi}_n$  at the reference point; these relations are developed in Appendix C.
    - 3.3 Idealize the pushover curve, as necessary, and define appropriate hysteretic rules for cyclic deformations.
    - 3.4 Compute the peak deformation  $D_n$  of the inelastic SDF system defined by the force-deformation relation developed in Step 3.3 and damping ratio  $\zeta_n$ , subjected to the ground acceleration  $\ddot{u}_g(t)$  at the reference support.
    - 3.5 Calculate the peak value of the reference-point displacement  $u_{rn}$  from  $u_{rn} = \Gamma_n \phi_{rn} D_n$ .

3.6 At the reference point displacement equal to  $u_{rg} + u_{rn}$ , note the value  $r_{n+g}$  of desired response from the pushover data.

4. The peak dynamic response is,  $r_o = r_{n+g} - r_g$ , where  $r_g$  is the contribution of gravity loads alone, computed earlier.

Note that the most-dominant mode to be considered in the dynamic analysis may depend on the response quantity under consideration, e.g., most-dominant mode for computation of the dynamic part of the drift at one bent may differ from that for another bent (see Appendix D). Therefore, the MPA procedure must be implemented for each mode that is identified to be the most-dominant mode for a seismic response of interest, implying the need for several such analyses. For bridges considered in this investigation, however, it was found that generally the same mode was the most-dominant mode for all seismic responses (see modal contribution factors in Tables 5.1 to 5.4), requiring a single implementation of the MPA procedure. Only in very few cases (such as the example bridge in Appendix D) did the most-dominant mode differ for different seismic responses. Even for such cases, implementation of the MPA procedure was needed for no more than two different modes.

### ***Pushover Curve and Reference-Point Displacement***

Figure 6.5 presents the pushover curves for the most-dominant mode – the one for drift bent 2 – of the eight selected bridges, together with the peak value of the transverse displacement at abutment 1, chosen as the reference displacement. Bridges with elastic shear keys, e.g., bridges 2, 4, 6, and 8, remain within the linear-elastic range during the dynamic part of the response (Figure 6.5) because the peak displacement is very small (Figures 6.3 and 6.4). Bridges without shear keys, e.g., bridges 1, 3, 5, and 7, on the other hand, are deformed beyond the elastic limit, but only slightly (Figure 6.5).

These results suggest that linear analysis may be adequate to estimate the dynamic part of the response of these bridges. To evaluate this approximation, the peak reference displacements determined by nonlinear and linear analyses are compared in Figure 6.6 for bridges without shear keys. This comparison shows that linear analysis underestimates slightly the reference displacement for bridges 1, 3, and 5 but provides an excellent estimate for bridge 7; however, the slight underestimation of the peak displacement appears to be well within the errors acceptable

for most practical applications. For practical implementation of linear analysis of the dynamic part of the response, two simple procedures are presented next.

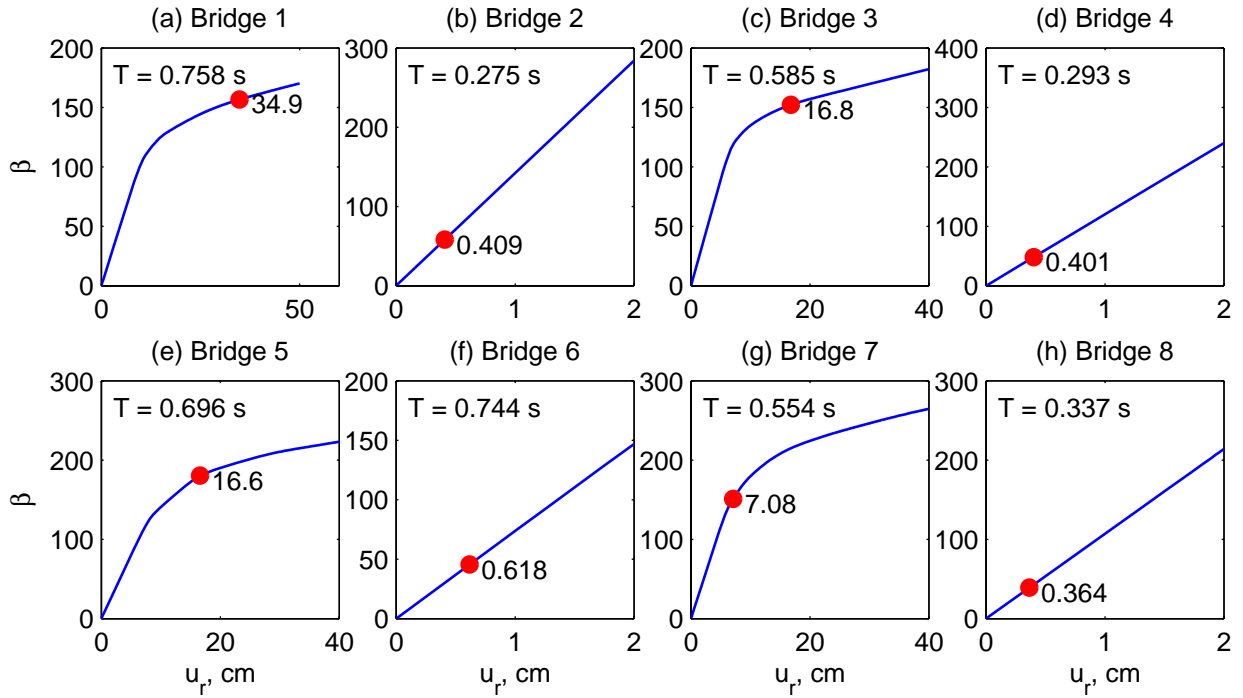


**Figure 6.5. Pushover curve and peak reference displacement for the most-dominant mode of the selected bridges.**

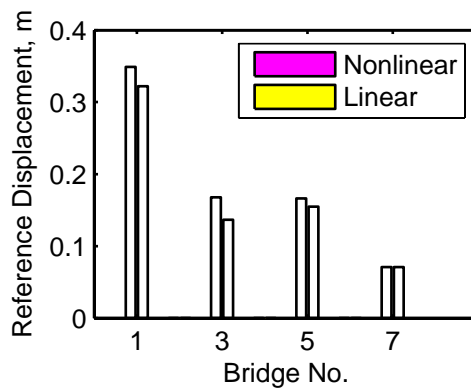


**Figure 6.6. Comparison of the reference displacement for the most-dominant mode from nonlinear and linear analyses.**

### 6.3.2 Linear Dynamic Analysis

The peak modal response of a structure due to one mode – the most dominant mode – can be determined by analysis of the bridge due to equivalent static forces (see Chopra, 2007: Section 13.1)

$$\mathbf{f}_n = \mathbf{s}_n A_n = \Gamma_n \mathbf{m} \phi_n A_n \quad (6.3)$$

in which  $\Gamma_n$  was defined in Step 2.3 of the MPA procedure, and  $A_n$  is determined from the pseudo-acceleration spectrum for the reference support acceleration  $\ddot{u}_g(t)$ . As demonstrated previously, this spectrum differs significantly from the CALTRANS SDC spectrum (see Figure 3.9). The linear dynamic analysis procedure is equivalent to the RSA procedure in Chapter 5 but specialized to consider only one mode – the most dominant mode.

The peak value,  $r_o$ , of the dynamic part of the response can be computed as follows:

1. Compute the vibration periods,  $T_n$ , and mode shapes,  $\phi_n$ , of the bridge.
2. Compute the “effective” influence vector,  $\mathbf{t}_{\text{eff}}$ , as the vector of displacements in the structural DOF obtained by linear static analysis of the bridge due to support displacements  $\alpha_l$  applied simultaneously in the appropriate direction: fault parallel or normal fault.
3. Identify the most-dominant mode by implementing Step 2.2 of the MPA procedure presented earlier and compute  $\Gamma_n = \phi_n^T \mathbf{m} \mathbf{t}_{\text{eff}} / \phi_n^T \mathbf{m} \phi_n$ .
4. Estimate  $r_o$  by linear analysis of the bridge due to equivalent static forces  $\mathbf{s}_n = \Gamma_n \mathbf{m} \phi_n A_n$ .

### 6.3.3 Linear Static Analysis

As demonstrated in Chapter 5, the peak value of the dynamic part of the response of linearly elastic bridges can be estimated to a sufficient accuracy simply by static analysis of the structure due to lateral forces  $= 2.5 \mathbf{m} \mathbf{t}_{\text{eff}} \ddot{u}_{go}$ ; computation of vibration periods and modes is no longer necessary. The same procedure is adopted for inelastic bridges because, as demonstrated earlier, the dynamic part of their response may be estimated by linear analysis. Thus, the peak value  $r_o$  of the dynamic part of the response can be computed as follows:

1. Compute the effective influence vector,  $\mathbf{t}_{\text{eff}}$ , as the vector of displacements in the structural

DOF obtained by linear static analysis of the bridge due to support displacements  $\alpha_l$  applied simultaneously.

2. Estimate  $r_o$  by linear static analysis of the bridge due to lateral forces  $= 2.5 \mathbf{m} \mathbf{l}_{\text{eff}} \ddot{u}_{go}$ .

#### 6.4 Accuracy of Approximate Procedures

The total (quasi-static plus dynamic) seismic demands for bridges oriented orthogonal to strike-slip faults due to fault-parallel ground motions estimated by the three approximate procedures are compared against results of “exact” nonlinear RHA. Recall that the three procedures are identical in their computation of the quasi-static response but differ in estimation of the dynamic response. The results presented in Figures 6.7 and 6.8 lead to the following observations:

First, the MPA procedure leads to estimates of deck displacements at abutments and column drifts that are generally slightly conservative but with some exceptions: column drift in bent 2 of bridges 5 and 7 is underestimated (Figure 6.8a). Second, the simpler linear dynamic analysis procedure is generally no less accurate than the computationally more demanding MPA procedure. Third, the linear static procedure, which is the simplest of the three approximate procedures, provides conservative, but not excessively conservative, estimates of deck displacements at abutments (Figure 6.7) and good estimates of column drifts (Figure 6.8). Although it underestimates the drift in bent 2 of bridges 3, 5, and 7 (Figure 6.8a), this underestimation is not much worse than in the MPA procedure. Therefore, linear static analysis is preferable over linear dynamic analysis or MPA for practical applications to “ordinary” bridges.

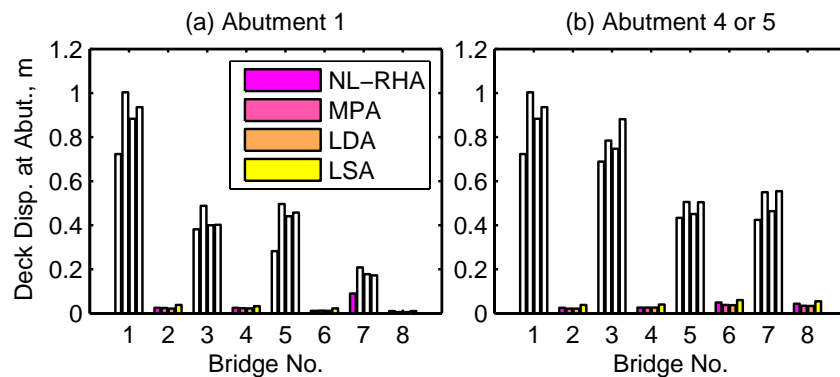


**Figure 6.7. Transverse deck displacement at abutment determined by three approximate procedures – MPA, linear dynamic analysis (LDA), and linear static analysis (LSA) – and “exact” nonlinear RHA (NL-RHA). Results are for fault-parallel ground motions associated with a vertical strike-slip fault.**

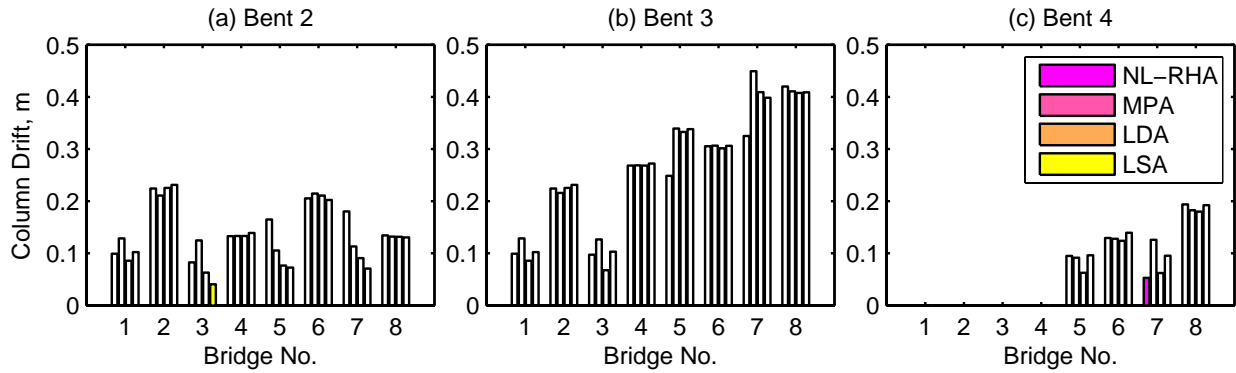


**Figure 6.8. Transverse column drifts at abutment determined by three approximate procedures – MPA, linear dynamic analysis (LDA), and linear static analysis (LSA) – and “exact” nonlinear RHA (NL-RHA). Results are for fault-parallel ground motions associated with a vertical strike-slip fault.**

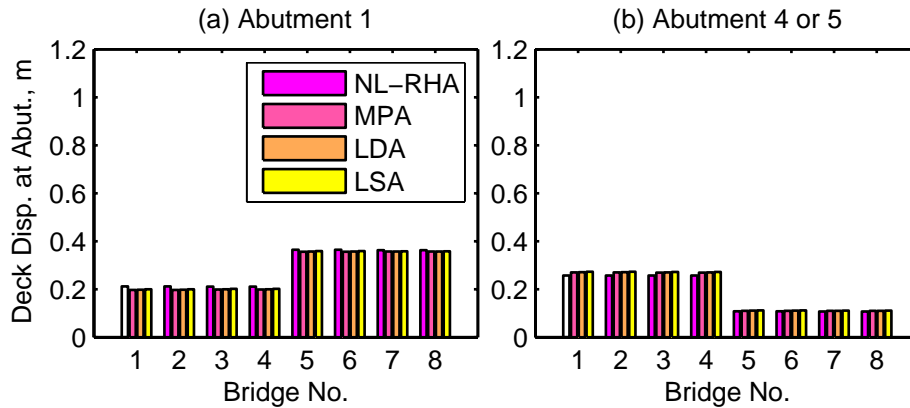


**Figure 6.9. Longitudinal deck displacement at abutment determined by three approximate procedures – MPA, linear dynamic analysis (LDA), and linear static analysis (LSA) – and “exact” nonlinear RHA (NL-RHA). Results are for fault-normal ground motions associated with a fault with dip of  $40^\circ$  and rake of  $110^\circ$ .**

The results presented in Figures 6.9 and 6.10 for fault-normal motions on a fault with dip of  $40^\circ$  and rake of  $110^\circ$  indicate that all three procedures – MPA, linear dynamic analysis, and linear static analysis – provide estimates that are essentially identical, and are very close to those from the “exact” nonlinear RHA. Thus, as before, the simpler linear static analysis is preferable over linear dynamic analysis or MPA for practical applications. In passing, observe that the longitudinal response of a bridge oriented orthogonal to the fault is not affected by shear keys (compare bridges 1 and 2, 3 and 4, 5 and 6, and 7 and 8 in Figures 6.9 and 6.10), because they provide restraint only in the transverse direction.

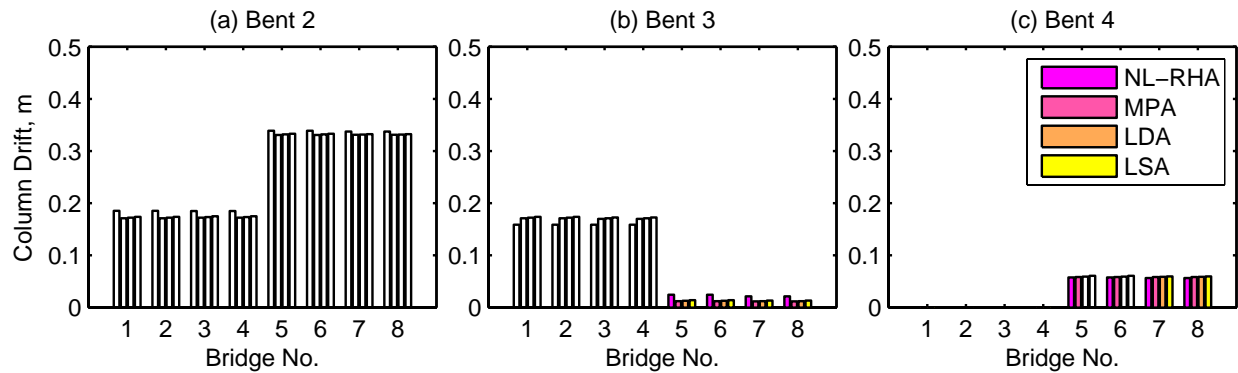


**Figure 6.10. Longitudinal column drifts at abutment determined by three approximate procedures – MPA, linear dynamic analysis (LDA), and linear static analysis (LSA) – and “exact” nonlinear RHA (NL-RHA). Results are for fault-normal ground motions associated with a fault with dip of 40° and rake of 110°.**

### 6.5 Application to Bridges with Nonlinear Shear Keys

Chapter 4 demonstrated that the earthquake response of bridges crossing fault-rupture zones is very sensitive to the strength of the shear keys. Computations of this response were shown to be unreliable for lack of experimental data and realistic nonlinear force-deformation models for shear keys. For this reason, it was proposed to estimate bridge response as the larger of responses computed by nonlinear analysis of the bridge for two shear key cases: no shear keys and elastic shear keys. Therefore, this upper bound of response is selected as the benchmark to evaluate approximate procedures presented in this investigation.

Figures 6.11 to 6.14 present the upper bound response of the four bridges considered in this investigation: three-span symmetric (3S), three-span unsymmetric (3U), four-span symmetric (4S), and four-span unsymmetric (4U) determined by the three approximate procedures – MPA, linear dynamic analysis, and linear static analysis – and nonlinear RHA. Included are results for transverse response due to fault-parallel ground motions on a strike-slip fault (Figures 6.11 and 6.12) and for longitudinal response due to fault-normal motions on a fault with a dip of 40° and rake of 110° (Figures 6.13 and 6.14).

The MPA procedure provides a conservative estimate of deck displacements at abutments. They are within about 10% of the result from nonlinear RHA for a few cases (bridges 3U and 4S in Figure 6.11a). For most of the remaining cases, the results from the MPA procedure are within about 30% of the estimate from nonlinear RHA (see bridge 3S and 3U in Figure 6.11a; bridges 3S and 4U in Figure 6.11b). The apparently much larger percentage discrepancy (bridge 4U in

Figure 6.11a) is inconsequential as the response under consideration is very small. The MPA procedure provides estimates of column drifts that are generally very close to the exact results (Figure 6.12), within about 5% for most cases (bridges 3S, 3U, and 4S in Figure 6.12a; bridges 3S, 3U, and 4U in Figure 12b; bridges 4S and 4U in Figure 6.12c), within 10% for one case (bridge 4S in Figure 6.12b), and about 30% for another case (bridge 4U in Figure 6.12a). While the MPA overestimated the deck displacements at abutments, it slightly underestimated the column drifts for a few cases (bridges 3S and 4U in Figure 6.12a; bridge 3S in Figure 6.12b; bridge 4U in Figure 6.12c).

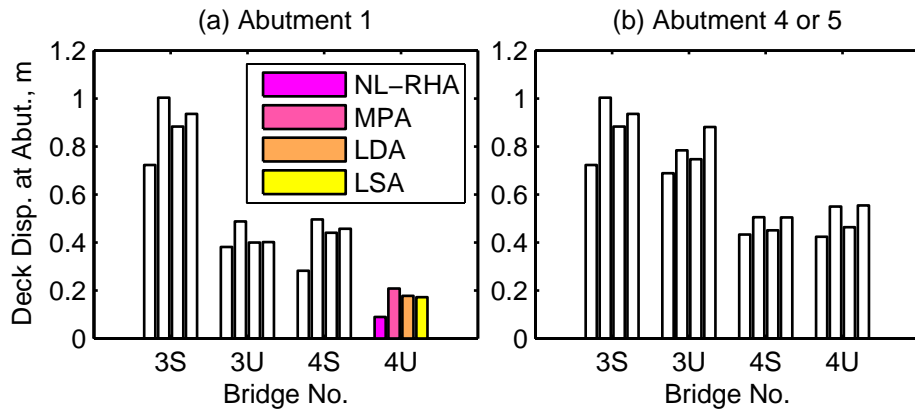


**Figure 6.11. Upper bound of transverse deck displacement at abutment determined by three approximate procedures – MPA, linear dynamic analysis (LDA), and linear static analysis (LSA) – and “exact” nonlinear RHA (NL-RHA). Results are for fault-parallel ground motions associated with a vertical strike-slip fault.**

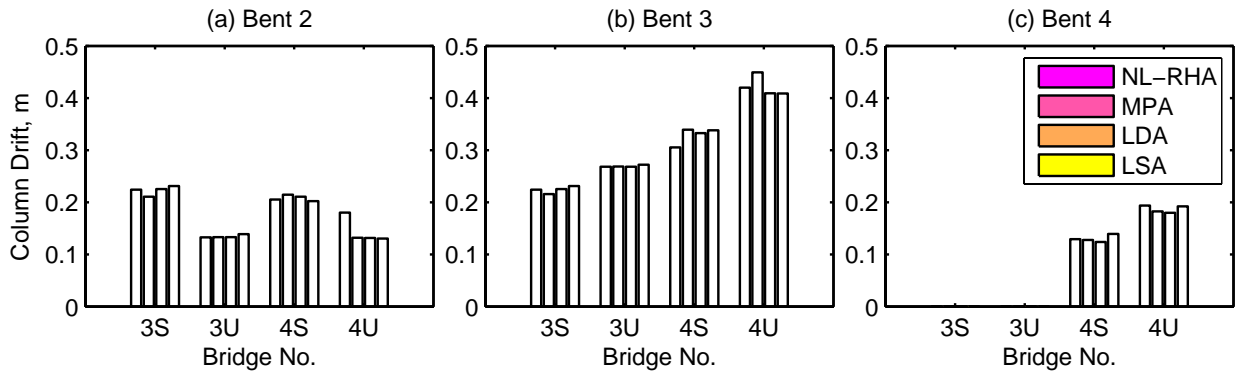


**Figure 6.12. Upper bound of transverse column drifts at abutment determined by three approximate procedures – MPA, linear dynamic analysis (LDA), and linear static analysis (LSA) – and “exact” nonlinear RHA (NL-RHA). Results are for fault-parallel ground motions associated with a vertical strike-slip fault.**

The linear dynamic analysis and linear static analysis procedures also provide conservative estimates of deck displacements at abutments (Figure 6.11a), but these procedures are generally slightly less conservative compared to the MPA procedure. The exception occurs for bridge 3U for which the linear static analysis procedure provides slightly more conservative estimate of deck displacements at abutments (Figure 6.11). The column drifts estimated by linear dynamic analysis and linear static analysis procedures are generally very similar to those from the MPA procedure (Figure 6.12).

The results presented in Figures 6.13 and 6.14 for longitudinal response due to fault-normal motions on a fault with a dip of  $40^\circ$  and rake of  $110^\circ$  indicate that the three approximate procedures – MPA, linear dynamic analysis, and linear static analysis – provide essentially identical estimates of deck displacements at abutments and column drifts, which are within about 5% of the “exact” results.

The three approximate procedures are much more accurate in estimating the upper bound of the response for the two shear-key cases (Figures 6.11 to 6.14) compared to that observed previously for the individual cases (see Figures 6.7 to 6.10). The accuracy of the linear static analysis procedure is generally no worse, and slightly better for many cases, compared to the MPA procedure or the linear dynamic analysis procedure. Therefore, the linear static analysis procedure, which is the simplest of the three approximate procedures, is preferable over MPA or linear dynamic analysis procedures.

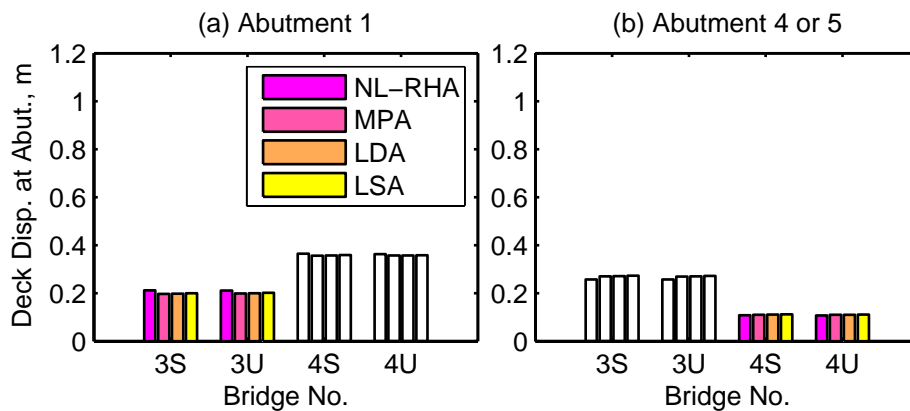


**Figure 6.13. Upper bound of transverse deck displacement at abutment determined by three approximate procedures – MPA, linear dynamic analysis (LDA), and linear static analysis (LSA procedures) – and “exact” nonlinear RHA (NL-RHA). Results are for fault-normal ground motions associated with a fault with dip of  $40^\circ$  and rake of  $110^\circ$ .**

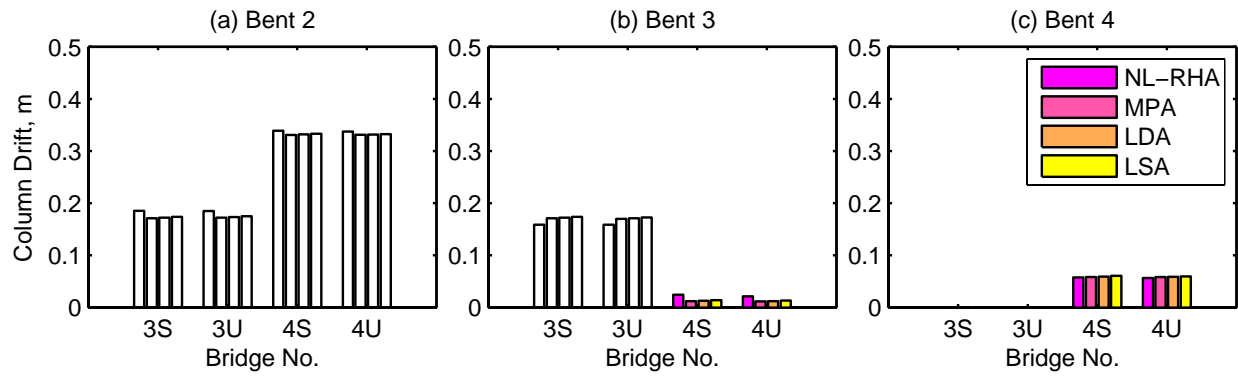


**Figure 6.14. Upper bound of transverse column drifts at abutment determined by three approximate procedures – MPA, linear dynamic analysis (LDA), and linear static analysis (LSA procedures) – and “exact” nonlinear RHA (NL-RHA). Results are for fault-normal ground motions associated with a fault with dip of 40° and rake of 110°.**

## 7. COMMENTS ON CURRENT PROCEDURES

### 7.1 Procedures based on Fault Rupture Load Cases

Gloyd et al. (2002) proposed a simple design approach for “ordinary” bridges crossing fault-rupture zones by consider the following two load cases, in addition to the standard CALTRANS load cases *I-VII*:

$$\text{Group VII}_{FR-1} = 1.0[1.0D + \beta_E E + 1.0B + 1.0SF + 1.0PS + 1.0EQ + 1.0FR_P] \quad (7.1a)$$

$$\text{Group VII}_{FR-2} = 1.0[1.0D + \beta_E E + 1.0B + 1.0SF + 1.0PS + 1.0FR_D] \quad (7.1b)$$

in which  $D$ ,  $E$ ,  $B$ ,  $SF$ ,  $PS$ ,  $EQ$ ,  $FR_P$ , and  $FR_D$  are demands due dead load, earth pressure, buoyancy load, stream-flow load, pre-stress load, earthquake load, probabilistic surface displacement (or fault-offset), and deterministic fault-offset, respectively, and  $\beta_E$  is the load multiplier for earth pressure. The  $VII_{FR-1}$  load case involves superposition of demands  $FR_P$  from static analysis of the bridge due to the fault-offset, estimated from probabilistic analysis, in the fault-parallel direction and  $EQ$  from dynamic analysis of the bridge to motions in the fault-normal direction. The  $VII_{FR-2}$  load case involves only demand  $FR_D$  from static analysis of the bridge to the fault-offset, estimated from deterministic analysis, in the fault-parallel direction. The demand  $EQ$  from dynamic analysis in the  $VII_{FR-1}$  load case is for ground motions in the fault-normal direction associated with the fault rupture. Under the guidance of a Technical Advisory Panel, this approach was used by the CALTRANS engineers and project consultants to design bridges in the SR210/I-215 interchange in San Bernardino, California.

In contrast, the structural-dynamics-based development presented in Chapter 5 demonstrates that analysis of bridges crossing fault-rupture zones due to an individual component of ground motion (fault-parallel or fault-normal) requires superposition of demands from a static analysis for fault-offset and a dynamic analysis for spatially-varying ground motion.

While the procedure proposed by Glyod et al. (2002) considers the static response due to fault offset, it either ignores the dynamic response or considers the dynamic response incorrectly. For example, the  $VII_{FR-1}$  load case combines the static response due to fault offset in the fault-parallel direction with the dynamic response due to excitation in the fault-normal direction. Obviously, the dynamic part of the response due to ground shaking in the fault-parallel direction

is ignored in this load case. The  $VII_{FR-2}$  load case ignores the dynamic response due to both fault-parallel and fault-normal ground motions.

## 7.2 A Simplistic Procedure

Recognizing the difficulty in implementing nonlinear RHA with spatially-varying ground motions, practicing engineers have devised a simple two-step procedure for design of bridges crossing fault-rupture zones (CALTRANS, 2007). The first step in this procedure estimates the displacement demands for the bridge, assumed to be linearly elastic by standard RSA. Implicit in this approach is the assumption that the bridge is located on one side of the fault and thus subjected to spatially-uniform excitation. The excitation is characterized either by a site-specific spectrum or the CALTRANS SDC spectrum that is modified for near-field effects; the magnification factor is zero for  $T \leq 0.5 \text{ sec}$ , 20% for  $T \geq 1 \text{ sec}$ , and varies linearly over the period range  $0.5 < T < 1 \text{ sec}$  (CALTRANS, 2006). The second step estimates the displacement capacity of the bridge by nonlinear static analysis wherein gravity loads are applied first, followed by fault rupture displacements applied at various supports of the bridge. One-half of the fault-rupture displacement is applied to the portion of the bridge on one side of the fault; the other one-half is applied in the opposite direction to the portion of the bridge on the other side of the fault. The preceding analysis in the second step may be interpreted as equivalent to the quasi-static analysis described in preceding sections. Finally, in the second step, lateral forces proportional to the structural mass distribution are applied to the bridge and monotonically increased until column plastic hinges reach their capacity and incremental displacement is noted. The bridge design is acceptable if the incremental displacement capacity determined by this pushover analysis exceeds the seismic displacement demand from RSA in the first step. The last step of the procedure suggests that the total seismic demand is estimated by superposition of nonlinear quasi-static response due to peak values of support displacements, and linear dynamic response of the bridge, assumed to be located one side of the fault, due to spatially-uniform support excitation.

Although combining quasi-static and dynamic responses in the above-described simplistic procedure appears to be similar to the superposition approach in the three approximate procedures proposed Chapter 6, there are two important discrepancies in computation of the dynamic part of the response. The first step of the simplistic procedure assumes the bridge to be

located on one side of the fault and thus subjected to spatially-uniform support excitation, which bears no resemblance to spatially-varying excitation with fault offset relevant for bridges crossing fault-rupture zones. The same assumption is implicit in the final part of the second step in the simplistic procedure. The mass-proportional lateral force distribution, which is equivalent to  $\mathbf{s}^* = \mathbf{m}\boldsymbol{\iota}$ , used in the pushover analysis of the simplistic procedure, may be appropriate for bridges located on one side of the fault that are subjected to spatially-uniform support excitation, but not for bridges crossing fault-rupture zones subjected to spatially-varying support excitation with fault offset. For bridges crossing fault-rupture zones, the appropriate force distribution is either that corresponding to the most-dominant mode, i.e.,  $\mathbf{s}_n^* = \mathbf{m}\boldsymbol{\phi}_n$ , or that considering the distribution of inertia forces on the bridge subjected to spatially-varying support motions with fault offset, i.e.,  $\mathbf{s}^* = \mathbf{m}\boldsymbol{\iota}_{\text{eff}}$ . As demonstrated in Chapter 5, the influence vector,  $\boldsymbol{\iota}$ , for spatially-uniform support excitation has no resemblance to the effective influence vector,  $\boldsymbol{\iota}_{\text{eff}}$ , for spatially-varying excitation with fault offset.

Second, the response spectrum used in the simplistic procedure is inappropriate for ground motions expected in close proximity to faults. This becomes apparent by comparing the CALTRANS SDC spectrum with the response spectrum for ground motions in fault-rupture zones, all presented in normalized form (see Figure 3.9).

In contrast, all three approximate procedures, MPA, linear dynamic analysis, and linear static analysis, presented in Chapter 6 recognize all the important features of the earthquake response of bridges crossing fault-rupture zones: spatial variations including fault offset in the support motions, and the characteristics of ground motions expected in close proximity to the causative fault. Linear static analysis, the simplest of the three procedures presented here, is especially attractive for practical application because it is even simpler than the simplistic procedure, and yet provides good estimates of seismic demands, because it is rooted in structural dynamics theory.

## 8. CONCLUSIONS

This investigation on analysis of “ordinary” bridges crossing fault-rupture zones has been implemented in three phases: (1) understanding the role of shear keys in seismic behavior, (2) development of linear analysis procedures, and (3) development of nonlinear analysis procedures. Finally, procedures currently being used by bridge engineers for analysis of “ordinary” bridges crossing fault-rupture zones are compared against the procedures developed during this investigation. Following are the conclusions and recommendations from this investigation. Although accuracy of the analytical procedures proposed in this report are demonstrated only for three- and four-span straight bridges perpendicular to the fault, these procedures are expected to provide accurate estimates of seismic demands for all bridges in general – bridges with larger number of spans, curved bridges, bridges skewed with respect to the fault – because the underlying theory used in development of these procedures is independent of the number of spans, curvature of the bridge, or orientation of the bridge relative to the fault.

### 8.1 Role of Shear Keys

The first phase of this investigation on how shear keys affect seismic behavior of bridges has led to the following conclusions:

1. The seismic demands for a bridge with nonlinear shear keys (shear keys that break-off and cease to provide transverse restraint if deformed beyond a certain limit) can generally be bounded by the demand computed for two shear-key cases: elastic shear keys (shear keys that do not break-off and continue to provide transverse restraint throughout the ground shaking), and no shear keys (transverse restraint due to shear keys is completely ignored). This conclusion is valid for bridges subjected to spatially-uniform ground motion as well as spatially-varying ground motion expected in fault-rupture zones.
2. The shear keys may be ignored in estimating an upper bound of seismic demands for a bridge subjected to spatially-uniform ground motion.
3. Estimating upper bound values of seismic demands for a bridge crossing a fault-rupture zone requires analysis for two shear-key cases: no shear keys and elastic shear keys. A bridge without shear keys generally provides an upper bound estimate of deck displacement at abutment, but a bridge with elastic shear keys generally provides an upper bound estimate of column drift.

4. Seismic response of bridges crossing fault-rupture zones may be very sensitive to the strength of shear keys indicating that computation of this response, even with nonlinear RHA, may be unreliable in the absence of realistic and accurate force-deformation models for shear keys.

Because ignoring transverse restraint due to shear keys may underestimate some seismic demands for a bridge crossing fault-rupture zones, it is recommended that such bridges be analyzed for both shear-key cases (elastic shear keys and no shear keys) to establish an upper bound of seismic demands. Shear keys may be ignored for such bridges only if they can be demonstrated to “truly” break-off before initiation of strong shaking expected during the maximum design earthquake.

While explicit consideration of nonlinear force-deformation relationship of shear keys may be the most accurate modeling for estimating seismic demands, it presents two complications. First, some seismic demands may be underestimated if the shear key happens to be stronger than the design strength. Second, nonlinear modeling of shear keys requires that the seismic demands be determined by nonlinear RHA of the bridge system. Upper and lower bounds for seismic demands *can* be obtained by analyses of two simpler nonlinear systems: bridge with elastic shear keys and bridge without shear keys.

## **8.2 Linear Analysis**

The second phase of investigation has led to development of two procedures – response spectrum analysis (RSA) procedure and linear static analysis procedure – for estimating peak responses of linearly-elastic “ordinary” bridges crossing fault-rupture zones. Although much simpler than response history analysis, these procedures provide estimates of peak seismic responses that are sufficiently “accurate” for most practical application.

The presented procedures idealize spatially-varying excitation as a proportional multiple-support excitation in which motions at various supports of the bridge are assumed to be proportional to the motion at a reference location. It has been demonstrated that this idealization is valid for spatially-varying ground motions in close proximity to faults with various dip and rake angles, and provides accurate estimates of peak seismic responses.

In the presented procedures, the peak value of seismic response of the bridge is computed by superposition of peak values of quasi-static and dynamic parts of the response. The peak quasi-

static response is computed by static analysis of the bridge with peak values of all support displacements applied simultaneously. Two procedures are presented for estimating the peak dynamic response. In the RSA procedure it is estimated directly from the response spectrum including all significant modes in the dynamic analysis. The linear static analysis procedure avoids computing the vibration periods of the bridge as well as estimating the rise time of the fault offset, and estimates the peak dynamic response by a much simpler static analysis of the bridge to appropriately selected forces. These procedures utilize the “effective” influence vector that differs from that for the spatially uniform excitation. Furthermore, the RSA procedure uses the response spectrum for ground motions expected in close proximity to the causative fault.

The natural vibration modes that are excited in bridges subjected to motions resulting from rupture on a fault passing under the bridge differ entirely from those excited in bridges on one side of the fault. Therefore, it is important to correctly identify the modes that need to be considered in the RSA procedure. For this purpose, the modal contribution factor concept is demonstrated to be useful.

It is shown that both the RSA procedure and the linear static analysis procedure provide estimates of peak total response that are very close to the peak response determined by “exact” response history analysis. Furthermore, it is shown that only one mode – the most dominant mode – is usually sufficient in the RSA Procedure.

### **8.3 Nonlinear Analysis**

The last phase of this investigation focused on computation of seismic demands in “ordinary” bridges crossing fault-rupture zones and deformed beyond their linear elastic limit. It is shown that the seismic demands for such bridges can be estimated to a useful degree of accuracy by superposition of the peak values of the quasi-static and dynamic parts of the response. The peak value of the quasi-static part of the response, including the effects of gravity loads, is computed by nonlinear static analysis of the bridge due to peak ground displacements applied simultaneously at all supports.

Three approximate procedures were presented for estimating the peak value of the dynamic part of the response. The linear static analysis procedure, which is simpler than the two other procedures, MPA and linear dynamic analysis, is recommended as the procedure for practical analysis of “ordinary” bridges. Although the other two are dynamics-based procedures, they

consider only the response contribution of the most-dominant mode; at the expense of additional computational effort, they can be extended to include higher mode contributions; as in the general MPA and RSA procedures, respectively. On the other hand, the linear static analysis procedure does not require computation of the vibration periods or modes of the structure, but indirectly considers contributions of all vibration modes and requires only a linear static analysis of the bridge due to lateral forces that recognize the ground offset across the fault and the shape of the response spectrum for fault ground motions in close proximity to the fault.

#### **8.4 Current Procedures**

It is demonstrated that procedure based on fault-rupture load cases recently used by bridge engineers to design bridges in the SR210/I-215 interchange in San Bernardino, California, is inappropriate for estimating seismic demands in bridges crossing fault-rupture zones: these procedures either ignore the dynamic part of the response or compute it incorrectly.

It is also demonstrated that the simplistic two-step procedure for design of bridges crossing fault-rupture zones is also inappropriate for analysis and design of bridges crossing fault-rupture zones. This procedure has two important discrepancies in computation of the dynamic part of the response. First, this procedure assumes the bridge to be located on one side of the fault and thus subjected to spatially-uniform support excitation, which bears no resemblance to spatially-varying excitation with fault offset relevant for bridges crossing fault-rupture zones. Second, the response spectrum used in this procedure is inappropriate for ground motions expected in close proximity to faults.

Finally, it is demonstrated that the mass-proportional lateral force distribution used in the pushover analysis of the simplistic procedure may not be for bridges crossing fault-rupture zones. For bridges crossing fault-rupture zones, the appropriate force distribution is either that corresponding to the most-dominant mode or that considering the distribution of inertia forces on the bridge subjected to spatially-varying support motions with fault offset.

In contrast, all three approximate procedures, MPA, linear dynamic analysis, and linear static analysis, developed in this investigation recognize all the important features of the earthquake response of bridges crossing fault-rupture zones: spatial variations including fault offset in the support motions, and the characteristics of ground motions expected in close proximity to the causative fault. Linear static analysis, the simplest of the three procedures

presented here, is especially attractive for practical application because it is even simpler than the simplistic procedure, and yet provides good estimates of seismic demands, because it is rooted in structural dynamics theory.

## REFERENCES

- Bozorgzadeh, A., Megally, S., and Restrepo, J. (2003). *Seismic Response of Sacrificial Exterior Shear Keys in Bridge Abutments: Recommended Design and Construction Details*. Report to CALTRANS, Contract No. 59A0337, Department of Structural Engineering, UC San Diego, April 30.
- Bozorgzadeh, A., Megally, S., Restrepo, J., and Ashford, S.A. (2006). "Capacity Evaluation of Exterior Sacrificial Shear Keys of Bridge Abutments," *Journal of Bridge Engineering*, 11(5):555-565.
- CALTRANS (2006). *Seismic Design Criteria: Version 1.4*, California Department of Transportation, Sacramento, CA. (<http://www.dot.ca.gov>)
- CALTRANS (2007). *Personal Communication*, June 5.
- Chopra, A.K. (2007). *Dynamic of Structures: Theory and Applications to Earthquake Engineering*, 3<sup>rd</sup> Edition, New Jersey: Prentice-Hall.
- Clayton, R. and B. Engquist (1977). "Absorbing Boundary Conditions for Acoustic and Elastic Wave Equations," *Bulletin of Seismological Society of America*, 67:1529-1540.
- Der Kiureghian, A. and Neuenhofer, A. (1992). "Response Spectrum Method for Multiple Support Seismic Excitation," *Earthquake Engineering and Structural Dynamics*, 21(8):713-740.
- Dreger, D (2006). "Scaling of Ground Motions in Fault-Rupture Zones for Different Rise Time," *Personal Communication*, February, 21.
- Dreger, D., Hurtado, G., and Chopra, A.K., and Larson, S. (2007). Near-Fault Seismic Ground Motions, *Report No. UCB/EERC-2007/03*, Earthquake Engineering Research Center, University of California, Berkeley, CA.
- Earthquake Engineering Research Institute (EERI), (2000). Chapter 18: Impact on Highway Structures in Kocaeli, Turkey, Earthquake of August 17, 1999 Reconnaissance Report, *Earthquake Spectra*, Supplement A to Volume 16.
- Earthquake Engineering Research Institute (EERI), (2001). Chapter 8: Highway Bridges in Chi-Chi, Taiwan, Earthquake of September 21, 1999 Reconnaissance Report, *Earthquake Spectra*, Supplement A to Volume 17.
- Ghasemi, H., Cooper, J.D., Imbsen, R., Piskin, H., Inal, F., and Tiras, A. (2000). *The November 1999 Duzce Earthquake: Post-Earthquake Investigation of the Structures in the TEM*. Publication No. FHWA-RD-00-146, U.S. Department of Transportation, Federal Highway Administration.
- Gloyd, S., Fares, R., Sánchez, A., and Trinh, C. (2002). "Designing Ordinary Bridges for Ground Fault Rupture," *Proceedings of the Third National Seismic Conference & Workshop on Bridges and Highways*, Portland, Oregon, April.
- Larsen, S. and C.A. Schultz (1995). ELAS3D: 2D/3D Elastic Finite-Difference Wave Propagation Code, *Lawrence Livermore National Laboratory Technical Report No. UCRL-MA-121792*, 19 pp.

McKenna, F. and Fenves, G. (2001). *The OpenSees Command Language Manual: Version 1.2*, Pacific Earthquake Engineering Center, University of California, Berkeley. (<http://opensees.berkeley.edu>).

Megally, S.H., Silva, P.F., and Seible, F. (2001). *Seismic Response of Sacrificial Shear Keys in Bridge Abutments*, Report No. SSRP-2001/23, Department of Structural Engineering, University of California, San Diego, CA.

Neuenhofer, A. (2007). "Multiple-Support Excitation." *Personal Communication*, June 27.

Somerville, P. G., K. Irikura, R. Graves, S. Sawada, D. Wald, N. Abrahamson, Y. Iwasaki, T. Kagawa, N. Smith, and A. Kowada (1999). "Characterizing Crustal Earthquake Slip Models for the Prediction of Strong Ground Motion," *Seism. Res. Lett.*, 70, 59-80.

Yen, W.-H. (2002). Lessons Learned about Bridges from Earthquake in Taiwan. *Public Roads*, U.S. Department of Transportation, Federal Highway Administration, Volume 65, No. 4.

## APPENDIX A. GROUND MOTIONS FOR OTHER EARTHQUAKE MAGNITUDES

This appendix describes a simplified procedure to generate fault-parallel ground motions for earthquakes with different magnitudes on a strike-slip fault. Such ground motions are utilized later to show that the normalized response spectrum for fault-parallel motions in the fault-rupture zone is independent of the earthquake magnitude, given the assumption of linear elasticity used to generate the motions. Although, such ground motions could be generated by seismological simulations similar to the one that led to motions described earlier for earthquake events in fault-rupture zone with different magnitudes, these simulations require considerable computational effort. A simpler approach is to utilize the relationships of earthquake magnitude,  $M_w$ , with rise time,  $T_R$ , and the total fault-offset,  $u_{go}$ , for motion in the fault-parallel direction (Somerville et al, 1999),

$$T_R = 10^{0.5(M_w - 6.69)} \quad (\text{A1a})$$

$$u_{go} = 10^{0.5(M_w - 2.91)} \quad (\text{A1b})$$

to scale the ground displacements generated previously for a magnitude 6.5 earthquake to obtain the ground displacement for other magnitude earthquakes. For this purpose, the time scale is multiplied by the ratio  $T_R(M_w)/T_R(M_w = 6.5)$ , and the displacement scale is multiplied by the ratio  $u_{go}(M_w)/u_{go}(M_w = 6.5)$ . Such scaling is appropriate for fault-parallel motions, the motions of interest, in fault rupture zone but not for fault-normal motions (Dreger, 2007: Personal Communication).

Equation A1 indicates that the average rise-time as well as the fault-offset would increase with increasing earthquake magnitude, which is verified by the results of Figure A1. The effects of earthquake magnitude (and hence rise-time) on the ground motions are presented in Figure A2. As expected, the ground displacement is a step function and the displacement-offset at the reference location, which is selected as one-half of the average fault-offset, increases with earthquake magnitude and rise-time (Figure A2a). The ground velocity is characterized by a single-sided pulse of increasing duration with increasing earthquake magnitude. However, the peak ground velocity remains essentially independent of the earthquake magnitude (Figure A2b). This is the case because of the assumption of constant stress drop, which yields a constant slip

velocity (Dreger, 2007: Personal communication, Feb, 21). This also occurs due to use of self-similar restrained empirical relationship of Somerville et al. (1999). The ground acceleration, which is characterized by a double-sided pulse, increases in duration but decreases in magnitude with increasing earthquake magnitude (Figure A2c). This is a direct result of the ground velocity with same peak value but increasing duration with increasing earthquake magnitude.

Note that the stress drop in actual earthquake events may vary somewhat from the constant value assumed in this investigation. As a result, time variation of ground velocity and accelerations may differ from those in Figure A2. However, the ground motions of Figure A2 are sufficient for the limited purpose of demonstrating the relative importance of quasi-static and dynamic responses in this investigation.

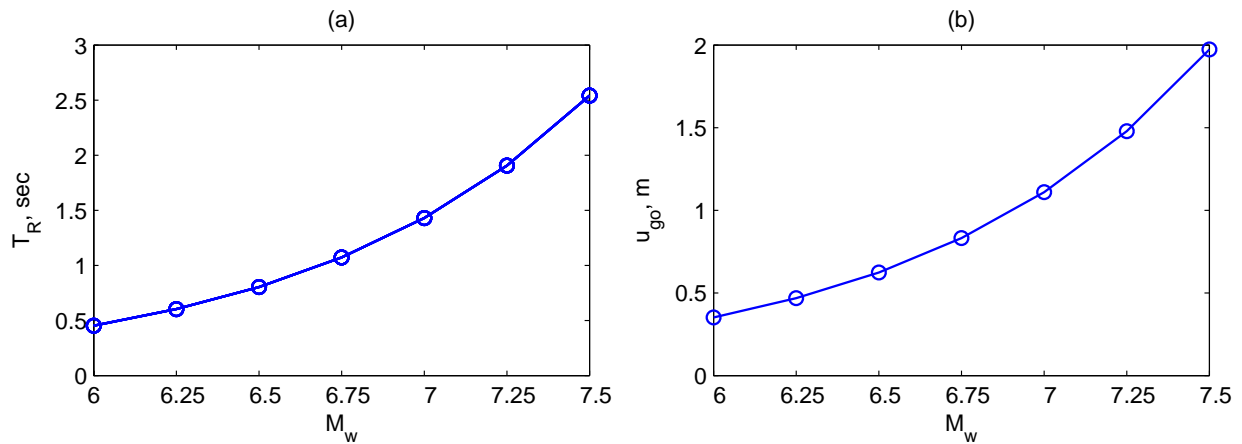


**Figure A1. Variation of (a) ground displacement rise time and (b) fault-offset with earthquake magnitude for fault-parallel motions on a strike-slip fault.**

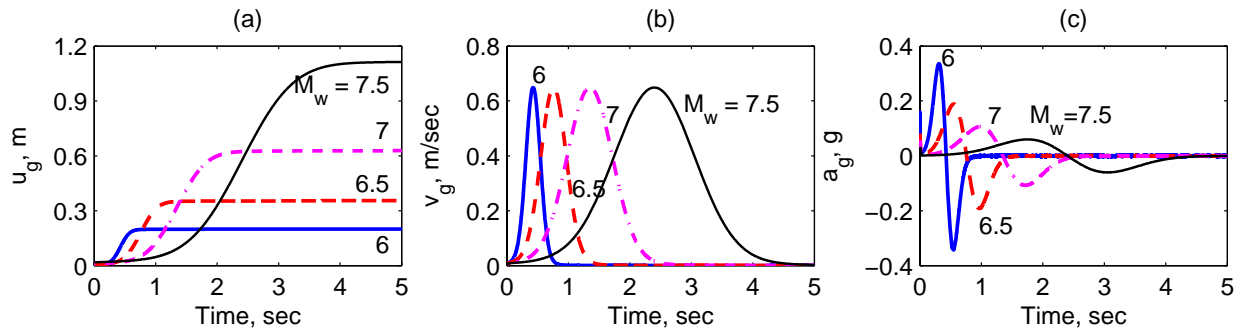


**Figure A2. Effects of earthquake magnitude on ground motions: (a) ground displacement; (b) ground velocity; and (c) ground acceleration for fault-parallel motions on a strike-slip fault.**

Figure A3a presents 5%-damped elastic response spectra for the ground motions of Figure A2. These results indicate lower peak ground accelerations, i.e., spectral acceleration at zero-period, for higher magnitude earthquake in fault-rupture zone even though the ground offset becomes larger for higher magnitude earthquakes (Figure A2). As explained previously, this occurs due to the assumption of constant stress drop in generating the ground motions, which the justification for restraining relationships in Equation A1 to follow self-similarity. Furthermore, higher spectral accelerations occur at short periods for low-magnitude earthquakes and at long periods for high-magnitude earthquakes. The peak in the spectral acceleration appears to occur at the period equal to rise-time of the ground displacement.

Figure A3b presents the normalized response spectrum: the vibration period,  $T_n$ , is normalized with the rise-time of the ground displacement,  $T_r$ , and the pseudo-acceleration  $A$  (or spectral acceleration), is normalized with the peak ground acceleration,  $\ddot{u}_{go}$ . These results indicate that the normalized average response spectrum becomes independent of the earthquake magnitude, as apparent from identical spectra for all magnitudes; the slight differences apparent in the response spectra are purely due to numerical errors in the computation procedure. As expected, the peak in the normalized spectrum occurs at  $T_n = T_r$ , and  $A/\ddot{u}_{go}$  approaches one at zero period.

The above noted trends in the ground motions and response spectra are for motions generated with constant stress drop. Furthermore, the scaling of ground motions with earthquake magnitude is for average values of fault offset and rise-time. These trends may differ slightly for earthquake ground motions generated for variable stress drop as well as more accurate modeling for fault offset and rise-time.

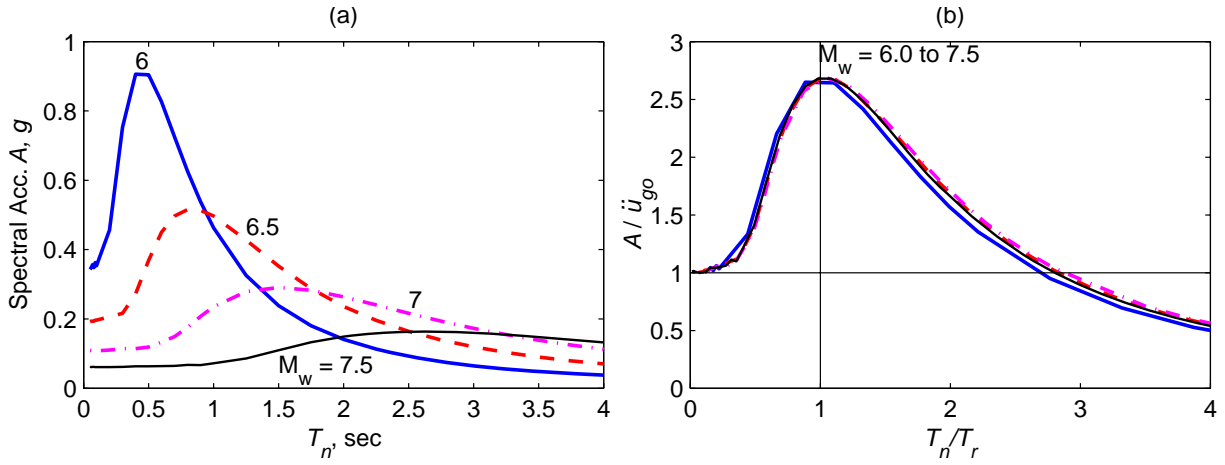


**Figure A3. 5%-Damped elastic response spectra for fault-parallel ground motions on a strike-slip fault: (a) Response spectrum; (b) Normalized response spectrum.**

## APPENDIX B. SHEAR-KEY MODELING

Presented in this appendix is the procedure used in this investigation to develop force-deformation behavior of external shear keys. For this purpose, the experimental work and the shear-key failure mechanisms reported elsewhere (Bozorgzadeh et al., 2003, 2006; Megally et al, 2001) have been utilized. Presented first is the procedure to evaluate the shear-key strength followed by the force-deformation relationship.

### B.1 STRENGTH OF SHEAR KEYS

Two failure mechanisms of external shear keys that are typically used by CALTRANS (Figure B1a) have been reported (see Bozorgzadeh et al., 2006 for details and other references): (1) sliding shear mechanism in which a single horizontal crack develops at the interface of the shear key and abutment stem wall; and (2) diagonal tension mechanism in which multiple diagonal cracks develop in the abutment stem wall. The nominal capacity (or strength) of the shear key in the sliding shear mechanism can be evaluated from (Bozorgzadeh et al., 2006):

$$V_n = \frac{\mu_f \cos \alpha + \sin \alpha}{1 - \mu_f \tan \beta} A_{vf} f_{su} \quad (\text{B1})$$

in which  $\alpha$  is the angle of kinking of the vertical bars with respect to the vertical axis ( $=37^\circ$ );  $\beta$  is the angle of include face of the shear key with respect to the vertical axis;  $\mu_f$  is the kinematic coefficient of friction of concrete ( $=0.36$ ); and  $f_{su}$  and  $A_{vf}$  are the ultimate tensile strength and area, respectively, of the vertical reinforcement crossing the shear plane.

The nominal capacity of the shear key in the diagonal tension mechanism can be computed from (Bozorgzadeh et al., 2006):

$$V_n = V_c + V_s \quad (\text{B2})$$

in which  $V_c$  is the contribution of concrete, and  $V_s$  is the contribution of steel. The value of  $V_c$  is given by

$$V_c = 0.2\sqrt{f'_c}bh \quad (\text{B3})$$

where  $f'_c$  is the compressive strength of concrete in MPa, and  $b$  and  $h$  are the width and height

in meters, respectively, of the abutment stem wall. Note that units of  $V_c$  from Equation (B3) are in MN, which can be converted to the units of kN by multiplying the answer from Equation (B3) by 1000. The contribution of steel,  $V_s$ , is given by

$$V_s = \left[ A_{s1}f_y h + A_{s2}f_y d + n_h A_{sh} f_y \frac{h^2}{2s} + n_v A_{sv} f_y \frac{d^2}{2s} \right] \left( \frac{1}{h+a} \right) \quad (B4)$$

where  $A_{s1}$  is the total area of the horizontal tie (or hanger) bars;  $A_{s2}$  is the total area of the inclined bars in the first row crossing the shear key interface;  $A_{sh}$  and  $A_{sv}$  are the area of single horizontal and vertical bars, respectively (see Figure B1a);  $n_h$  and  $n_v$  are the number of side faces with horizontal and vertical side reinforcement, respectively;  $s$  is the spacing of horizontal and vertical bars;  $d$  is the thickness of shear key at the interface with abutment stem wall;  $a = 0.167d$ ; and  $f_y$  is the yield strength of steel assumed to be identical for all reinforcing bars.

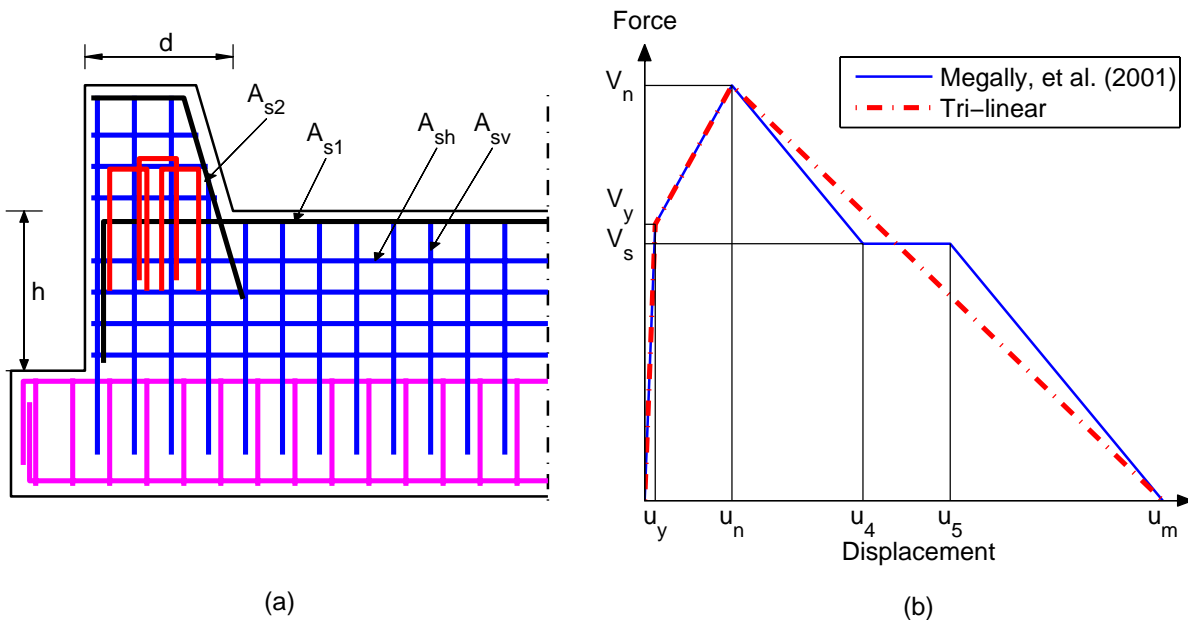


**Figure B1. (a) Shear-key details, and (b) shear-key force-deformation relationship.**

Under the action of a horizontal force (or shear) applied to the shear key, one of the two aforementioned mechanisms would develop in exterior shear keys. Depending on the reinforcement details and construction joint of a shear key, a mechanism that requires the lowest shear force would develop at the failure limit state.

## B.2 FORCE-DEFORMATION RELATIONSHIP OF SHEAR KEY

In addition to the shear key strength described in the preceding section, this investigation needed a complete description of the force-deformation relationship. While a force-deformation relationship is not currently available for the sliding shear mechanism, a simple relationship has been developed for the diagonal tension mechanism (Megally et al., 2001). In this relationship, shown in Figure B1b, the displacements at various levels are given as:

$$u_y = \sqrt{2}\varepsilon_y (L_d + L_a) \frac{(h+d)}{\sqrt{h^2 + d^2}} \quad (\text{B5a})$$

$$u_n = \sqrt{2}\varepsilon_y (L_d + L_a) \frac{(h+d)}{s} \quad (\text{B5b})$$

$$u_4 = \sqrt{2}\varepsilon_{0.005} (L_d + L_a) \frac{(h+d)}{s} \quad (\text{B5c})$$

$$u_5 = \sqrt{2}\varepsilon_{0.007} (L_d + L_a) \frac{(h+d)}{s} \quad (\text{B5d})$$

where  $\varepsilon_y$  is the yield strain in steel,  $\varepsilon_{0.005} = 0.005$ ,  $\varepsilon_{0.007} = 0.007$ ,  $L_a$  is equal to width of the stem wall, and  $L_d$  is the reinforcement development length. The displacement  $u_m$  is obtained by assuming the slope of the curve between  $u_5$  and  $u_m$  to be the same as that between  $u_n$  and  $u_4$ . Finally, the force  $V_y$  is defined as

$$V_y = V_s + V_c \frac{u_y}{u_n} \quad (\text{B6})$$

In this investigation, the force-deformation relationship presented by Megally et al. (2001) has been idealized by a tri-linear curve (Figure B1b). The hysteretic rule, however, is similar to that presented by Megally et al. (2001). Furthermore, the force-deformation relationship of the shear key is based only on the diagonal tension mechanism, i.e., the possibility of sliding shear mechanism for which force-deformation relations is not currently available has been excluded. Such simplifications are not likely to significantly alter the observations and conclusions.

Development of the shear-key force-deformation relationship using the aforementioned procedure requires that the abutment design, i.e., size and reinforcement details, be available. In this parametric investigation, however, such details were not available. One option was to scale experimental results from the shear key Test Unit 4A with details currently used by CALTRANS and tested at UCSD (Bozorgzadeh et al, 2006). This unit was built at 1:2.5 scale of a prototype abutment design. Therefore, the force-deformation relationship developed for the details of the test unit using Equations B5 and B6 was scaled as follows to obtain the force-deformation relationship of the prototype abutment: multiply the displacements and forces of the test unit by a factor of 2.5 and 6.25, respectively. Unfortunately, the shear key in the prototype abutment obtained by such scaling was too strong (it remained essentially elastic) for the structural systems considered in this investigation.

The alternative procedure used in this investigation first selected the target strength,  $V_T$ , of the shear key to be equal to 30% of the dead load reaction at the abutment. Second, the scale factor,  $sf = \sqrt{V_T/V_n}$ , was computed in which  $V_n$  was the strength of the test unit. Next, size and reinforcement details of the abutment-shear-key system in the bridge system under consideration were obtained by scaling the design of the test unit. Finally, the force-deformation relationship was developed from Equations B5 and B6 for the size and reinforcement details of scaled abutment design.

Note that the procedure used in this investigation to develop the force-deformation behavior of shear key may not be “accurate” theoretically; however, such a simple procedure is sufficient for this parametric investigation because the observations and conclusions are not likely to be significantly affected by the shear-key force-deformation relationship. Although results are not presented here for brevity, force-deformation relationship of the test unit directly without any scaling led to the identical observations and conclusions.

## APPENDIX C. PROPERTIES OF INELASTIC SDF SYSTEM

The MPA procedure considering lateral force distribution corresponding to only one mode – the most-dominant mode – is based on the assumption that response of a nonlinear multi-degree-of-freedom (MDF) system occurs due to that mode alone. This implies that response due to other modes and the coupling between modes due to system nonlinearity is ignored. For such an assumption, Equation (1) for dynamic response of a nonlinear MDF system may be re-written as

$$\mathbf{m}\ddot{\mathbf{u}} + \mathbf{c}\dot{\mathbf{u}} + \mathbf{f}_s(\mathbf{u}, \dot{\mathbf{u}}) = -\mathbf{s}_n\ddot{u}_g(t) \quad (\text{C1})$$

in which  $\mathbf{s}_n = \Gamma_n \mathbf{m} \boldsymbol{\phi}_n$ ,  $\Gamma_n = \boldsymbol{\phi}_n^T \mathbf{m} \boldsymbol{\iota}_{\text{eff}} / \boldsymbol{\phi}_n^T \mathbf{m} \boldsymbol{\phi}_n$ , and  $n$  is the number of the most-dominant mode. Pre-multiplying Equation (C1) by  $\boldsymbol{\phi}_n^T$  and using the mass- and classical damping-orthogonality property of modes gives

$$\ddot{q}_n + 2\zeta_n \omega_n \dot{q}_n + \frac{F_{sn}}{M_n} = -\Gamma_n \ddot{u}_g(t) \quad (\text{C2})$$

where  $F_{sn} = \boldsymbol{\phi}_n^T \mathbf{f}_s(\mathbf{u}, \dot{\mathbf{u}})$  and  $M_n = \boldsymbol{\phi}_n^T \mathbf{m} \boldsymbol{\phi}_n$ . The response of the MDF nonlinear system then can be computed from

$$\mathbf{u} = \mathbf{u}_n = \boldsymbol{\phi}_n q_n = \Gamma_n \boldsymbol{\phi}_n D_n \quad (\text{C3})$$

and displacement at any reference location from

$$u_{rn} = \Gamma_n \boldsymbol{\phi}_{rn} D_n \quad (\text{C4})$$

in which  $D_n$  is governed by

$$\ddot{D}_n + 2\zeta_n \omega_n \dot{D}_n + \frac{F_{sn}}{L_n} = -\ddot{u}_g(t) \quad (\text{C5})$$

with  $L_n = \boldsymbol{\phi}_n^T \mathbf{m} \boldsymbol{\iota}_{\text{eff}}$ . Note that Equation (A5) is the governing equation of motion of an inelastic SDF system with  $\omega_n$  (or  $T_n$ ),  $\zeta_n$ , and force-deformation behavior defined by the  $F_{sn}/L_n$  relationship subjected to ground motion at a reference support. Utilizing Equations (C4) and (C5), the force-deformation relationship of the inelastic SDF system needed in the MPA procedure can be obtained from that of the MDF system from:

$$\frac{F_{sn}}{L_n} = \frac{\phi_n^T \mathbf{f}_s}{L_n} \quad (\text{C6a})$$

$$D_n = \frac{u_{rn}}{\Gamma_n \phi_{rn}} \quad (\text{C6b})$$

The pushover analysis for the most-dominant mode involves applying increasing intensity of the force distribution given by

$$\mathbf{f}_s = \beta_n \mathbf{m} \phi_n \quad (\text{C7})$$

in which  $\beta_n$  is the force-scale factor during pushover analysis. Utilizing Equation (C7) into Equation (C6a) gives

$$\frac{F_{sn}}{L_n} = \frac{\phi_n^T \mathbf{f}_s}{L_n} = \frac{\beta_n \phi_n^T \mathbf{m} \phi_n}{L_n} = \frac{\beta_n M_n}{L_n} = \frac{\beta_n}{\Gamma_n} \quad (\text{C8})$$

Therefore, the pushover curve for a MDF system can be converted to the  $F_{sn}/L_n - D_n$  curve of the inelastic SDF system by Equations (C8) and (C6b).

Although not essential, the  $F_{sn}/L_n - D_n$  relation is often idealized as a bilinear (or multi-linear) curve because most readily available computer programs for solving response of inelastic SDF system utilize such force-deformational idealization. The initial slope of this curve is equal to  $\omega_n^2$  indicating that the vibration period  $T_n$  of the inelastic SDF system is given by

$$T_n = 2\pi \left( \frac{L_n D_{ny}}{F_{sny}} \right)^{1/2} \quad (\text{C9})$$

in which subscript y indicates the yield values. This value of  $T_n$ , which may differ from the period of the corresponding linear system, should be used for estimating deformation of the inelastic SDF system.

The pushover curves for a multi-story building is plot of base shear,  $V_{bn}$ , versus roof displacement,  $u_{rn}$ . From such a pushover curve,  $F_{sn}/L_n$  for the  $n$ th mode inelastic SDF systems is computed from

$$\frac{F_{sn}}{L_n} = \frac{V_{bn}}{M_n^*} \quad (\text{C10})$$

in which  $M_n^* = L_n \Gamma_n$  is the effective modal mass. The relationship of Equation (C10) for a multi-story building is a special case of Equation (C8), which becomes evident from the following equations:

$$V_{bn} = \mathbf{1}^T \mathbf{f}_{sn} = \beta_n \mathbf{1}^T \mathbf{m} \boldsymbol{\phi}_n = \beta_n \boldsymbol{\phi}_n^T \mathbf{m} \mathbf{1} = \beta_n L_n \quad (\text{C11})$$

$$\frac{V_{bn}}{M_n^*} = \frac{V_{bn}}{\Gamma_n L_n} = \frac{\beta_n L_n}{\Gamma_n L_n} = \frac{\beta_n}{\Gamma_n} \quad (\text{C12})$$

which utilize the fact that  $\boldsymbol{\iota}_{\text{eff}} = \boldsymbol{\iota} = \mathbf{1}$  for buildings subjected to spatially-uniform support excitation.

While the  $V_{bn} - u_{rn}$  pushover curve is useful for design and evaluation of buildings, where it can provide useful insight into nonlinear behavior and potential weak spots of the selected building, it may not be appropriate for bridges crossing fault-rupture zones because the most-dominant mode, which often involves torsional motions about a vertical axis, may induce little or no base shear. The value of  $\beta_n$  would always be non-zero during pushover analysis using force distributions for all types of modes. Therefore, the  $\beta_n - u_{rn}$  pushover curve is more appropriate for bridges crossing fault-rupture zones.

## APPENDIX D. EXAMPLE ANALYSIS

### D.1 STATEMENT OF THE PROBLEM

The estimation of seismic demands in nonlinear bridge crossing fault-rupture zone is illustrated for the Magnolia Avenue UC Bridge. This three-span continuous box-girder bridge is located on section of a road with a horizontal curve of radius 853.4 m (1800 ft) and a vertical curve of radius 579.1 m (1900 ft). It is supported on two seat-type abutments, with skew-angle of about  $19.75^\circ$  at abutment 1 and  $30^\circ$  at abutment 4, and two single-column bents. Due to large radius of horizontal and vertical curves, this bridge can be idealized as three straight spans of 43.6 m (143 ft), 41.8m (137 ft), and 39.6 m (130 ft) (Figure D1). The bridge deck has a 4% slope across its width (Figure D2). The deck, a 13 m (42.5 ft) wide and 1.75 m (5.75 ft) deep multi-cell box girder, is expected to accommodate two traffic lanes (Figure D3). The lower portion of the column is octagonal in shape with a total depth of 2.14 m (7 ft) (Figure D4). The upper 6.4 m (21 ft) of the column has a parabolic flare with a total depth across the bridge deck varying from 2.14 m (7 ft) to 4.28 m (14 ft). The primary longitudinal steel in the column cross section is arranged in a circular pattern and consists of a total of 30 bundles of 2 bars each with an area of  $10.1 \text{ cm}^2$  (#11 bar) (Figure D4). The transverse reinforcement consists of circular hoops of 2.54 cm diameter bar (#8 bar) at a spacing of 11.4 cm (4.5 inch).

For the purpose of this example, this bridge is assumed to cross a strike-slip fault, located between bents 2 and 3. The bridge is analyzed for the fault-parallel motions due to an earthquake of magnitude of 6.5 (Figure 3.3). The results are presented for transverse response of the bridge without shear keys.

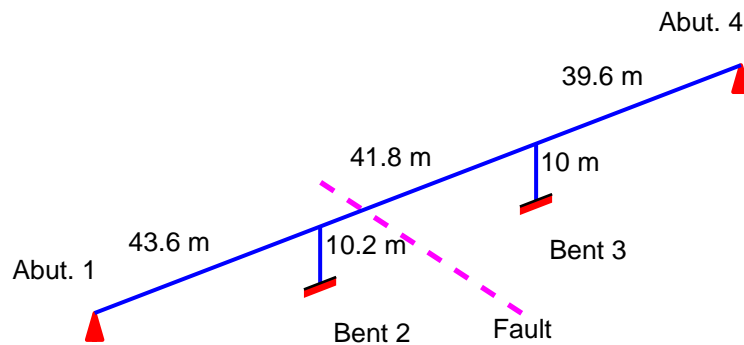


**Figure D1. Magnolia Avenue UC Bridge.**

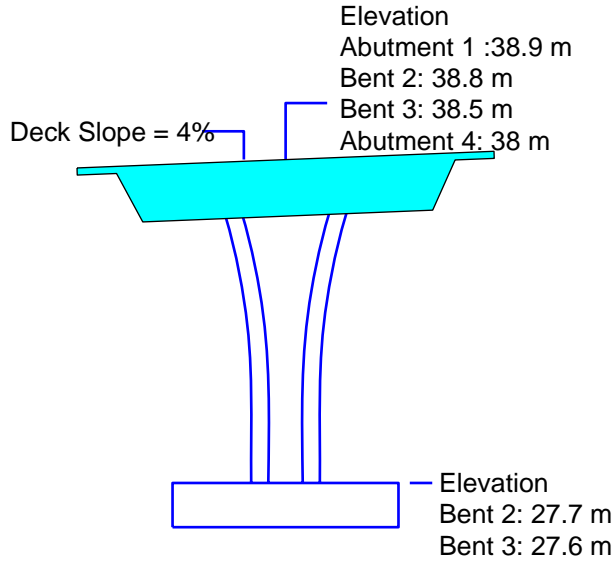


**Figure D2. Section of the Magnolia Avenue UC Bridge.**

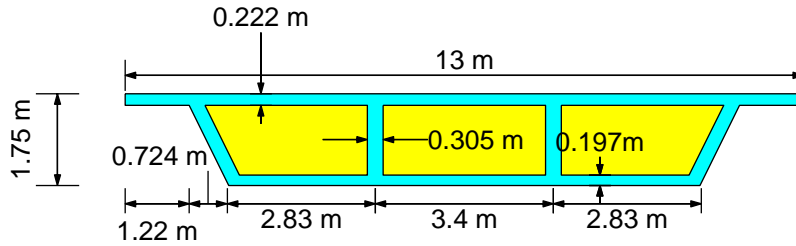


**Figure D3. Deck cross section for the Magnolia Avenue UC Bridge.**

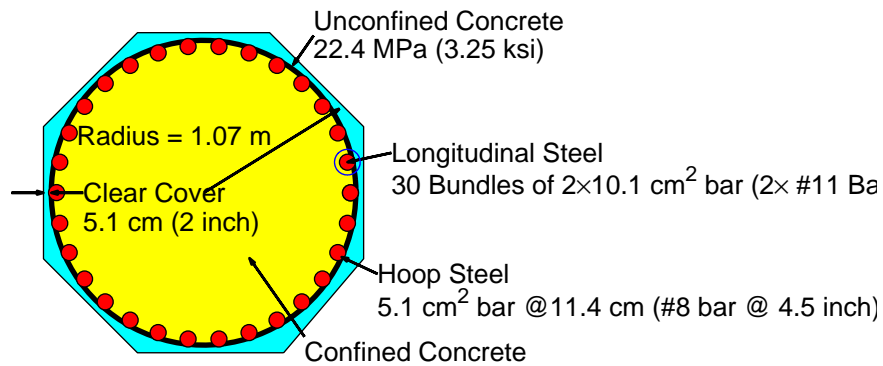


**Figure D4. Column cross section for the Magnolia Avenue UC Bridge.**

The selected bridge is analyzed using the structural analysis software *OpenSees* (McKenna and Fenves, 2001). The deck girder is modeled by linearly-elastic beam column elements. In order to capture the distribution of mass along the length of the deck, five elements per span

were used. Consistent with the CALTRANS recommendations (CALTRANS, 2006), the gross values for moment of inertia and polar moment of inertia were used for pre-stressed multi-cell box deck girder. For linear analysis, the column is modeled with single linear beam-column element with effective moment of inertia obtained from section moment-curvature analysis. For nonlinear analysis, column is modeled with nonlinear beam-column element with cross-sectional properties specified based on a circular fiber section.

The inherent damping for the selected bridge is modeled with Rayleigh's damping (Chopra, 2007):  $\mathbf{c} = a_0\mathbf{m} + a_1\mathbf{k}$ , where  $\mathbf{m}$  is the mass matrix of the system,  $\mathbf{k}$  is the initial elastic stiffness matrix of the system, and  $a_0$  and  $a_1$  are the mass- and stiffness-proportionality coefficients. In order to keep damping ratio to be about 5% in most significant modes of the selected systems, values of  $a_0$  and  $a_1$  were selected to be 0.4134 and 0.004837, respectively

## D.2 VIBRATION PERIODS AND MODES

The implementation of the MPA and linear dynamic analysis procedures requires computation of the mode-shapes, vibration periods, and modal contribution factors of the linear-elastic bridge. The modal contribution factors are then used to identify the most-dominant mode that needs to be considered in these procedures. The first six mode shapes and vibration periods of the bridge are presented in Figure D5. The computed mode shapes indicate coupling between transverse and torsional motions of the bridge: the mode shapes of the selected bridge occur in pairs with the first two modes forming the first pair whereas fourth and fifth modes forming the second pair of coupled transverse-torsional modes. The third mode is coupled vertical-longitudinal mode and the sixth mode is a predominantly vertical mode.

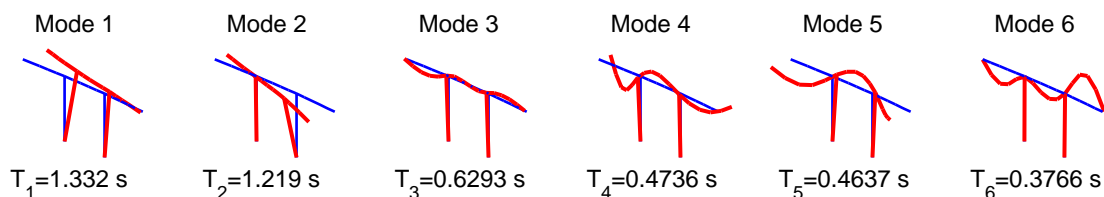


**Figure D5. First six mode shapes and vibration periods of the bridge.**

## D.3 MODAL CONTRIBUTION FACTORS

Illustrated next is computation of the modal contribution factors for various modes of the bridge. For this purpose, the effective influence vector is computed by statically applying displacement

equal to +1 at abutment 1 and at the base of bent 2, and  $-1$  at the base of bent 3 and at abutment 4. The deflected shape of the bridge associated with the effective influence vector is shown in Figure D6. It is apparent from this deflected shape that the effective influence vector for ground motions in fault-rupture zones exhibits significant torsional motions about the vertical axis of the bridge and therefore the selected ground motion is likely to excite modes of the bridge that involve torsional motions about its vertical axis.

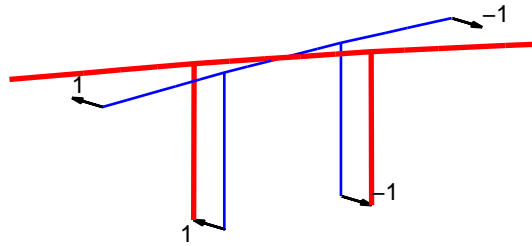


**Figure D6. Deflected shape of the bridge associated with the effective influence vector.**

In order to compute the modal contribution factors, forces  $\mathbf{s} = \mathbf{m}\mathbf{u}_{\text{eff}}$  (Figure D7a) are applied statically to the fixed-base, linear-elastic bridge to compute its deflections (Figure D7b). The drifts in the column of bent 2 and 3 are  $c_2^{\text{st}} = 0.0406$  and  $c_3^{\text{st}} = -0.0315$ , respectively; and deck displacement at abutment 1 and 4 are  $d_1^{\text{st}} = 0.132$  and  $d_4^{\text{st}} = -0.109$ , respectively. Note that units of these deformation quantities are not important as they would cancel out later during computation of the modal contribution factor.

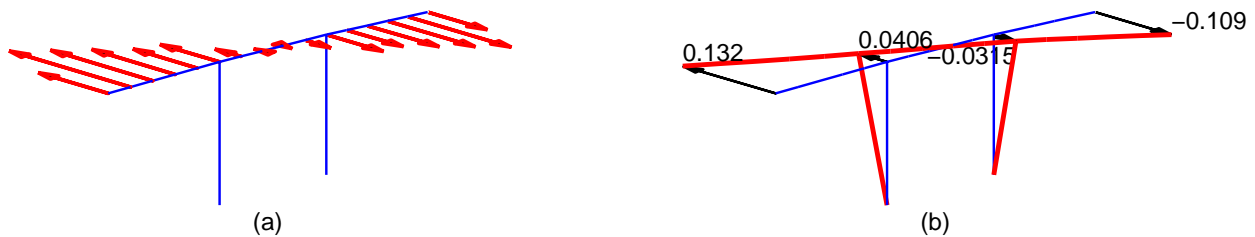


**Figure D7: (a) Forces  $\mathbf{s} = \mathbf{m}\mathbf{u}_{\text{eff}}$ ; and (b) Deflected shape of the bridge due to forces,  $\mathbf{s} = \mathbf{m}\mathbf{u}_{\text{eff}}$ .**

Next, forces corresponding to the 1<sup>st</sup> mode,  $\mathbf{s}_1 = \Gamma_1 \mathbf{m}\boldsymbol{\phi}$  (Figure D8a), are applied statically to the linear-elastic bridge to compute the deflected shape (Figure D8b). The drift in bent 2 and 3

are  $c_{21}^{st} = 0.0441$  and  $c_{31}^{st} = 0.0167$ , respectively; and deck displacement at abutment 1 and 4 are  $d_{11}^{st} = 0.085$  and  $d_{41}^{st} = -0.00734$ , respectively.

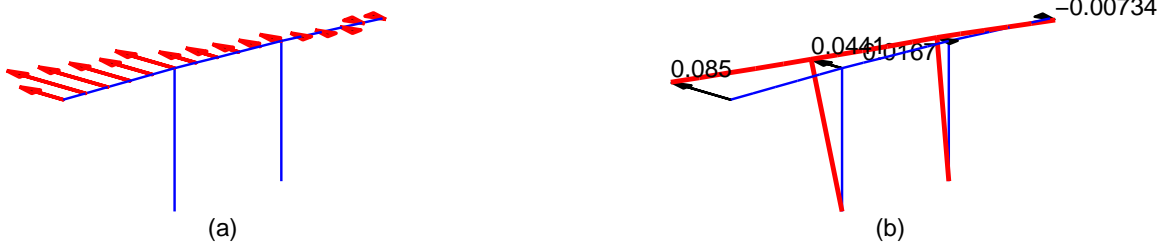


**Figure D8: (a) Forces  $s_1 = \Gamma_1 m \phi$ ; and (b) Deflected shape of the bridge due to forces,  $s_1 = \Gamma_1 m \phi$ .**

The first mode modal contribution factor for drifts in bent 2 and 3 are  $\bar{c}_{21} = c_{21}^{st}/c_1^{st} = 0.0441/0.0406 = 1.086$  and  $\bar{c}_{31} = c_{31}^{st}/c_3^{st} = 0.0167/-0.0315 = -0.530$ , respectively; and deck displacement at abutment 1 and 4 are  $\bar{d}_{11} = d_{11}^{st}/d_1^{st} = 0.085/0.132 = 0.644$  and  $\bar{d}_{41} = d_{41}^{st}/d_4^{st} = -0.00734/-0.109 = 0.0673$ , respectively.

The aforementioned process is repeated for the first six modes of the bridge to obtain the modal contribution factors listed in Table D1. This table shows that the modal contribution factors are the largest for the first two modes – the first pair of coupled transverse-torsional modes (Figure D5). Although the modal contribution factors for the fourth and fifth modes, the second pair of coupled transverse-torsional modes (Figure D5), are non-zero, the small values indicate negligibly small participation of these modes. The modal contribution factors for the third and sixth modes, the two predominantly longitudinal modes, are zero implying that these modes are not excited. The modal contribution factors presented in Table D1 also indicate that the first mode is the most dominant mode for deck displacement at abutment 1 and drift in bent 2 but second mode is the most-dominant mode for deck displacement at abutment 4 and column drift in bent 3.

Table D1. Modal contribution factors.

Mode	Abut. 1	Abut. 4.	Bent 2	Bent 3
1	0.643	0.068	1.086	-0.530
2	0.359	0.929	-0.088	1.531
3	0	0	0	0
4	-0.001	0.001	0.001	-0.001
5	-0.001	0.001	0.001	0.000
6	0	0	0	0

#### D.4 QUASI-STATIC RESPONSE

Required in the three approximate procedures presented in this report is the peak value of the quasi-static response, including gravity load effects,  $r_{o+g}^s$ . For calculating  $r_{o+g}^s$ , the gravity loads are applied to the structure followed by static application of peak support displacements of +0.35 m, +0.35 m, -0.35 m, and -0.35 m on base of abutment 1, bent 2, bent 3, and abutment 4, respectively, that occur at these supports due to the selected ground motion. Since the shear keys are not engaged in the example bridge, the support displacements at abutment 1 and abutment 4 do not induce deformations in the bridge. A nonlinear static analysis of the selected bridge to the gravity loads and the aforementioned support displacements leads to the quasi-static displacements shown in Figure D9. Note that the support displacements are applied in small increment during the nonlinear static analysis in order to keep the numerical errors within acceptable level. The peak drift in bents 2 and 3 are computed as  $c_{2o+g}^s = |(0.323) - (0.350)| = 0.027\text{m}$  and  $c_{3o+g}^s = |(-0.322) - (-0.350)| = 0.028\text{m}$ , respectively; and deck displacement at abutments 1 and 4 as  $d_{1o+g}^s = |(0.991) - (0.350)| = 0.641\text{m}$  and  $d_{4og}^s = |(-0.930) - (-0.350)| = 0.580\text{m}$ , respectively. The contributions of gravity loads to the selected response quantities are negligibly small.

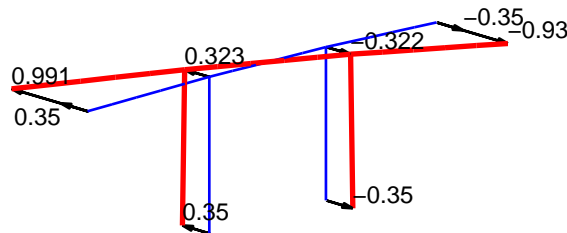


Figure D9. Peak values of nonlinear quasi-static displacement of the selected bridge.

## D.5 PEAK DYNAMIC RESPONSES

Three approximate procedures are implemented to estimate the dynamic response: MPA, linear dynamic analysis, and linear static analysis.

### D.5.1 MPA Procedure

Application of Steps 1 and 2 of the MPA procedure led to mode shapes and periods in Figure B5 and effective influence vector in Figure D6. These mode shapes along with the effective influence vector were used to generate the modal contribution factors in Table D1. It was found that the first mode is the most dominant mode for deck displacement at abutment 1 and drift in bent 2 but second mode is the most-dominant mode for deck displacement at abutment 4 and column drift in bent 3. The implementation of Steps 3 and 4 of the MPA procedure is illustrated next.

#### Step 3.

The peak value of dynamic response,  $r_{no}$ , in the most dominant modes is computed from the pushover analysis as follows:

#### Step 3.1.

Figures D10a and D11a show the pushover curves  $\beta_1 - u_{r1}$  and  $\beta_2 - u_{r2}$  for the first and second “mode” force distributions,  $\mathbf{f}_1^* = \beta_1 \mathbf{m} \phi_1$  and  $\mathbf{f}_2^* = \beta_2 \mathbf{m} \phi_2$ , respectively. Recall that first mode is the most dominant mode for deck displacement at abutment 1 and drift in bent 2 and second mode is the most-dominant mode for deck displacement at abutment 4 and column drift in bent 3. Reference location for developing these pushover curves is selected as the node on the deck at abutment 1 of the bridge.

#### Step 3.2.

The pushover curve of Figures D10a and D11a are converted to the force-deformation relationships for the first- and second-“mode” inelastic SDF system by utilizing  $F_{sn}/L_n = \beta_n/\Gamma_n$  and  $D_n = u_{rn}/\Gamma_n \phi_{rn}$ . These relationships are shown in solid line in Figures B10b and B11b.

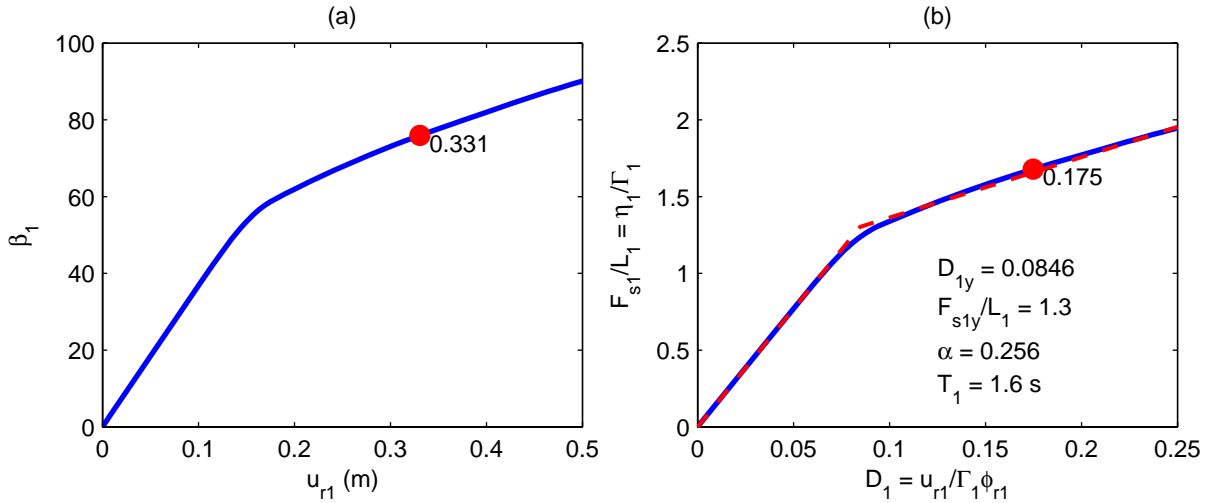


**Figure D10. (a) First-“Mode” pushover curve; and (b)  $F_{sn}/L_n - D_n$  relationship for the first “mode” inelastic SDF system.**

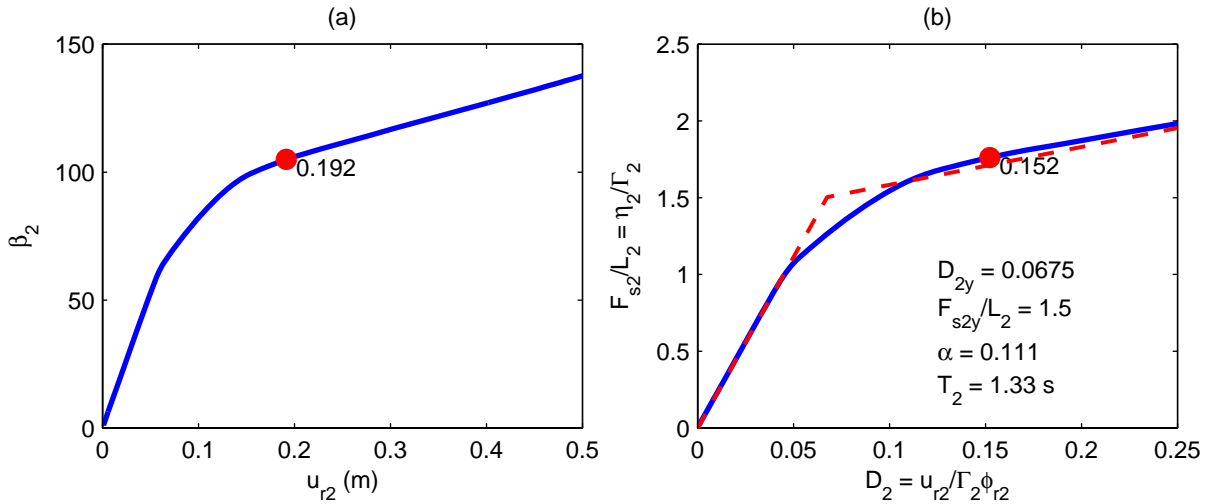


**Figure D11. (a) Second-“Mode” pushover curve; and (b)  $F_{sn}/L_n - D_n$  relationship for the second “mode” inelastic SDF system.**

*Step 3.3.*

The force-deformation relationships of the first- and second-“mode” inelastic SDF system are idealized in Figures D10b and D11b by a bilinear curve (dashed line). These idealizations provide yield displacement, yield force, and post-yield stiffness ratio of 0.0846, 1.3, and 0.256 for the first-“mode” SDF system (Figure D10b); and 0.0675, 1.5, and 0.111 for the second-“mode” SDF system (Figure D11b).

*Step 3.4.*

Analyses of the first- and second-“mode” inelastic SDF systems defined by the idealized bilinear

force-deformation relations of Figures D10b and D11b subjected to the selected ground acceleration at the reference location provide  $D_1 = 0.175\text{m}$  and  $D_2 = 0.152\text{m}$ ; the damping ratios computed from specified Rayleigh's damping with  $a_0 = 0.4134$  and  $a_1 = 0.004837$ , for first and second mode are  $\zeta_1 = 5.52\%$  and  $\zeta_2 = 5.26\%$ , respectively. Note that the initial elastic vibration period of the inelastic SDF system obtained from the force-deformation relationship (Figures D10b and D11b) are slightly longer than the first- and second-“mode” vibration period of the linearly elastic bridge (Figure D5).

*Step 3.5.*

The peak reference point displacements associated with the first- and second-“mode” are computed as  $u_{r1} = 0.331\text{m}$  and  $u_{r2} = 0.192\text{m}$ . These displacements are also noted on the pushover curves of Figures D10a and D11a.

*Step 3.6.*

First-“mode” pushover analysis of the bridge to the peak reference location displacement of  $0.331\text{ m}$  leads to drift in bent 2 and 3 of  $c_{21o+g} = 0.194\text{m}$  and  $c_{31o+g} = 0.0793\text{m}$ , respectively; and deck displacement at abutment 1 and 4 of  $d_{11o+g} = 0.331\text{m}$  and  $d_{41o+g} = 0.0283\text{m}$ , respectively (Figure D12). Similarly, second-“mode” pushover analysis of the bridge to the peak reference location displacement of  $0.192\text{ m}$  leads to drift in bent 2 and 3 of  $c_{22o+g} = 0.0798\text{m}$  and  $c_{32o+g} = 0.330\text{m}$ , respectively; and deck displacement at abutment 1 and 4 of  $d_{12o+g} = 0.192\text{m}$  and  $d_{41o+g} = 0.580\text{m}$ , respectively (Figure D13).

*Step 4.*

Since contributions due to gravity loads are negligibly small, the peak values of the dynamic response are:  $c_{2o} = 0.194\text{m}$ ,  $c_{3o} = 0.330\text{m}$ ,  $d_{1o} = 0.331\text{m}$ , and  $d_{4o} = 0.580\text{m}$ . Note that the deck displacement at abutment 1 and drift in bent 2 are selected from the first-“mode” pushover analysis and deck displacement at abutment 4 and drift in bent 3 are selected from the second-“mode” pushover analysis.

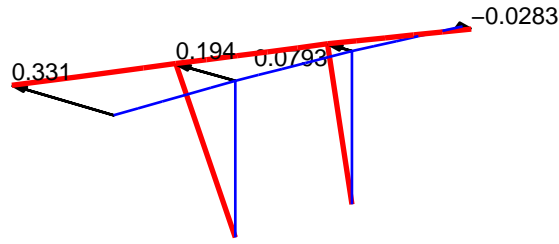


**Figure D12. Deflected shape of the example bridge at reference displacement of 0.331m from the first-“mode” pushover analysis.**

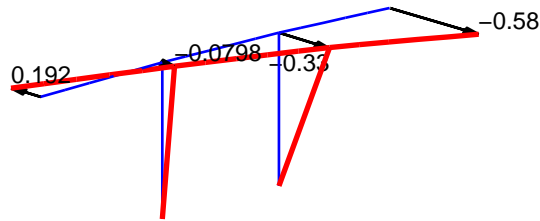


**Figure D13. Deflected shape of the example bridge at reference displacement of 0.192m from the second-“mode” pushover analysis.**

The total response of the bridge are:  $c_{2o}^t = 0.027 + 0.194 = 0.221\text{m}$ ,  $c_{3o}^t = 0.028 + 0.330 = 0.358\text{m}$ ,  $d_{1o}^t = 0.640 + 0.331 = 0.971\text{m}$ , and  $d_{4o}^t = 0.580 + 0.580 = 1.16\text{m}$ .

### ***D.5.2 Linear Dynamic Analysis***

Application of Steps 1 and 2 of the linear dynamic analysis procedure led to mode shapes and periods in Figure D5 and the effective influence vector of Figure D6. The modal contribution factors computed in the MPA procedure indicated that the first mode is the most dominant mode for deck displacement at abutment 1 and drift in bent 2 but second mode is the most-dominant mode for deck displacement at abutment 4 and column drift in bent 3. The implementation of Steps 3 and 4 of the linear dynamic analysis procedure is illustrated next.

#### ***Step 3.***

Using mode shapes of Figure D5 and effective influence vector of Figure D6, the values of  $\Gamma_n$  are computed as:  $\Gamma_1 = 45.2$  for the first mode and  $\Gamma_2 = 59.6$  for the second mode.

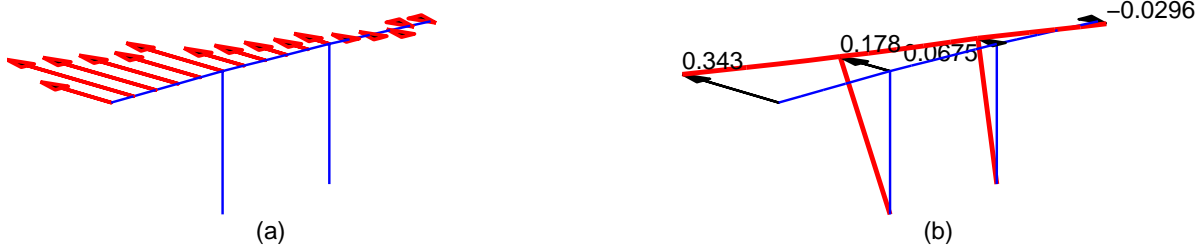


**Figure D14: (a) Force  $s_1 = \Gamma_1 \mathbf{m} \phi_1 A_1$ ; and (b) Deflected shape of the linear-elastic example bridge due to  $s_1 = \Gamma_1 \mathbf{m} \phi_1 A_1$ .**

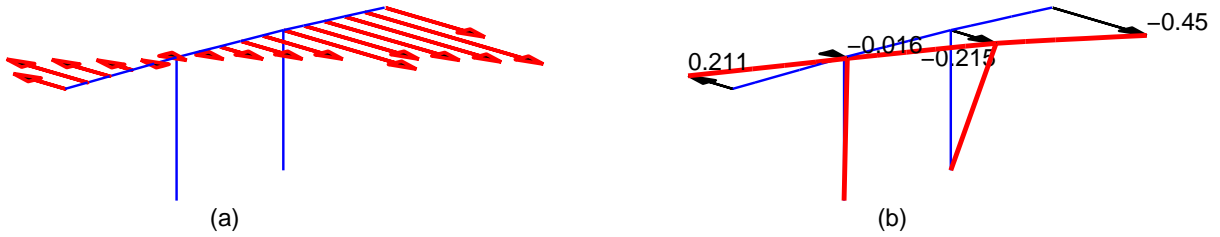


**Figure D15: (a) Force  $s_2 = \Gamma_2 \mathbf{m} \phi_2 A_2$ ; and (b) Deflected shape of the linear-elastic example bridge due to  $s_2 = \Gamma_2 \mathbf{m} \phi_2 A_2$ .**

*Step 4.*

The equivalent lateral forces corresponding to the first mode equal to  $s_1 = \Gamma_1 \mathbf{m} \phi_1 A_1$  (Figure D14a) are applied to linear-elastic bridge to obtain peak values of dynamic drift in bent 2 and 3 as  $c_{2o} = 0.178\text{m}$  and  $c_{3o} = 0.0675\text{m}$ , respectively; and deck displacement at abutment 1 and 4 as  $d_{1o} = 0.343\text{m}$  and  $d_{4o} = 0.0296\text{m}$ , respectively (Figure D14b). Similarly, equivalent lateral forces corresponding to the second mode equal to  $s_2 = \Gamma_2 \mathbf{m} \phi_2 A_2$  (Figure D15a) are applied to linear-elastic bridge to obtain peak values of dynamic drift in bent 2 and 3 as  $c_{2o} = 0.016\text{m}$  and  $c_{3o} = 0.215\text{m}$ , respectively; and deck displacement at abutment 1 and 4 as  $d_{1o} = 0.211\text{m}$  and  $d_{4o} = 0.450\text{m}$ , respectively (Figure D15b).

The total response of the bridge are:  $c_{2o}^t = 0.027 + 0.178 = 0.205\text{m}$ ,  $c_{3o}^t = 0.028 + 0.215 = 0.243\text{m}$ ,  $d_{1o}^t = 0.640 + 0.343 = 0.983\text{m}$ , and  $d_{4o}^t = 0.580 + 0.450 = 1.03\text{m}$ .

### ***D.5.3 Linear Static Analysis***

Application of Steps of the linear static analysis procedure led to the effective influence vector of Figure D6. The implementation of Step 2 of the linear static analysis procedure is illustrated

next.

*Step 2.*

Linear analysis of the bridge for equivalent lateral forces  $= 2.5\mathbf{m}t_{\text{eff}}\ddot{u}_{go}$  (Figure D16a) leads to dynamic drift in bents 2 and 3 as  $c_{2o} = 0.270\text{m}$  and  $c_{3o} = 0.221\text{m}$ , respectively; and deck displacements at abutment 1 and 4 as  $d_{1o} = 0.881\text{m}$  and  $d_{4o} = 0.726\text{m}$ , respectively (Figure D16b).

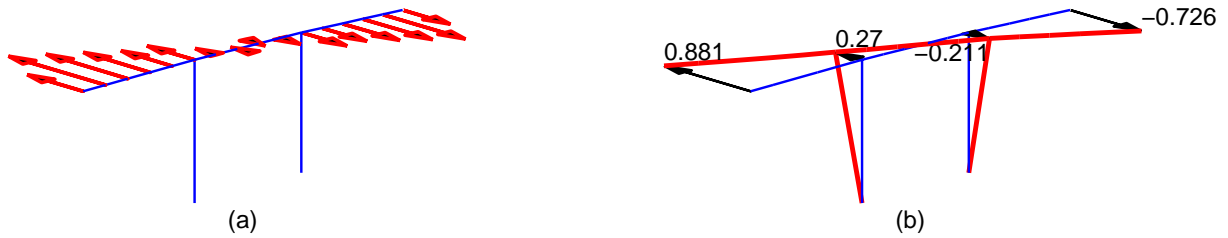


**Figure D16: (a) Forces  $2.5\mathbf{m}t_{\text{eff}}\ddot{u}_{go}$ ; and (b) Deflected shape of the bridge due to forces  $= 2.5\mathbf{m}t_{\text{eff}}\ddot{u}_{go}$ .**

The peak values of the total responses of the bridge are:  $c_{2o}^t = 0.027 + 0.270 = 0.325\text{m}$ ,  $c_{3o}^t = 0.028 + 0.211 = 0.239\text{m}$ ,  $d_{1o}^t = 0.640 + 0.881 = 1.52\text{m}$ , and  $d_{4o}^t = 0.580 + 0.726 = 1.31\text{m}$ .